B56 Subunits in --Adrenergic Regulation of Cardiac Type 2A Phosphatases

Ranieri, Antonella

Awarding institution:
King's College London

B56 Subunits in β-Adrenergic Regulation of Cardiac Type 2A Phosphatases

Antonella Ranieri

Thesis undertaken for the degree of Doctor of Philosophy in Cardiovascular Biology

3-year PhD studentship funded by the British Heart Foundation

King's College London

Cardiovascular Division
The Rayne Institute
St Thomas' Hospital
London SE1 7EH

Submitted in June 2015

Abstract

Protein phosphatase 2A (PP2A) holoenzymes are present in most cell types, including cardiac myocytes, where they provide a large proportion of serine (Ser, S) and threonine (Thr, T) phosphatase activity. PP2A family members comprise a catalytic C subunit, a scaffold A subunit and a B-type subunit, which regulates subcellular targeting, substrate specificity and catalytic activity. Previous studies in our laboratory showed that in adult rat ventricular myocytes (ARVM) the subcellular localization of the regulatory B56α subunit is altered in response to isoprenaline (ISO) stimulation. This encouraged further studies of B56 subunits in β-adrenergic regulation of cardiac PP2A, which form the basis of this PhD project.

Immunoblot analysis of ARVM samples revealed that in this cell system regulatory B56α, -γ and -δ subunits are expressed at protein level. Protein expression of PP2A scaffold and catalytic subunits was also confirmed. The subcellular distribution and ISO-induced translocation of PP2A subunits was investigated by fractionation of ARVM. B56α was depleted from the myofilament/nuclear compartment and was enriched in the cytosolic/membrane compartment of ISO-stimulated myocytes. This was observed also for PP2A scaffold and catalytic subunits.

Potential ISO-induced phosphorylation of B56δ, which is phosphorylated by protein kinase A (PKA) at S573 in non-cardiac cells, was explored. Use of the Phos-tag™ SDS-PAGE system suggested that B56δ was phosphorylated in ARVM in response to ISO stimulation. In further studies, by using a phospho-site-specific antibody, increased phosphorylation of S573 was revealed. Studies with propranolol, a non-selective β-adrenergic receptor (β-AR) antagonist, confirmed that the response is mediated by β-ARs. Studies with CGP 20712A (a β_1-selective antagonist) and ICI 118,551 (a β_2-selective antagonist) indicated that the response is mediated primarily by β_1-ARs. Studies with compounds that inhibit (H89 and PKI) or activate (N^6-Benz-cAMP) PKA showed that the activity of PKA is necessary and sufficient for the response.

To explore the functional role of B56δ phosphorylation at S573, adenoviral vectors encoding GFP-tagged human B56δ in wild type (WT) or mutated form, in which S573 is replaced by non-phosphorylatable alanine (Ala, A), were constructed and post-infection protein expression profiles in ARVM were characterized. The studies confirmed that heterologous WT B56δ is phosphorylated at S573 in response to ISO stimulation and that heterologous S573A B56δ is not phosphorylated at this site. Overexpression of WT B56δ but not S573A B56δ appeared to amplify ISO-induced phosphorylation of some PKA substrates. Further studies are now necessary to identify the direct targets of B56δ-PP2A and the impact of altered B56δ phosphorylation, and in particular to determine the physiological role of B56δ phosphorylation at S573 in β-adrenergic regulation of cardiac function.

Acknowledgements

First and foremost, I wish to thank my supervisor, Professor Metin Avkiran. Metin: thank-you for giving me the opportunity to be a member of your lab, for supporting and encouraging me throughout these years, and for always providing prompt and helpful advise or feedback. I thank my second supervisor, Professor Ali El-Armouche, for further encouragement and am grateful to Professor Angus Nairn and Professor Veerle Janssens, for their collaboration.

I would like to thank Dr Alexandra Candasamy for her help. Alex: thank-you for welcoming me into the lab at the beginning of my PhD and for teaching me the basic techniques that have enabled me to carry out my studies. Thank-you for all the support you have given me, whilst at the Rayne and after you left. Another person I wish to say a special thank-you to is Dr Elizabeth Kemp. Elizabeth: thank-you for helping me construct the adenoviral vectors – without your guidance, part of my studies would not have been possible. A very big thank-you goes to Dr Kate Weeks. Kate: thank-you for being such a wonderful colleague, teacher and friend! I have enjoyed our time together, especially our morning chats and sushi lunches, and will miss you when you leave. Other people I would like to thank are: Dr Shiney Reji for the endless number of myocyte isolations, Dr Elizabeth Ehler for the advice on confocal microscopy, and Dr Seda Eminaga for all her invaluable suggestions.

An enormous thank-you goes to my mum and dad, for loving me and supporting me. Thank-you both for being so encouraging and for putting up with me (and my moods!) whilst writing this thesis.

Finally, I would like to thank all the colleagues and friends that have been there for me, at work and outside of work, that I have not mentioned individually.

List of Publications

Papers

Longman MR, **Ranieri A**, Avkiran M and Snabaitis AK. Regulation of PP2AC carboxylmethylation and cellular localisation by inhibitory class G-protein coupled receptors in cardiomyocytes. *PLoS One*. 2014;9:e86234.

Abstracts

Ranieri A, Avkiran M. Role of B56 regulatory/targeting subunits in β-adrenergic of cardiac type 2A phosphatases. *J Mol Cell Cardiol*. 65:PS1-P106. *XXI ISHR World Congress, San Diego, July 2012 (poster).*

Table of Contents

List of Figures

List of Tables

Abbreviations

AdV	Adenovirus serotype 5
AKAP	A-kinase anchoring protein
ARE	AU-rich element
ARVM	Adult rat ventricular myocytes
ATP	Adenosine triphosphate
BSA	Bovine serum albumin
CaMK	Calcium/calmodulin kinase
cAMP	Cyclic adenosine 3',5'-monophosphate
CKIP-1	Casein kinase-2 interacting protein-1
cMyBP-C	Cardiac myosin-binding protein-C
CRE	cAMP response element
CREB	cAMP response element-binding protein
cTnI	Cardiac troponin I
Cx	Connexin
DARPP-32	Dopamine- and cAMP-regulated neuronal phosphorotein
ECC	Excitation-contraction coupling
Epac	Exchange protein activated by cAMP
ERK	Extracellular signal-regulated kinase
GAPDH	Glyceraldehyde 3-phosphate dehydrogenase
GDP	Guanosine diphosphate
GFP	Green fluorescent protein
GOI	Gene of interest
GPCR	G protein-coupled receptor
GRK	GPCR kinase
GSK3β	Glycogen synthase kinase 3β
GST	Glutathione S-transferase
GTP	Guanosine triphosphate
HA	Hemagglutinin
HDAC	Histone deacetylase
HEAT	Huntington-elongation-A subunit-TOR-like
HEK293	Human embryonic kidney 293
HF	Heart failure
H2B	Histone 2B
I-1	Inhibitor-1
I-2	Inhibitor-2
I1-PP2A	Inhibitor-1 of PP2A

I2-PP2A	Inhibitor-2 of PP2A
IP	Immunoprecipitation
ISO	Isoprenaline
KO	Knock out
LCMT-1	Leucine carboxyl methyltransferase 1
LIZ	Leucine/isoleucine zipper
LTCC	L-type calcium channel
Luteinizing hormone	LH
LV	Left ventricular
mAKAP	Muscle-specific AKAP
MAP	Microtubule-associated protein
MAPK	Mitogen-activated protein kinase
MEF2	Myocyte enhancer factor 2
MOI	Multiplicity of infection
myr-PKI	Myristoylated PKI 14-22 amide
N^6-Benz-cAMP	N^6-Benzoyl-cAMP
CPA	N^6-cyclopentyladenosine
NKA	Sodium/potassium ATPase
OA	Okadaic acid
Pak1	p21-activated protein 1
PBS	Phosphate-buffered saline
PCR	Polymerase chain reaction
PDE	Phosphodiesterase
PDF	Polyvinylidene fluoride
PFU	Plaque forming unit
PI3K	Phosphoinositide 3-kinase
PKA	Protein kinase A
PKC	Protein kinase C
PLB	Phospholamban
PLM	Phospholemman
PME-1	Protein phosphatase methyl esterase 1
PP1	Protein phosphatase 1
PP2A	Protein phosphatase 2A
PPP	Phosphoprotein phosphatase
RT	Room temperature
RyR2	Type 2 ryanodine receptor
SDS-PAGE	Sodium dodecyl sulfate polyacrylamide gel electrophoresis
Ser, S	Serine
SERCA2a	SR calcium ATPase
SR	Sarcoplasmic reticulum

STP	Ser/Thr phosphatase
TBST	Tris-buffered saline-Tween-20
$TCID_{50}$	Tissue infectivity dose 50
Thr, T	Threonine
Tyr, Y	Tyrosine
UTR	Untranslated region
WT	Wild type
β-AR	β-Adrenergic receptor

1 General Introduction

1.1 Protein phosphorylation

Protein phosphorylation is a regulatory post-translational modification that alters the biological properties of proteins, usually by inducing conformational changes.[1] The phosphorylation status of a given protein reflects the balance between the activities of protein kinases and protein phosphatases. As illustrated in Figure 1.1, protein kinases phosphorylate proteins on Ser, Thr and tyrosine (Tyr, Y) residues and protein phosphatases remove the added phosphate group. Protein phosphorylation is implicated in the regulation of many cellular processes (e.g. growth and proliferation, metabolism, apoptosis, membrane transport, gene transcription, and contraction) and aberrant phosphorylation of proteins underlies a diverse range of diseases, including heart disease.[2-4]

1.2 β-Adrenergic regulation of cardiac protein phosphorylation

1.2.1 Cardiac adrenergic receptor signaling

Adrenaline and noradrenaline regulate cardiac function through stimulation of ARs. Cardiac ARs, which include α-ARs (α_{1A}, α_{1B} and α_{1D}) and β-ARs (β_1, β_2 and β_3), are G protein-coupled receptors (GPCRs) and as such, signal via heterotrimeric G proteins.[5-7] The G_α subunit binds guanosine diphosphate (GDP) or guanosine triphosphate (GTP) and GPCR stimulation promotes G protein activation by inducing the exchange of GDP for GTP. The G_α and $G_{\beta\gamma}$ subunits dissociate and signal to distinct effector proteins, including enzymes and ion channels. The hydrolysis of GTP to GDP is mediated by the GTPase activity of the G_α subunit and promotes reformation of the G protein complex.[6,8] The responses induced by GPCR stimulation depend on the effector protein(s) activated downstream of the receptor. This in turn largely depends on the type of G_α subunit comprised in the coupled G protein. As an example, β-ARs couple to $G_{\alpha s}$ and $G_{\alpha i}$ proteins and the receptors thus signal via PKA. In contrast, α-ARs couple to $G_{\alpha q}$ proteins and therefore signal via protein kinase C (PKC).[6,8]

In the physiological mammalian heart β-ARs represent the largest population of ARs. The β_1 and β_2 subtypes, which are most abundant, are expressed at a ratio of ~80:20 and their stimulation gives rise to the positive inotropic, chronotropic and lusitropic effects of adrenergic stimuli (i.e. adrenaline and noradrenaline).[5-7] Both β_1- and β_2-ARs couple to $G_{\alpha s}$ (stimulatory) proteins and their activation leads to the accumulation of cyclic adenosine 3′,5′-monophosphate (cAMP) and activation of PKA, via stimulation of adenylyl cyclase (Figure 1.2).[9] As described in more detail in subsequent sections, this signaling pathway, referred to as the classical β-AR signaling pathway, is critical in the regulation of cardiomyocyte contractility (acute effects) and can induce cardiac hypertrophy and failure (chronic effects).[10]

The catalytic subunits of PKA, which are released from the regulatory subunits upon cAMP binding, mediate a large number of cardiac responses to β-adrenergic stimuli by

phosphorylating target proteins on Ser and Thr residues.[11-13] The subcellular targeting of PKA holoenzymes is mediated by A-kinase anchoring proteins (AKAPs), which contribute to PKA signaling specificity by colocalizing the kinase with enzymes that counterbalance its activation and its effects.[14,15] Phosphodiesterases (PDEs) regulate PKA activation (and protein phosphorylation) by degrading cyclic nucleotide second messengers, including cAMP. Furthermore, they compartmentalize cAMP signals such that selected pools of PKA are activated in response to a given stimulus.[16-21] Protein phosphatases, which can also be found in AKAP complexes,[22] oppose the effects of PKA by reversing phosphorylations.

Although PKA is considered to be the main effector of cAMP, the second messenger can elicit effects that are independent of PKA. For example, cAMP directly regulates hyperpolarization-activated cyclic nucleotide-gated channels[23] and PDEs.[24] Another target (and effector) of cAMP is Epac, a guanine nucleotide exchange protein directly activated by cAMP.[25] Epac is expressed in the heart and the affinity of cAMP for Epac is comparable to the affinity for PKA.[26] Although the cardiac effects of Epac are less well characterized than the effects of PKA, evidence suggests that Epac activity impacts on intracellular calcium, affecting contractility.[27] It has been shown that in adult ventricular myocytes Epac induces calcium release from the sarcoplasmic reticulum (SR) in a signaling pathway that sequentially involves phospholipase Cε, PKCε and calcium/calmodulin kinase (CaMK) II.[28] Epac may also play a role in gene transcription and cardiac hypertrophy and in adult myocytes, where it induces a perinuclear increase in calcium, its sustained activation leads to the nuclear export of histone deacetylase (HDAC) 5.[29]

Some of the responses to β-adrenergic stimuli are mediated by CaMKII,[30] whose activity is at least partly dependent on the frequency and amplitude of calcium signals.[31] For example, CaMKII activity impacts on β-adrenergic regulation of contractility through phosphorylation of calcium-handling proteins, phospholamban (PLB)[32] and the type-2 ryanodine receptor (RyR2)[33] being the best examples. Besides these acute effects, studies have shown that CaMKII activity is responsible for some of the detrimental effects of chronic β_1-AR activation, including apoptosis.[34]

The function of β-ARs is subject to post-translational regulation, primarily by phosphorylation. This is accomplished by GPCR kinases (GRKs, also known as β-AR kinases) and PKA, which phosphorylate the receptors at sites in their intracellular domains.[35] The phosphorylation of β-ARs by GRKs leads to the recruitment of β-arrestins. By binding to the receptors, these impede its interaction with the G protein and thereby avoid the potentially harmful effects of chronic receptor activation.[36] β-Arrestins can induce G protein-independent signaling pathways, which include cytoprotective pathways.[37] β-Arrestin, recruited to β_1-ARs via GRK5/6, can transactivate the extracellular growth factor receptor, for example.[38] This receptor then activates pro-survival signaling pathways involving extracellular signal-regulated kinase (ERK) and Akt, protecting the heart against sustained β_1-ARs stimulation.[38]

Alternative signaling pathways can also occur downstream of β_2-ARs, which additionally couple to $G_{\alpha i}$ (inhibitory) proteins. The consequences of β_2-AR stimulation, including the effects on contractility, are species-dependent and age-dependent and are different in physiological and pathological hearts.[39-41] Whilst the $G_{\alpha i}$ subunit fine-tunes cAMP signals by inhibiting the activity of adenylyl cyclase, its counterpart $G_{\beta\gamma}$ subunit can induce parallel signaling pathways.[40] For example, the anti-apoptotic effects of β_2-AR stimulation arise from activation of phosphoinositide 3-kinase (PI3K) and Akt.[42] The induction of this signaling pathway is believed to protect cardiac myocytes from apoptosis, induced by the parallel $G_{\alpha s}$ pathway downstream of β_1-ARs.[42]

1.2.2 Role in the regulation of excitation-contraction coupling

Amongst the many cardiac proteins phosphorylated by PKA in β-adrenergic signaling are the calcium-handling and myofilament proteins that modulate excitation-contraction coupling (ECC). Phosphorylation of voltage-dependent L-type calcium channels (LTCCs) at S1928 increases the calcium influx upon channel opening[43] and phosphorylation of RyR2 at S2808 increases SR calcium release.[44] Phosphorylation of PLB at S16 enhances SR calcium reuptake by SR calcium ATPase (SERCA2a), promoting relaxation.[45] Phosphorylation of phospholemman (PLM) at S68 stimulates the activity of the sodium/potassium ATPase (NKA) in the sarcolemma. This helps maintain the trans-

sarcolemmal sodium gradient and thereby facilitates the extrusion of calcium via the sodium/calcium exchanger.[46] Phosphorylation of the myofilament proteins troponin I (cTnI) at S23 and S24[47] and myosin binding protein-C (cMyBP-C) at S273, S282 and S302[48] promotes earlier onset of relaxation (by reducing myofilament calcium sensitivity) and force generation (by accelerating actin-myosin cross-bridge cycling). As previously mentioned, CaMKII additionally phosphorylates the RyR2 at S2814 and PLB at T17. Some of the proteins that regulate ECC, PLB being one example, can also be regulated by PKA indirectly, via inhibitor-1 (I-1) of protein phosphatase 1 (PP1). The phosphorylation of I-1 at T35 increases its inhibitory activity towards PP1. By reducing PP1 activity, substrate phosphorylation is amplified.[49]

1.2.3 Role in the regulation of gene and protein expression

The stimulation of β-ARs can induce long-term changes by modulating gene/protein expression. PKA can induce gene expression via cAMP response element binding protein (CREB).[50] PKA phosphorylates the transcription factor at S133 and thereby stimulates the expression of genes that feature a cAMP response element (CRE) in their promoter region.[50] For example, the β_2-AR gene promoter includes a CRE and expression of the β_2-AR increases in response to receptor-mediated increase in cAMP.[51] HDACs, which repress the expression of fetal cardiac genes (and hypertrophy) by inhibiting myocyte enhancer factor 2 (MEF2),[52] are another important class of nuclear proteins regulated in response to β-adrenergic stimulation. Studies suggest that acute stimulation of β-ARs promotes nuclear retention of HDAC4[53] and HDAC5[54] by PKA-dependent cleavage and PKA-mediated phosphorylation, respectively and thereby inhibits MEF2 activity. However, there is also evidence that β-AR stimulation induces HDAC5 nuclear export and MEF2 activation through a phosphorylation-independent manner.[55]

1.2.4 Role in the regulation of metabolism

The stimulation of β-ARs impacts on the activity of metabolic enzymes and thus metabolism, to meet the energy demand of increased contractility. The oxidation of fatty acids provides a major source of energy for contraction in the adult heart under

physiological conditions[56] and acetyl-CoA carboxylase, which regulates fatty acid synthesis, is inhibited by PKA through phosphorylation.[57] Ultimately, by inhibiting the synthetic pathway, the oxidative pathway can proceed. Studies in neonatal cardiac myocytes suggest that β-AR stimulation enhances insulin-induced glucose uptake and regulates the function of the insulin receptor in signaling pathways that involve Akt.[58] Whilst short-term stimulation of β-ARs facilitates glucose uptake, long-term stimulation of the receptors leads to impaired insulin sensitivity.[58]

As described in this section, it is clear that the stimulation of β-ARs impacts on a diverse range of cellular processes, primarily through activation of protein kinases and protein phosphorylation. Although PKA plays a dominant role, the effects of β-AR stimuli can be mediated by other protein kinases (e.g. CaMKII, ERK, Akt and GRK) all of which can phosphorylate target proteins on Ser and Thr residues. Protein phosphatases reverse these phosphorylations and a large proportion of the cardiac Ser/Thr phosphatase activity is derived from PP1 and PP2A.[59-61]

1.3 Regulation of protein phosphorylation at Ser and Thr residues

1.3.1 Kinases versus phosphatases

Protein kinases represent one of the largest eukaryotic gene families. In humans, over 400 kinases are Ser/Thr kinases, the majority of which comprise a catalytic and a regulatory domain encoded by the same gene.[62-64] The number of catalytic subunits for Ser/Thr phosphatases (STPs) is limited to ~30 and thus, STPs were considered non-specific enzymes.[65-67] The catalytic subunit of most STPs does not function as a monomer and functional enzymes comprise a catalytic subunit associated with one or more regulatory subunits.[66] As discussed in more detail in subsequent sections of this general introduction, the diverse range of cellular STPs thus results from the combination of a small number of catalytic subunits with a large number of regulatory subunits.

1.3.2 STP classification

In the initial classification scheme, STPs were classified as either a type-1 (PP1) or type-2 (PP2) phosphatase. PP1 dephosphorylated the β subunit of phosphorylase kinase and was inhibited by I-1 and inhibitor-2 (I-2). PP2 dephosphorylated the α subunit of phosphorylase kinase and its activity was not sensitive to either inhibitor. The PP2 family was divided into subtype 2A, 2B and 2C; PP2B was calcium and calmodulin-dependent and PP2C was magnesium-dependent.[67] This classification has been revised and STPs are now classified into three families.[66] While metal-dependent protein phosphatases and aspartate-based phosphatases represent the smaller families, phosphoprotein phosphatases (PPPs) represent the largest family and include PP2A, which is the focus of this thesis.

The PPP family is divided into seven subfamilies: PP1, PP2A, PP2B (calcineurin), PP4, PP5, PP6 and PP7 (Figure 1.3, panel A). With the exception of PP5, the cellular functions of PPP catalytic subunits are governed by regulatory subunits, which are specific for the individual family members.[65,66] Substrate dephosphorylation by the catalytic core domain,

which is conserved in all family members, is assisted by divalent metal ions (Figure 1.3, panel B).[66] These ions are coordinated by six active site residues and activate a molecule of water, such that it can perform a nucleophilic attack on phosphorous. The phosphate group is removed as an orthophosphate (PO_4^{3-}) group and the hydroxyl side chain on the substrate Ser/Thr residue is restored.[66]

1.4 Structure and regulation of PP2A

1.4.1 Structure of PP2A

PP2A is ubiquitously expressed and in some tissues accounts for up to 1% of the total cellular protein. The enzyme is highly conserved from yeast to humans and exhibits multiple functions in cells.[68,69] PP2A is a tumor suppressor and its dysfunction in cancer is well documented.[70-73] PP2A dysfunction in the brain underlies neurodegenerative diseases, including Alzheimer's.[74,75] Importantly, PP2A is not a single enzyme but comprises a large family of distinct holoenzymes with complex mechanisms of regulation.[69,76,77]

The structure of PP2A and the classification of its subunits are shown in Figure 1.4. PP2A holoenzymes are complexes of three subunits: a 36-kDa catalytic subunit (C subunit), a 65-kDa scaffold subunit (A or PR65 subunit) and a regulatory subunit (B-type subunit) of variable molecular weight.[66,77] The A and C subunits together represent the "PP2A core enzyme" and are encoded by PPP2R1 and PPP2C gene families, respectively. For each subunit two isoforms (α and β) exist. Cα and Cβ comprise 309 amino acids, exhibit 97% sequence homology and are ubiquitously expressed at a ratio of 10:1. Despite the similarity between the two isoforms, Cβ cannot compensate for the absence of Cα and mice lacking the latter isoform die *in utero*.[78-81] Aα and Aβ exhibit ~86% sequence similarity. They are ubiquitously expressed but Aα is more abundant.[82] The A subunit, which comprises 15 Huntington-elongation-A subunit-TOR-like (HEAT) motifs repeated in tandem, mediates the interaction between the C and B-type subunit and facilitates the formation and regulation of the holoenzyme.[83-86] B-type subunits, are classified into four families: B (B55/PR55), B' (B56/PR61), B'' (PR72) and B''' (PR93/PR110).[87] These subunits are discussed in more detail in subsequent sections of this general introduction. Although most cellular PP2As are of the "ABC" type, smaller pools of dimeric structures exist; in these, the C subunit is associated with the α4 protein, which stabilizes the subunit in a latent form during PP2A biogenesis.[87-89]

1.4.2 Regulation of PP2A

1.4.2.1 **Regulation by post-translational modification of the core enzyme**

PP2A C subunits are regulated by covalent post-translational modifications at the C-terminus. Amino acids 304 to 309 constitute the conserved "TPDYFL" motif (T, threonine; P, proline; D, aspartic acid; Y, tyrosine; F, phenylalanine; L, leucine), which is subject to methylation and phosphorylation. Methylation occurs on the free carboxyl group of leucine 309 and is regulated by leucine carboxyl methyltransferase 1 (LCMT-1) and protein phosphatase methyl esterase 1 (PME-1). This modification regulates holoenzyme formation through B-type subunit selection.[90-93] B (B55/PR55) subunits are methylation-sensitive and their association with the core enzyme relies on C subunit methylation. In contrast, B' (B56/PR61), B'' (PR72) and B''' (PR93/PR110) subunits are methylation-insensitive and associate with the core enzyme regardless of methylation.[94,95] C subunit phosphorylation occurs on Y307. *In vitro* p60v-src, p56lck, epidermal growth factor receptor and insulin receptor Tyr kinases phosphorylate this site.[96] The physiological kinase(s), however, are unknown. Phosphorylation on Y307 inactivates PP2A.[96,97] As suggested by studies *in vitro* with phospho-mimetic mutants this modification might also inhibit the recruitment of selected B (B55/PR55) and B' (B56/PR61) subunits.[77,98] Although C subunit methylation and phosphorylation are the best-characterized, other post-translational modifications have been reported. In endothelial cells, nitration of Y307 prevents phosphorylation of the site and increases PP2A activity.[99] Phosphorylation of the A subunit was also recently reported and was proposed to interfere with C subunit binding.[100]

1.4.2.2 **Regulation by endogenous inhibitory proteins**

Endogenous inhibitors of PP2A were purified from bovine kidney cell extracts.[101] By analogy with the PP1 inhibitors, they were named I-1 and I-2 of PP2A (I1-PP2A and I2-PP2A). Their physiological and pathophysiological roles are best-characterized in cancer, where PP2A's tumor suppressor activity is inhibited by the increased expression or altered post-translational modification of these proteins.[102-104] Although the mechanistic

details remain to be elucidated, evidence suggests that I2-PP2A inhibits the enzyme by binding to the C subunit.[74]

1.4.2.3 **Regulation by associated B-type subunits**

B-type subunits are regulatory subunits that determine subcellular targeting and substrate selectivity.[65,105] The classification of B-type subunits is based on primary amino acid sequences, which are conserved only in members of the same family. As shown in Figure 1.4, human B-type subunits are encoded by fifteen genes and the products of these genes are grouped into four families: B (B55/PR55), B' (B56/PR61), B'' (PR72) and B''' (PR93/PR110).[77,87] Each family comprises between three and five isoforms, some of which have alternative splice variants. Thus, B-type subunits represent the most variable PP2A subunit and in human cells at least 96 holoenzymes exist, despite the existence of only two catalytic subunits.[77] The expression of B-type subunits is spatially and temporally regulated[106-108] such that selected holoenzymes can exist in a given cell at a given time. The targeting functions of B-type subunits arise from the presence (or absence) of localization signals. For example B'α, B'β and B'ε contain nuclear export signals that localise PP2A to non-nuclear (cytosolic) compartments. In contrast, B'γ lacks this sequence and targets PP2A to nuclear compartments.[109-111] B-type subunits increase PP2A substrate affinity[112] and structural studies of Bα-PP2A-mediated dephosphorylation of the microtubule-associated tau protein were the first to provide insight on how this might occur.[113] Accordingly, regulatory subunits provide substrate-docking motifs that facilitate the initial binding of the substrate to the holoenzyme.[113] Furthermore, B-type subunits fine-tune PP2A catalytic activity and post-translational modifications of selected subunits can enhance or inhibit such activity.[114,115]

Human B' subunits, henceforth referred to as B56 subunits, were first described in the 1990s and form the primary focus of this project.[108,116-118] As shown in Figure 1.5, these subunits are encoded by five genes (*PPP2R5A*, *PPP2R5B*, *PPP2R5C*, *PPP2R5D* and *PPP2R5E*), which localize to chromosome regions 1q41, 11q12, 3p21, 6p21.1, and 7p11.2-p12, respectively.[117] B56 family members include α, β, γ, δ and ε isoforms and splice

variants of γ and δ result from alternative gene splicing. With nine isoforms, the B56 family thus represents the largest family of B-type subunits.

1.4.2.3.1 *Structure, expression and distribution of B56 subunits*

The first crystal structure of a B56-containing PP2A holoenzyme (B56γ_1-PP2A) was published in 2006.[84] This structure provided insight on holoenzyme formation and on the function of the B-type subunit. A surface representation of the crystallized holoenzyme is shown in Figure 1.6. The A subunit adopts a horseshoe-shaped conformation and interacts with the C and B-type subunits. The B-type subunit, which shields a part of the C subunit, displays a superhelical structure that comprises 18 α helices, divided into 8 HEAT motifs. These are indicated in Figure 1.7. Residues within HEAT2, HEAT4 and HEAT5 interact with the A subunit and residues within HEAT2, HEAT5, HEAT6, HEAT7 and HEAT8 interact with the C subunit.[84] As also shown in Figure 1.7, most residues are conserved in B56α, -β, -δ and -ε isoforms, suggesting a common mode of subunit interaction with the core enzyme. In the crystalized holoenzyme, a concave region on the B56 subunit is unoccupied; this region comprises acidic residues and likely serves as a substrate docking region.[84] These structural studies indicate that regulatory subunits modify PP2A substrate selectivity by altering the environment around the catalytic site and by providing contact regions for substrate recruitment (Figure 1.8).[84] Whilst the central (core) domain of B56 subunits is conserved between the family members, sequences at the N-terminus and C-terminus are different and determine isoform-specific functions. As an example, in cardiac cells B56α localises to the sarcomeric M-line.[119] This distribution is determined by a physical interaction with ankyrin-B and is mediated by 13 amino acids present only at the C-terminus of B56α.[119] The expression of B56 subunits is tissue-specific and at messenger RNA (mRNA) level B56α and B56γ are most abundant in skeletal and cardiac muscle. In contrast, B56β and B56δ are highly expressed in the brain.[108,116,118,120]

1.4.2.3.2 *Post-translational modification of B56 subunits*

With the exception of B56γ_1, B56 proteins are phosphoproteins[110] and cellular PP2A function can be further regulated by external stimuli, through B56 subunit phosphorylation. As exemplified in this section, phosphorylation can alter the abundance,

substrate affinity, activity and localization of holoenzymes. The precise consequences of the modification depend on the isoform, the site of phosphorylation and cell type. The phosphorylation of B56γ_3 at S510, mediated by ataxia telangiectasia mutated kinase in response to DNA damage, enhances the stability of the isoform.[121] This leads to increased abundance of B56γ_3-PP2A complexes and furthermore, increases the affinity of this holoenzyme for its substrate p53.[121] PKA and PKC, activated in distinct signaling pathways, phosphorylate B56δ at S573[114,122] and this phosphorylation stimulates the activity of the associated catalytic subunit. In contrast, the phosphorylation of the same isoform at S37 by checkpoint kinase 1 promotes association of the subunit with the PP2A core enzyme.[123] The phosphorylation of B56α at S41 by PKC inhibits the activity of the associated catalytic subunit.[115] In contrast, its phosphorylation at S28 by protein kinase R promotes translocation of the holoenzyme from the nucleus to mitochondria.[124] Although most studies decribe phosphoregulation of B56 isoforms, a recent publication indicates that redox regulation can also occur. Accordingly, in an oxidative intracellular milieu B56δ is nitrated at Y289 and this interferes with formation of B56δ-PP2A.[125] The cellular mechanisms of PP2A regulation are summarised in Figure 1.9.

1.5 PP2A holoenzymes in the heart

A common approach taken to study the functions of PP2A in cells/tissues entails the use of naturally occurring cell-permeant phosphatase inhibitors. The most widely used of these is okadaic acid (OA), a small molecule toxin produced by marine organisms.[126] OA selectively inhibits PP2A at lower concentrations (IC_{50} 0.1-0.3 nM) and additionally inhibits PP1 at higher concentrations (IC_{50} 15-50 nM).[126] PP2B is relatively insensitive to this inhibitor (IC_{50} 4μM).[126] In cells, PP2A activity is thus the phosphatase activity that is inhibited by the lower concentration of OA and PP1 activity is comprised in the phosphatase activity inhibited by the inhibitor at a higher concentration. Notwithstanding the unintentional inhibition of PP1 that may occur in the cellular environment, most of the cardiac roles of PP2A have been inferred from studies with OA.

1.5.1 PP2A in cardiac physiology

1.5.1.1 **Role in the regulation of ECC**

The first indication that protein phosphatases impact on cardiac ECC was provided by Neumann *et al*.[59] OA mimicked the effects of β-AR stimulation, increasing the force of contraction and the rate of relaxation, by inhibiting PP1 and PP2A[59] and PP2A has since been implicated in dephosphorylation of several proteins that regulate ECC. De Arcangelis *et al*. showed that PP2A activity was increased in isolated myocytes subjected to acute β-AR stimulation with ISO.[127] This increase in activity reduced PKA-mediated phosphorylation of cTnI and PLB and was attenuated by the presence of PKI, a compound that inhibits PKA.[127] It was thus proposed that in β-adrenergic signaling, the increase in PP2A activity represents a negative feedback system that regulates the phosphorylation of PKA targets.[127] Further evidence for a role of PP2A in the regulation of ECC has come from studies of the LTCC. PP2A was detected in immunoprecipitates of rat brain LTCCs and was found to be constitutively associated with the channel's α_1 subunit.[128] In functional assays with the isolated channel complex, PP2A dephosphorylated the α_1 subunit at the PKA site.[128,129] Studies of cardiac LTCCs showed that PP2A binds two motifs at the C-terminus of the α_1 subunit and that the basal and ISO-induced inward calcium currents is increased

when PP2A is displaced from these sites.[130] Therefore, these studies suggest that PP2A regulates the activity of LTCCs under basal condition and in response to β-adrenergic stimulation. Marx *et al*. detected PP2A in RyR2 macromolecular complexes together with PP1, PKA and the its regulatory RII subunit, and muscle-specific AKAP (mAKAP).[131] In these studies, the functional role of PP2A was not reported and the possibility that PP2A regulates RyR2 phosphorylation (at the PKA or CaMKII sites) remains to be established.

1.5.1.2 **Role in the antiadrenergic effects of adenosine and acetylcholine**

Adenosine is derived from adenosine triphosphate (ATP) and is generated in the extracellular environment, where it activates purinergic receptors.[132] The stimulatory effects of catecholamines on the heart are opposed by adenosine, primarily via activation of adenosine A1 receptors.[132] Gupta *et al*. showed that ISO-induced phosphorylation of PLB was reduced in isolated myocytes co-stimulated with N^6-phenylisopropyladenosine, an agonist at adenosine A1 receptors.[133] Although adenosine A1 receptors are $G_{\alpha i}$ GPCRs, this response was independent of changes in cAMP and therefore, it was proposed that adenosine A1 receptor stimulation induces dephosphorylation of PLB by activating protein phosphatases.[133] Liu and Hofmann studied the anti-adrenergic effects of adenosine further, in rat myocardial preparations.[134] In isolated hearts, the adenosine A1 receptor agonist N^6-cyclopentyladenosine (CPA) attenuated the positive inotropic effect of ISO and this effect was abrogated by PP2A inhibition.[134] Similarly, in isolated myocytes CPA reduced the basal and ISO-induced phosphorylation of PLB and cTnI, and this effect was also dependent on the activity of PP2A.[134] Acetylcholine, which stimulates muscarinic M2 receptors ($G_{\alpha i}$ GPCRs), also exhibits anti-adrenergic effects and evidence suggests that activation of PP2A downstream of the receptors is responsible for this.[135,136]

1.5.1.3 **Role in β-AR resensitization**

Vasudevan *et al*. showed that PP2A activity is critical for resensitization of cardiac β-ARs.[137] PI3Kγ inhibits the resensitization of the receptors by regulating their dephosphorylation at the cell membrane.[137] This results from the inhibition of PP2A activity at the receptor complex and relies on PI3Kγ-mediated phosphorylation of the PP2A inhibitory protein (I2-PP2A) at S9 and S93.[137]

1.5.1.4 **Role of association with Pak1**

An emerging concept in cardiac PP2A signaling is the holoenzyme's association with p21-activated kinase 1 (Pak1). Pak1 is a Ser/Thr kinase activated by Rho GTPases Cdc42 and Rac1.[138] PP2A and Pak1 form signaling complexes in the brain[139] and studies in isolated myocytes suggested that these complexes exist in the heart.[140] In isolated myocytes, adenoviral expression of constitutively active Pak1 caused a reduced myofilament protein phosphorylation.[140] Furthermore, it was associated with reduced PP2A C subunit Y307 phosphorylation, suggesting that PP2A activity was increased in these cells.[140] Sheehan *et al*. proposed a signaling scheme in which cardiac PP2A is associated with Pak1 and is activated by Cdc42/Rac1 downstream of $G_{\alpha i}$ GPCRs.[141] It was proposed that this mode of PP2A activation might regulate the phosphorylation of PKA substrates in response to sympathetic stimulation.[141]

1.5.2 PP2A in cardiac pathophysiology

1.5.2.1 **Role in cardiac hypertrophy and failure**

Heart failure (HF) is a progressive disease. It is the end point of a wide range of cardiovascular disorders and is a leading cause of morbidity and mortality.[142] The cause of HF may be abrupt (e.g. myocardial infarction), gradual (e.g. hypertension) or hereditary (e.g. familial hypertrophic cardiomyopathy); in all cases the heart deteriorates to a point at which it can no longer sustain the needs of the peripheral organs.[143] Insults to the heart can induce pathological hypertrophy and adverse remodeling, which correlate with increased expression of the fetal cardiac genes and decreased expression of the adult cardiac genes.[144] In the early stages of heart disease the body initiates adaptive responses (e.g. neurohormonal activation) to restore the cardiac output.[145] Nevertheless, over time these persistent alterations cause further damage to the heart and hasten its demise.[145]

An increasing body of evidence indicates that PP2A expression and activity is altered in a diverse range of human and animal models of heart disease. For example, Boknik *et al*. proposed that in settings of pathological hypertrophy and HF, contractile dysfunction is caused by the reduced phosphorylation of proteins that regulate ECC through the

increased activity of protein phosphatases.[146] This was suggested on the basis of studies in a rat model of hypertrophy induced by long-term stimulation of β-ARs.[146] In this model, left ventricular (LV) dysfunction was associated with reduced phosphorylation of PLB at S16 and T17, and increased activity of PP1 and PP2A.[146]

Increased activity of cardiac PP2A was also reported in a mouse model of alveolar hypoxia with associated cardiac diastolic dysfunction.[147] In mice, the diastolic dysfunction was attributed to the reduced phosphorylation of PLB at S16, through the increased expression of PP2A induced by increased levels of circulating interleukin-18.[147] This was supported by observations (in isolated cardiac cells) that this inflammatory cytokine induced an increase in the expression of PP2A and a parallel decrease in the phosphorylation of PLB.[147]

PP2A has been implicated in dephosphorylation of gap junctions in human and experimental models of HF.[148] Gap junctions are channels that allow the exchange of metabolites and ions between cells and are formed from connexin (Cx) proteins. Cx43 is expressed in the heart and reduced Cx43 phosphorylation promotes arrhythmias by altering the electrical coupling of the cells.[149] Ai *et al*. showed that the phosphorylation of Cx43 was reduced in LV tissue of failing human and rabbit hearts.[148] They showed that PP2A activity was increased and furthermore, that in ventricular cells isolated from arrhythmogenic failing rabbit hearts its colocalization with Cx43 was increased.[148] In further studies, it was shown that Pak1 and PP2A are comprised in macromolecular complexes of Cx43.[150] Ai *et al*. reported that Pak1 activity was increased in failing human and rabbit hearts and attributed the reduced phosphorylation of Cx43 to complexes of Pak1-PP2A.[148,150] Related to this, studies in a feline model of right ventricular pressure overload-induced hypertrophy indicate that increased Pak1-PP2A signaling contributes to the adverse remodeling of the cytoskeleton.[151] In this model, Pak1-PP2A signaling was increased in a manner that was dependent on activation of β_1-ARs.[151] The increase in Pak1-associated PP2A activity caused dephosphorylation of microtubule-associated protein (MAP) 4 and thereby caused an increase in microtubule density.[151]

Decreased cardiac PP2A expression and activity was reported in a mouse model of sepsis.[152] Sepsis is a systemic inflammatory response to an infection[153] and cardiac depression is a frequent complication in this condition.[154] In this context, the isolated cardiac myocytes of septic rats and mice exhibit an impaired contractility through the sustained phosphorylation of cTnI (S23/24) and increased myofilament calcium sensitivity.[152,155] As suggested by studies in mice, increased cTnI phosphorylation is the consequence of the reduced expression and activity selected PP2A holoenzymes (i.e. B56α-PP2A).[152]

As described in an earlier section of this general introduction, class II HDACs prevent the onset of hypertrophy by repressing MEF2 in the nucleus.[52] Hypertrophic stimuli induce nuclear export of class II HDAC, resulting in increased transcription of MEF2 genes.[52] Studies in transgenic mice with increased cardiac expression of casein kinase-2 interacting protein-1 (CKIP-1) suggest that PP2A represses hypertrophy and the proposed signaling pathway involves dephosphorylation of HDAC4 at S246 by CKIP-1-recruited PP2A.[156]

The aforementioned studies show that the expression and the activity of PP2A is altered in multiple settings of heart disease and that these alterations correlate with changes in protein phosphorylation and cardiac dysfunction. However, they do not show that changes in PP2A expression and activity *cause* heart dysfunction. In this context, the importance of cardiac PP2A is underscored by the phenotype of transgenic mice. Cardiac-specific overexpression of the catalytic subunit (α isoform) induced hypertrophy and dilatation of the myocardium, tissue necrosis and fibrosis, and a depressed contractility.[157] As one might expect, the transgenic hearts exhibited reduced phosphorylation of proteins, including PLB (S16 and T17), cTnI and eukaryotic elongation factor 2 (eEF2).[157] The phosphorylation sites of the latter proteins were not reported. It was suggested that reduced phosphorylation of eEF2 might underlie cardiac hypertrophy through increased mRNA translation and protein synthesis.[157] Cardiac-specific over-expression of CaMKIIδ_B in mice is paralleled by increased expression and activity of PP2A and interestingly, these mice also develop hypertrophy and exhibit a diminished phosphorylation of PLB at S16 and T17.[158]

Transgenic mice with muscle-specific expression of a mutant PP2A scaffold subunit (AΔ5) have also been studied.[159] The mice expressed a dominant negative mutant of the human protein lacking HEAT5, hence AΔ5.[159] This mutated subunit, which binds the C subunit but not the B-type subunit, caused a form of dilated cardiomyopathy.[159] The expression of AΔ5 was associated with an increase in the core enzyme-to-holoenzyme ratio and, albeit by unknown mechanisms, induced an increase in heart weight-to-body weight ratio at birth.[159] The chambers of the heart were enlarged, their walls were thinner and the systolic function was impaired.[159]

1.5.2.2 **Role in ischaemia/reperfusion-induced injury**

Liu and Hofmann reported a role for PP2A in oxidative stress-induced apoptosis.[160] p38 mitogen-activated protein kinase (MAPK) and ERK signal in opposing pathways and whilst p38 MAPK is pro-apoptotic, ERK is anti-apoptotic.[161] Studies in isolated cardiac cells show that reactive oxygen species activate p38 MAPK and ERK simultaneously, and suggest that during oxidative stress p38 MAPK attenuates ERK phosphorylation (and activation) by stimulating PP2A activity.[160] The underlying mechanism for this response was not defined.

Snabaitis *et al*. showed that PP2A regulates NHE1 activity downstream of adenosine A1 receptors.[162] NHE1 is a sodium and hydrogen exchanger that regulates intracellular pH and its activity is increased by phosphorylation.[163] In isolated myocytes, phenylephrine induces p90 ribosomal S6 kinase-mediated phosphorylation of NHE1 and this is inhibited by co-stimulation with CPA.[162] Snabaitis *et al*. showed that CPA caused the accumulation of PP2A at the cell membrane and that PP2A activity was necessary for the inhibitory effect of CPA on phenylephrine-induced NHE1 phosphorylation and activation.[162] Therefore, in the context of adenosine A1 receptor stimulation during ischemia and reperfusion, this study suggests a cardio-protective role for PP2A.

1.5.3 Cardiac roles of specific B-type subunits

The importance of PP2A targeting in the heart is highlighted by the cardiac phenotype (dilated cardiomyopathy) of transgenic mice expressing AΔ5, which binds the C subunit but not the B-type subunit.[159] Knowledge of the *in vivo* functions of distinct B-type

subunits is limited by the scarcity of appropriate mouse models and the first report on the consequences of knocking out an individual B-type subunit (B56δ) in mice appeared only in 2011.[120] Thus, much of the relevant information to date has been obtained from studies in isolated cardiac myocytes or inferred from studies in immortalized cell lines.

1.5.3.1 **B56 subunits**

1.5.3.1.1 ***B56α***

Ankyrin proteins organize, transport and anchor membrane proteins to the cytoskeleton[164] and ankyrin-B has been implicated in the targeting of B56α.[119] In mouse ventricular myocytes, B56α is localized at the M-line and a smaller population is localized at the Z-disk.[119] This distribution is governed by the interaction with ankyrin-B and results from an ankyrin-binding motif at the C-terminus of the regulatory subunit.[119] The sequence of 14 amino acids is conserved in human, mouse and rat isoforms and does not exist in other B56 family members, suggesting that only B56α binds ankyrin-B.[119] The critical role of this adaptor protein in the targeting of B56α is highlighted by the near-complete loss of its M-line localization in cardiac myocytes of ankyrin-B-null mice.[119] Nevertheless, a minor population of B56α localizes in a manner that is not dependent on the presence of ankyrin-B.[119] In related studies it was determined that ankyrin-B and PP2A are localized at the M-line by obscurin.[165] The targets of ankyrin-B-targeted PP2A were not reported in either study.

Studies in our laboratory showed that in isolated ARVM, ISO altered the subcellular distribution of B56α.[166] This was initially revealed by proteomics analysis of the cardiac myofilament subproteome and was confirmed by immunofluorescence studies of B56α in isolated "skinned" cardiac cells.[166] B56α localized at the Z-disc and M-line in unstimulated cells and was lost from both regions following β-AR stimulation.[166] Overall, these studies suggested the intriguing possibility that dynamic changes in PP2A targeting regulate protein phosphorylation in response β-AR stimulation.

MicroRNAs are molecules of ~20 nucleotides that regulate gene expression.[167] MicroRNAs inhibit mRNA translation or promote mRNA degradation, by annealing with the target

mRNA.[167] MiR-1, a muscle-specific microRNA, is up-regulated in HF[168] and the functional role of this micro-RNA was explored in isolated ARVM with heterologous expression of miR-1.[169] In these cells, the amplitude of the inward calcium current and the frequency of spontaneous SR calcium release were increased.[169] Respectively, these effects were caused by increased phosphorylation of LTCCs (site not reported) and increased phosphorylation of RyR2s (S2814).[169] These alterations resulted from the reduced expression of B56α through translational inhibition of the mRNA transcript.[169] At the molecular level this was explained by the presence of a seed sequence in the 3'-untranslated region (UTR) of the B56α mRNA transcript, which is complementary to miR-1.[169] Therefore, miR-1 altered calcium signaling in the isolated cells by down-regulating a population of PP2A holoenzymes, i.e. B56α-PP2A.

The stress-induced cardiac hypertrophy and remodeling in HF is partly mediated by MAPK signaling.[170] Stress-induced changes in PP2A gene expression were studied in isolated cardiac cells with sustained activation of stress-activated c-Jun N-terminal kinase.[171] In these cells, the abundance of B56α protein was reduced through a reduction in the stability of the mRNA transcript and this was attributed to the presence of AU-rich elements (AREs) in the 3'-UTR.[171] AREs are targeted by ARE/poly(U)-binding/degradation factor 1 (which is up-regulated in this cell model of cardiac stress) and thereby contribute to mRNA instability.[171] Although there is no evidence that this is the case, such stress-induced reduction in B56α mRNA stability might explain the loss of cardiac B56α protein in septic mice, described in section 1.5.2.1.

Increased cardiac expression of B56α in mice results in a parallel increase in PP2A activity and altered phosphorylation of proteins that regulate ECC.[172] The transgenic hearts exhibited reduced basal phosphorylation of cTnI (S23/24) and cMyBP-C (S282) and increased basal LV contractility.[172] Nevertheless, the response to ISO stimulation was impaired by reduced phosphorylation of PLB at S16. Consistent with a role for PP2A in regulating the phosphorylation of cTnI, increased phosphorylation of this myofilament protein in the hearts of mice with endotoxemia-induced sepsis was associated with a loss of B56α-PP2A.[152]

1.5.3.1.2 *B56γ*

Gigena *et al*. studied the subcellular distribution of B56γ_1 in isolated rat ventricular myocytes with heterologous expression of hemagglutinin (HA)-tagged B56γ_1. Confocal images of the cells showed that HA-B56γ_1 was primarily localized in the nucleus and that it was concentrated in nuclear speckles, which are rich in transcription factors and splicing factors.[111] In contrast, HA-B56α was found in non-nuclear regions and localized in the myofilaments.[111] In related studies, Zhou *et al*. used an affinity-based proteomic strategy to identify the cardiac binding partners of B56γ_1.[173] This method relied on using glutathione S-transferase (GST)-tagged B56γ_1 to extract B56γ_1-PP2A binding partners from homogenates of mouse heart tissue.[173] ~30 putative binding partners, including SERCA2a, were identified in the analysis and the results were supplemented by functional studies in ARVM expressing HA-B56γ_1.[173] Over-expression of B56γ_1 was associated with reduced phosphorylation of the pre-mRNA splicing factor ASF/SF2 and reduced phosphorylation of PLB at S16.[173] ASF/SF2 has been implicated in mRNA splicing activity in hypertrophic cardiac growth and HF[174,175] but the potential involvement of B56γ_1 in this setting was not described. The functional studies were focused on ECC; over-expression of B56γ_1 caused a reduction in the peak twitch contraction under basal conditions, but did not affect ISO-induced contractility.[173]

Recent studies in B56γ-null mice indicate that B56γ-PP2A activity is necessary in heart development such that the absence of B56γ causes the incomplete formation of the intraventricular septum.[176]

1.5.3.1.3 *B56δ*

Studies performed in mouse brain cells showed that B56δ is phosphorylated by PKA at S573 and that this results in increased activity of PP2A.[114] A potential relevance of this to cardiac cells was suggested by studies with heterologous expression of proteins in human embryonic kidney 293 (HEK293) cells.[177] Dodge-Kafka *et al*. proposed a scheme in which PKA and PP2A (tethered by mAKAP) form a signaling complex that regulates the activity of PDE type 4 isoform D3 (PDE4D3) and degradation of cAMP.[177] In the proposed scheme, cAMP-activated PKA phosphorylates PDE4D3 at S54, stimulating the cAMP degradation.

Simultaneously, PKA phosphorylates B56δ at S573, stimulating PP2A activity. PP2A then attenuates PDE4D3 activation and cAMP degradation by dephosphorylating S54.[177] Although mice with global deletion of B56δ exist,[120] the cardiac phenotype of these mice was not reported and the specific cardiac roles of this regulatory subunit are unknown.

1.5.3.2 **B'' (PR130) subunits**

Leucine/isoleucine zippers (LIZs) are coiled repeats of leucine and isoleucine residues present in RyR2s, which interact with LIZs in the adaptor (or targeting) subunits of PKA, PP1 and PP2A.[178] B'' subunits contain two calcium-binding sites formed by small helix-loop-helix motifs, known as EF hands.[179] PR130 is expressed in the heart and was proposed to target PP2A to RyR2, on the basis of GST pull-down assays *in vitro* with GST-RyR2 and canine ventricular SR membrane preparations.[178] The phosphorylation of RyR2 is increased at the PKA site in human HF and this hyperphosphorylation causes defects in channel function.[180] Furthermore, when compared to control hearts, the association of PP1 and PP2A with RyR2 appears reduced in HF.[180] At present, however, it is not known whether PR130-PP2A regulates the phosphorylation of RyR2 in physiological conditions or indeed in pathophysiological conditions.

1.6 Project objectives

The targeting of PP2A, its substrate specificity and its catalytic activity are regulated by B-type subunits.[66] While studies in transgenic mice with cardiac-specific over-expression of the PP2A catalytic subunit suggest that dysregulated PP2A activity is detrimental for the heart, the specific importance of B-type subunits in the regulation of cardiac PP2A is highlighted by the phenotye of transgenic mice with muscle-specific expression of AΔ5, which is defective in binding to these subunits.[159] Our understanding of the cardiac roles and regulation of individual B-type subunits is limited and an improved understanding may facilitate the targeted modulation of cardiac PP2A holoenzymes for therapeutic benefit. Towards this objective, the following specific aims were addressed in this project:

- Determine the expression of PP2A regulatory B56 subunits in ARVM.
- Determine the basal subcellular distribution of B56 subunits in ARVM and investigate potential changes in this distribution in response to β-AR stimulation.
- Determine whether B56δ is phosphorylated in ARVM exposed to the β-AR agonist ISO.
- Characterize the signaling pathway that underlies ISO-induced phosphorylation of B56δ.
- Investigate the role of B56δ phosphorylation in β-AR-mediated regulation of cardiac protein phosphorylation and PP2A activity.

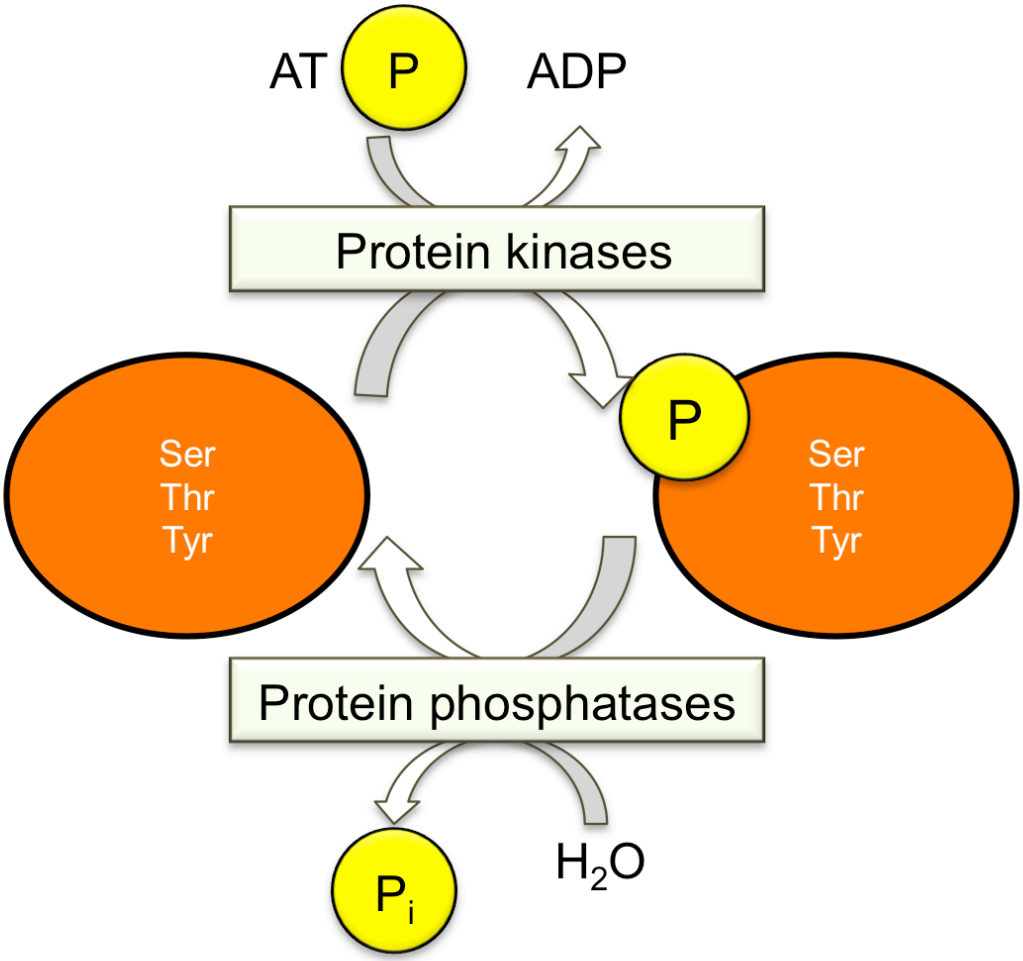

Figure 1.1 Protein phosphorylation and dephosphorylation

Protein kinases phosphorylate proteins by transferring the terminal phosphate group in ATP to Ser, Thr and Tyr residues. The phosphate group is removed by protein phosphatases through hydrolysis.

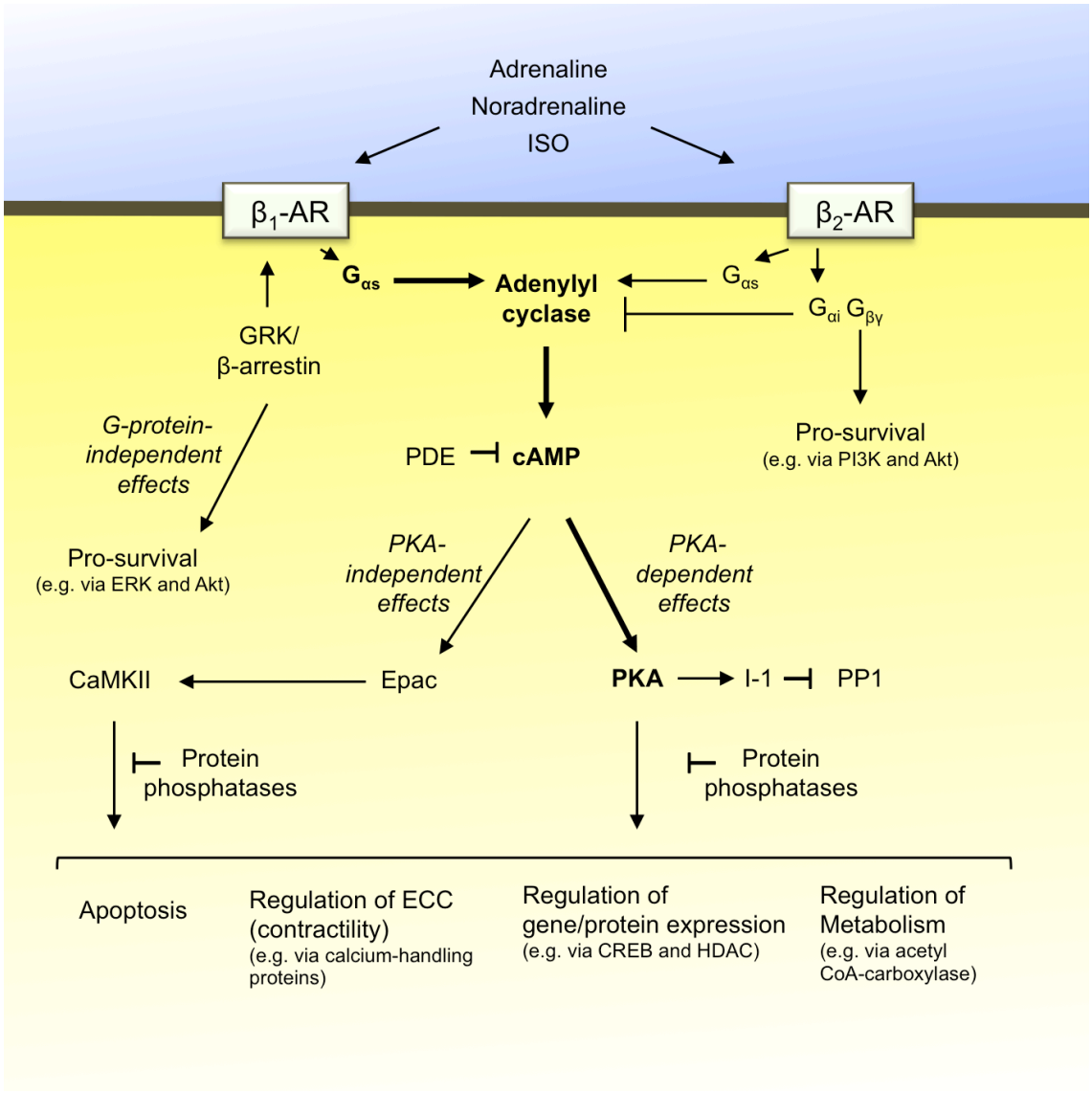

Figure 1.2 Cardiac β-adrenergic signaling

The cardiac effects of β-adrenergic stimuli are mediated by β_1- and β_2-ARs. Several signaling pathways can be activated downstream of the receptors and of these, the cAMP and PKA signaling pathway predominates. This signaling pathway is indicated by bold arrows.

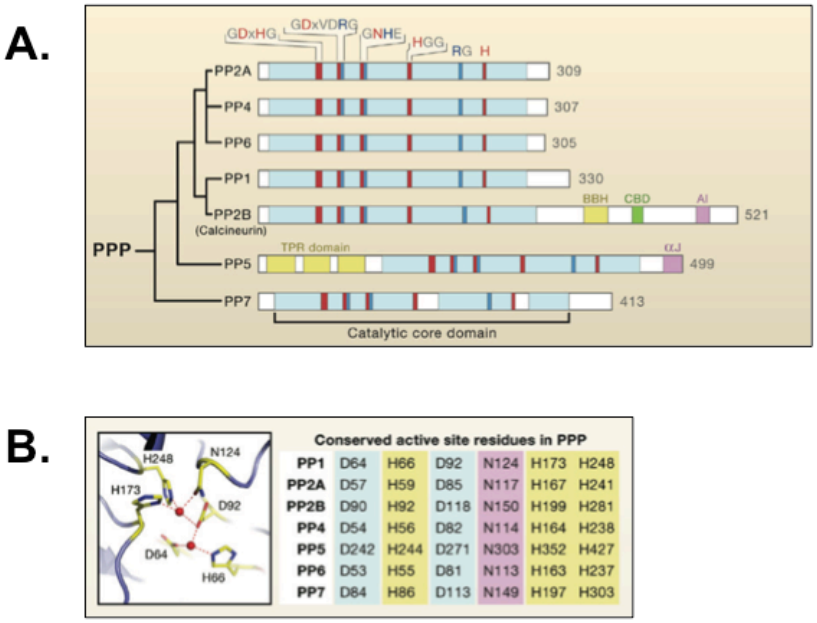

Figure 1.3 Structure and catalytic mechanism of PPPs

A. The PPP family includes seven sub-families with a conserved catalytic core domain. Residues that coordinate the metal ions are coloured in red. Residues that contribute to phosphate binding are coloured in blue. **B**. The catalytic site of PPPs contains six conserved residues that coordinate two divalent metal ions (red circles). The metal-binding scheme of PP1 is shown on the left and the corresponding residues in PP2A, PP2B, PP4, PP5, PP6 and PP7 are shown on the right. (G, glycine; D, aspartic acid; x, any amino acid; H, histidine; V, valine; R, arginine; N, asparagine; E, glutamic acid). Figures taken from Shi.[66]

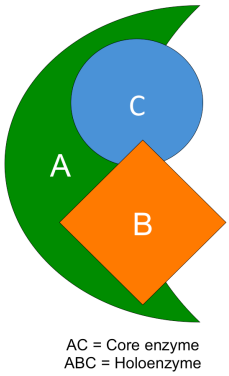

SUBUNIT FAMILY	GENE	ISOFORM	ALTERNATIVE NAMES
A	*PPP2R1A*	Aα	$PP2A_{Aα}$
	PPP2R1B	Aβ	$PP2A_{Aβ}$
C	*PPP2CA*	Cα	$PP2A_{Cα}$
	PPP2CB	Cβ	$PP2A_{Cβ}$
B (B55/PR55)	*PPP2R2A*	Bα	PR55α, B55α
	PPP2R2B	Bβ	PR55β, B55β
	PPP2R2C	Bγ	PR55γ, B55γ
	PPP2R2D	Bδ	PR55δ, B55δ
B'(B56/PR61)	*PPP2R5A*	B'α	PR61α, B56α
	PPP2R5B	B'β	PR61β, B56β
	PPP2R5C	B'γ (3)	PR61γ, B56γ
	PPP2R5D	B'δ (3)	PR61δ, B56δ
	PPP2R5E	B'ε	PR61ε, B56ε
B'' (PR72)	*PPP2R3A*	B''α (2)	PR130, PR72
	PPP2R3B	B''β	PR70, PR48
	PPP2R3C	B''γ	G5PR
B''' (PR93/PR110)	*STRN*	Striatin	
	STRN3	Striatin-3	
	STRN4	Striatin-4	

Figure 1.4 PP2A structure and subunit classification

The structure of PP2A is shown on the left. The holoenzyme comprises a scaffold A subunit, a catalytic C subunit and a regulatory B-type subunit. A and C represent the core enzyme. A, B and C represent the holoenzyme. The classification of PP2A subunits is shown on the right. The A and C subunits are each transcribed from two genes. B-type subunits are classified into B, B', B'' and B''' families. Alternative family names are shown in brackets. Each family comprises multiple isoforms transcribed from separate genes. Numbers in brackets indicate splice variants. Alternative subunit names are shown. Table adapted from Janssens et al.[77]

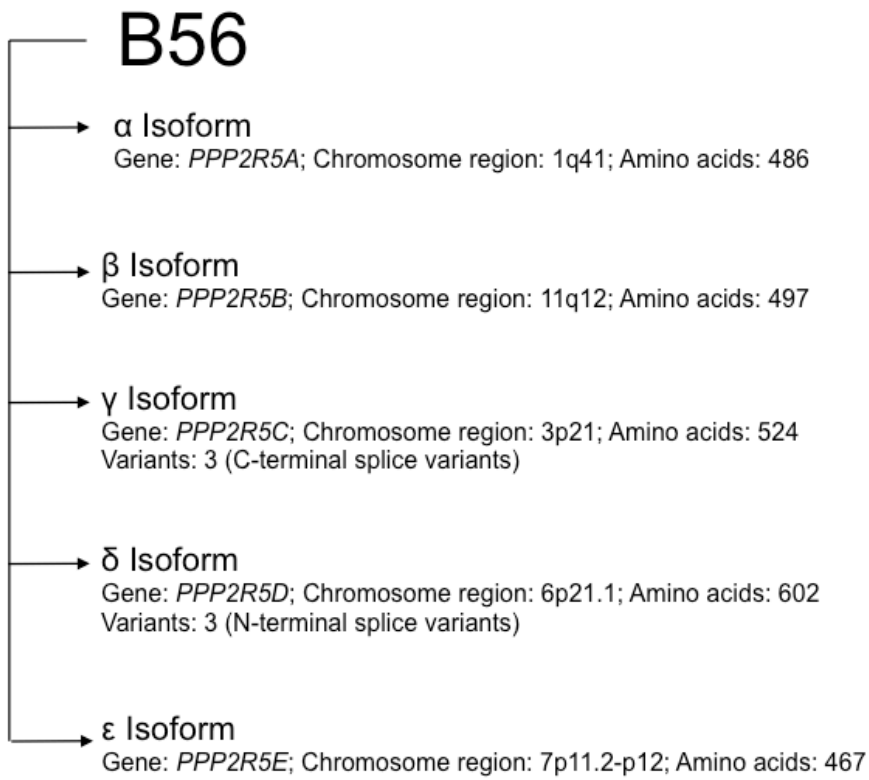

Figure 1.5 Human B56 subunits

Human B56 isoforms include α, β, γ, δ and ε isoforms. The isoforms are encoded by separate genes, which localise to distinct chromosome regions. Splice variants exist for γ and δ isoforms. For these, the length of the longest splice variant is shown.

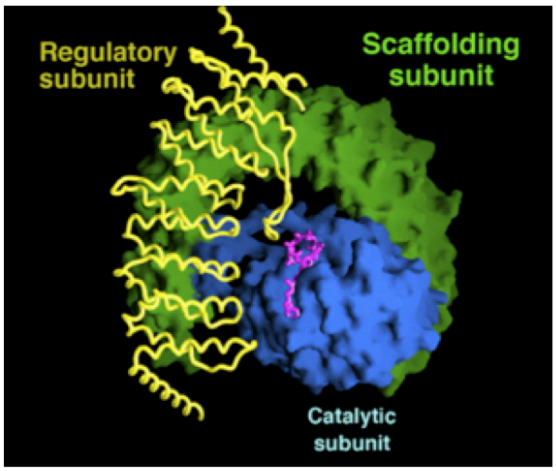

Figure 1.6 Surface representation of the PP2A holoenzyme

The scaffold (Aα), catalytic (Cα) and regulatory ($B56\gamma_1$) subunits are shown in green, blue and yellow, respectively. Microcystin-LR is shown in magenta. Figure taken from Xu *et al*.[84]

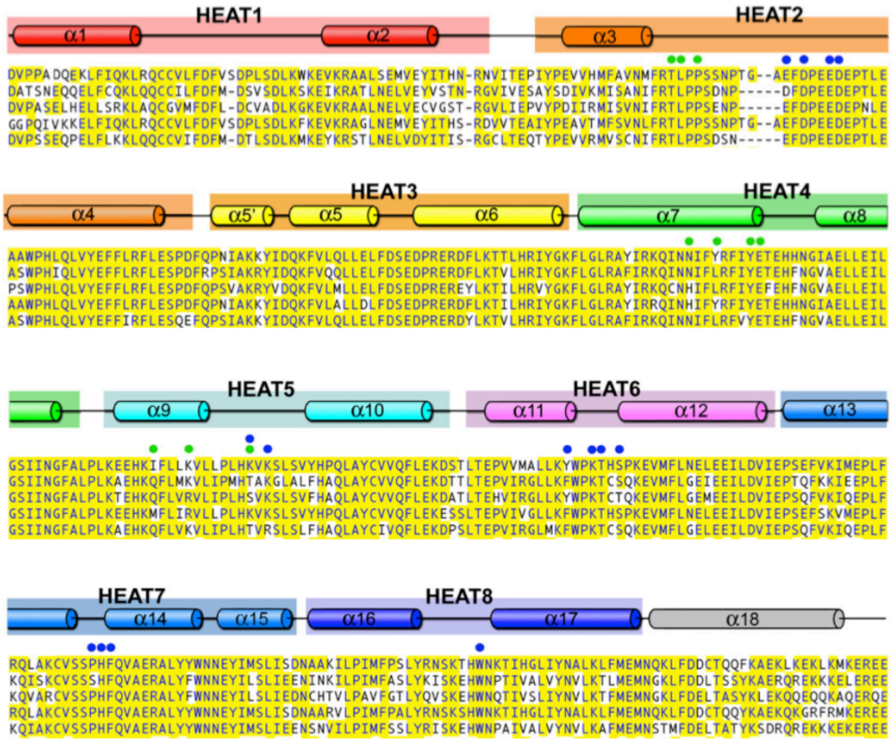

Figure 1.7 The B56 core domain

Sequence alignment of B56 isoforms. Secondary structural elements are indicated above the sequences. Sequences are listed in the order: γ_1, α, β, δ and ε. HEAT repeats are represented by different colour. Conserved residues are highlighted in yellow. Residues that interact with Aα and Cα subunits are indicated by green and blue circles, respectively. Note that these sequences are not the full sequence and include only the subunit's central (core) domain. Figure taken from Xu *et al*.[84]

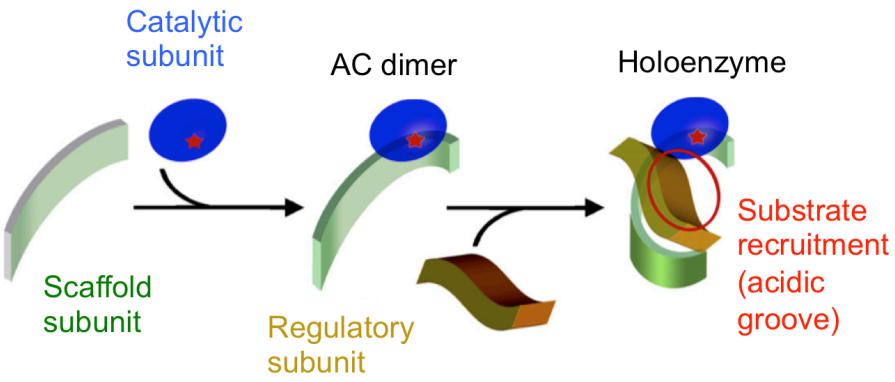

Figure 1.8 Structure-based model for PP2A assembly and regulation

The first step in holoenzyme assembly is the association of the free scaffold subunit with the catalytic subunit. The AC dimer then associates with a regulatory B56 subunit to form the holoenzyme. The B56 subunit recruits substrate proteins using its acidic, concave groove. The red star denotes the catalytic active site. Figure taken from Xu *et al*.[84]

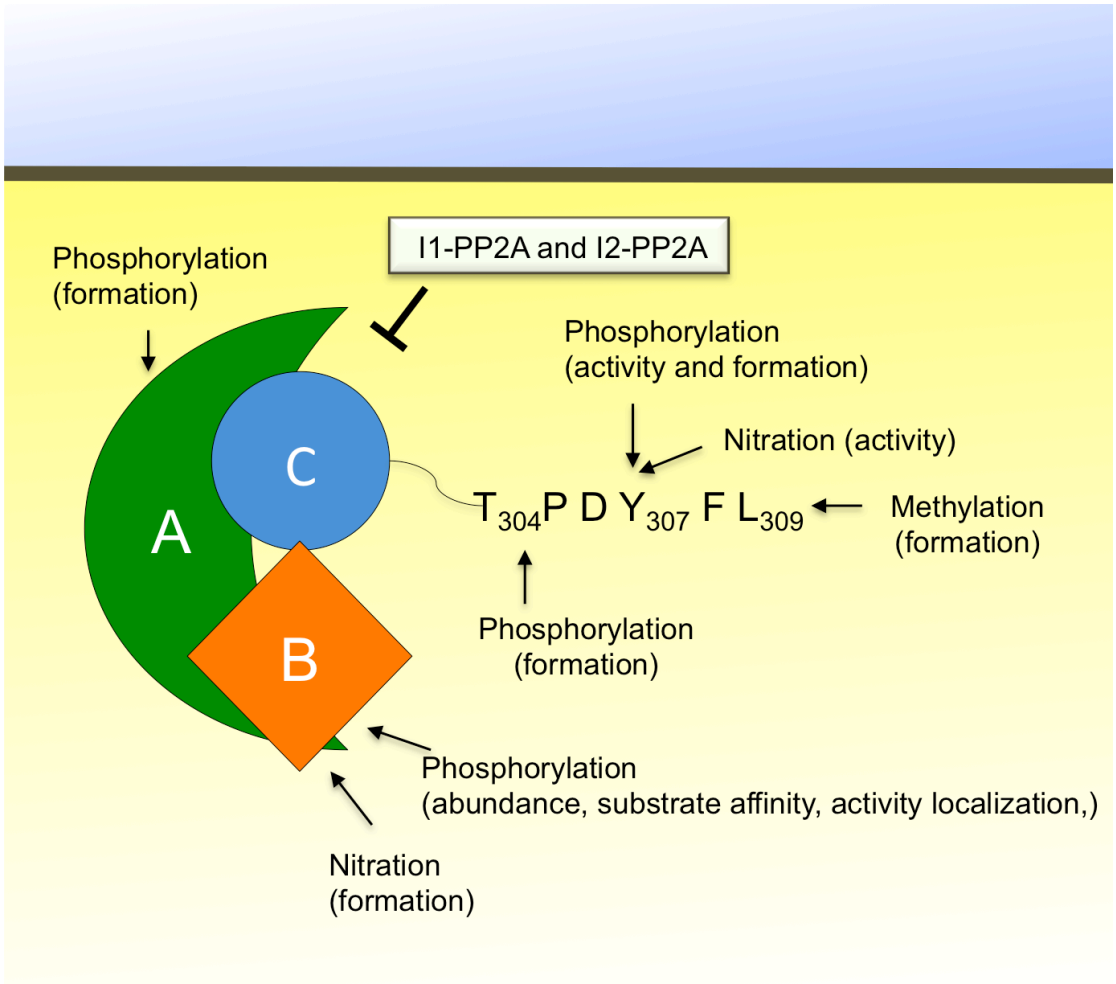

Figure 1.9 Cellular mechanisms of PP2A regulation

PP2A is regulated by post-translational modifications and by endogenous inhibitors. The C-terminal (TPDYFL) motif of the C subunit can be methylated, phosphorylated and nitrated. The A subunit can be phosphorylated. The B-type subunit can be phosphorylated and nitrated. The consequences of these events are indicated in brackets. I1-PP2A and I2-PP2A are endogenous inhibitory proteins.

2 Methods

2.1 Preparation and use of ARVM

2.1.1 Isolation

ARVM were isolated from the hearts of adult male Wistar rats (body weight 200-250g; B&K Universal Ltd.) by collagenase-based enzymatic digestion, as previously described.[166] Rats were anesthetized and heparinized by intraperitoneal injection with sodium pentobarbitone (60 mg/kg) and sodium heparin (100 units). To expose the heart, an incision was made below the sternum; the abdominal cavity was opened and the diaphragm and rib cage were removed. The excised heart was placed in cold (4^{o}C) modified Tyrode solution and was attached to the stainless steel cannula of the perfusion rig via the aorta, using a 4-0 surgical suture. The heart was perfused in the Langendorff mode, by retrograde perfusion of the aorta, with (i) modified Tyrode solution containing 0.75 mM $CaCl_2$ for 2 min, (ii) Ca^{2+} free modified Tyrode solution containing 0.2 mM EGTA for 4 min and (iii) modified Tyrode solution containing 0.1 mM $CaCl_2$ and 125 U/mL type II collagenase (Worthington) for 8 min. The solutions were gassed with 100% O_2 and maintained at 37^{o}C throughout the procedure. The heart was removed from the rig and non-ventricular tissue was removed. The right ventricle was removed and the left ventricle was cut into small pieces. These were incubated in the aforementioned collagenase solution, gently gassed with 100% O_2 for up to 10 min. The tissue was triturated gently by using a 2 mL plastic dropping pipette for < 2 min, until a uniform suspension was obtained. This was filtered through a nylon mesh (pore size 200 μM) into two 50 mL conical tubes. The cells were allowed to settle for 8-10 min. The supernatant was removed and the cells were resuspended in modified Tyrode solution containing 0.5 mM $CaCl_2$ and 10 mg/mL bovine serum albumin (BSA). Again, the cells were allowed to settle for 8-10 min. The supernatant was removed; the cells were resuspended in 30 mL of

modified Tyrode solution containing 1 mM $CaCl_2$ and cultured, as described in section 2.1.2.

2.1.2 Culture

ARVM were cultured in wells of plastic 6-well cell culture plates or in 28 mm single cell culture wells. The wells were coated with laminin prior to cell culture using Natural Mouse Laminin (Invitrogen). This was diluted in ddH_2O to 15 µg/mL and 1.5 mL of the solution was added to each well. Plates and single cell culture wells were left in a sterile environment for at least 1 h. Laminin was removed and the wells were washed with pre-warmed modified M199 medium (Invitrogen). Tyrode solution was removed from the 50 mL conical tube and myocytes, settled at the bottom of the tube, were washed with pre-warmed modified M199 medium. Following centrifugation (300 rpm, 2 min) the cells were resuspended in the appropriate volume of modified M199 medium (48 mL for ARVM isolated from one rat heart). 2 mL of the resulting suspension was added to each culture well. The cells were incubated for 2 h at 37°C (5% CO_2) after which, the culture medium was replaced with 2 mL of fresh modified M199 medium. Unless otherwise stated, the cells were incubated for 18 h (overnight) before the experiments were performed.

2.1.3 Infection with adenoviruses

Adenoviral infection of ARVM was performed 2 h post-seeding, before overnight incubation. The culture medium was replaced with 1 mL of fresh culture medium and cells were counted using an eyepiece graticulate that covered an area of 1 mm^2. The cells were counted in three distinct regions of the well, to obtain an average cell count per mm^2. From this, the total number of cells per well and the volume of virus required for that well were calculated as follows:

Cells per well = cells per mm^2 x 962 mm^2 (i.e. surface area of the well)

Volume of adenovirus per well = (MOI x cells per well) ÷ Titer of adenovirus (MOI is the multiplicity of infection)

2.1.4 Pharmacological treatment

Details of the compounds used in the experiments described in this thesis are provided in Table 2.1. Details of the treatment protocols are provided in the methods section of the relevant experimental chapters.

Table 2.1 Compounds used in pharmacological experiments

Compound	Supplier and catalogue no.	Solvent
CGP 20712A	Sigma Aldrich, C231	ddH_2O
H89	Calbiochem, 371962	DMSO
ICI 118,551	Sigma Aldrich, I127	ddH_2O
ISO	Sigma Aldrich, I5627	ddH_2O
Myr-PKI	Calbiochem, 476485	ddH_2O
N^6-Benz-cAMP	BioLog, B009	ddH_2O
Propranolol	Sigma Aldrich, P0084	ddH_2O

2.1.5 Subcellular fractionation

ARVM were lysed in cold cell lysis buffer (200 µL per well). The plates were frozen on liquid nitrogen and thawed at RT. The cells were detached from the bottom of the well using a cell scraper, whilst resting the plate on ice. Lysates were transferred to a microcentrifuge tube and maintained on ice for 5 min, with frequent vortexing. For each condition, lysates were pooled from four wells. For immunoblot analysis of total protein expression, 100 µL of lysate was transferred to a microcentrifuge tube and to this, 50 µL of 3X Laemmli sample buffer was added. The remaining 700 µL of lysate was subjected to centrifugation (14000 g, 30 min, 4^{o}C). The supernatant, containing soluble proteins, was transferred to a microcentrifuge tube and to this, 350 µL of 3X Laemmli sample buffer was added. The pellet, containing insoluble proteins, was resuspended in 1X Laemmli sample buffer (1050 µL to study relative subunit distribution or 300 µL to study translocation). A schematic overview of the fractionation method is shown in Figure 2.1.

2.2 Preparation of mouse heart samples

Flash-frozen hearts from homozygous B56δ knock out (KO) and WT littermate mice were a kind gift from Veerle Janssens (KU Leuven, Belgium).[120] The hearts were ground to a powder and homogenized on ice, in cold tissue lysis buffer (1 mL per 100 mg tissue), using a tight-fitting glass dounce homogenizer. The homogenates were diluted in urea-based sample buffer (100 µL per 100 µL homogenate) and heat-denatured at 95°C for 5 min.

2.3 Protein Biochemistry

2.3.1 Determination of protein concentration

Protein concentration was determined in the Bradford assay, using the Bio-Rad Protein Assay Dye Reagent Concentrate (Bio-Rad, 500-0006). The dye was prepared by diluting 1 part of Dye Reagent Concentrate with 4 parts of ddH_2O. BSA standards containing between 0.1 and 0.5 mg/mL BSA were prepared in wells of a 96-well microtitre plate using a 1 mg/mL BSA working solution, as indicated in Table 2.2. 200 µL of the dye reagent was added to each standard and the colour was allowed to develop for 5 min at RT. Absorbance was measured at 595 nm in a BioTek ELx808 Plate Reader. A standard curve was plotted and used to determine the protein concentration of the samples.

Table 2.2 Preparation of BSA standards

Standard	BSA (µL)	ddH_2O (µL)
1	1	9
2	2	8
3	3	7
4	4	6
5	5	5

2.3.2 Electrophoretic protein separation

Proteins were separated by sodium dodecyl sulfate polyacrylamide gel electrophoresis (SDS-PAGE). The gels were hand-cast using 1.5 mm thick spacer plates and consisted of a lower resolving gel and an upper stacking gel. The acrylamide content of the resolving gel was determined by the molecular weight of the protein of interest. The composition of the gels is indicated in Table 2.3. Cell or tissue samples were heat-denatured at 95°C for 5 min immediately before use. Electrophoresis was performed in 1X reservoir buffer at a constant voltage of 150 V.

Table 2.3 Composition of resolving and stacking gels used for SDS-PAGE

Resolving gel	Composition
7.5%	2.5 mL 4X resolving buffer, 2.5 mL 30% (w/v) acrylamide, 5 mL ddH_2O, 100 µL APS, 10 µL TEMED
10%	2.5 mL 4X resolving buffer, 3.35 mL 30% (w/v) acrylamide, 4.15 mL ddH_2O, 100 µL APS, 10 µL TEMED
12%	2.5 mL 4X resolving buffer, 4 mL 30% (w/v) acrylamide, 3.5 mL ddH_2O, 100 µL APS, 10 µL TEMED
15%	2.5 mL 4X resolving buffer, 5 mL 30% (w/v) acrylamide, 2.5 mL ddH_2O, 100 µL APS, 10 µL TEMED
Stacking gel	Composition
3.5%	2.5 mL 4X stacking buffer, 1.5 mL 30% (w/v) acrylamide, 6 mL ddH_2O, 100 µL TEMED, 10 µL APS

2.3.3 Electrophoretic protein transfer

For semi-dry protein transfer, the gels were equilibrated in semi-dry transfer buffer for 10 min before electrophoretic protein transfer to a polyvinylidene fluoride (PVDF) blotting membrane. Blotting papers and membranes were pre-soaked in transfer buffer and a transfer sandwich was assembled in a semi-dry transfer unit. Protein transfer proceeded at a constant current of 45 mA per gel (maximum of six gels per transfer unit) for 2 h at room temperature (RT). For wet protein transfer, the gels were equilibrated in wet transfer buffer for 10 min before electrophoretic transfer of proteins to a PVDF blotting membrane. Blotting papers and membranes were pre-soaked in transfer buffer and a transfer sandwich was assembled on a gel holder cassette of a Bio-Rad Criterion Blotter. Proteins were transferred towards the positive electrode at a constant voltage of 90 V (maximum of two gels per blotting tank) for 90 min at 4°C.

2.3.4 Immunoblot analysis

Non-specific binding was blocked by incubating the membranes in TBS containing 0.1% (v/v) Tween-20 (TBST) and 10% (w/v) milk powder for 2 h at RT. Subsequently, the membranes were incubated in primary antibody overnight at 4°C. The membranes were washed four times in TBST (15 min per wash) and were incubated in HRP-conjugated secondary antibody for 2 h at RT. The membranes were washed four times in TBST (15

min per wash). Proteins were detected by chemiluminescence, using ECL Western Blotting Detection Reagents (GE Healthcare). Each membrane was incubated for 2 min in equal volumes of solutions A and B. The membranes were positioned in an X-ray film cassette and X-ray films (GE Healthcare) were exposed to the membranes for different lengths of time. The films were developed in a Fuji RGII automatic processor (Fuji) and the optical density of protein bands was determined using a GS-800 Calibrated Densitometer and Quantity One software (Bio-Rad). Details of primary and secondary antibodies used for immunoblot analysis are provided in Table 2.4 and Table 2.5, respectively.

Table 2.4 Primary antibodies used for immunoblot analysis

Primary antibody	Supplier and catalogue no.	Dilution
α-Actinin	Sigma Aldrich, A7732	1:5000
α_1NKA	Calbiochem, 05-369	1:1000
B56α	BD Biosciences, 610615	1:1000
B56γ	Abcam, Ab94633	1:500
B56δ	Bethyl Laboratories, A301-100A	1:1000
pS573 B56δ	Gift from Angus Nairn	1:2000
cMyBP-C	Gift from Mathias Gautel	1:30 000
pS282 cMyBP-C	Enzo Life Sciences, ALX-215-057-R050	1:2000
cTnI	Cell Signaling Technology, 4002	1:1000
pS23/24 cTnI	Cell Signaling Technology, 4004	1:1000
GAPDH	Abcam, Ab9482	1:5000
GFP	Roche, 11814460001	1:500
Histone 2B	Abcam, ab1790-100	1:1000
Phospho-PKA substrate	Cell Signaling Technology, 9624	1:3000
PLB	Cell Signaling Technology, 8595	1:1000
pS16 PLB	Badrilla, A010-12AP	1:1000
PP2A catalytic	Cell Signaling Technology, 2038	1:1000
PP2A scaffold	Santa Cruz Biotechnology, sc-74580	1:1000

Table 2.5 Secondary antibodies used for immunoblot analysis

Secondary antibody	Supplier and catalogue no.	Dilution
Anti-mouse IgG, HRP-conjugated	Dako, P0446	1:2000
Anti-rabbit IgG, HRP-conjugated	GE Healthcare, NA934	1:2000

2.3.5 Phos-tag™ SDS-PAGE and immunoblot analysis

Proteins were separated by electrophoresis under reducing and denaturing conditions in a discontinuous polyacrylamide gel system. Gels were hand-cast using 1 mm thick spacer plates and consisted in a lower resolving gel and an upper stacking gel. 50 µM acrylamide-pendant Phos-tag™ (Wako Pure Chemical Industries) and 100 µM $MnCl_2$ were included in the resolving gel. The composition of the resolving and stacking gel is indicated in Table 2.6. Electrophoresis was performed in 1X reservoir buffer at a constant current of 25 mA per gel. The Gels were equilibrated in wet transfer buffer with 2 mM EDTA for 15 min then in transfer buffer without EDTA for 10 min. Proteins were transferred to a PVDF

membrane by wet transfer, as described in section 2.3.3. Immunoblot analysis and protein detection were carried out as described in section 2.3.4.

Table 2.6 Composition of resolving and stacking gels used for Phos-tag™ SDS-PAGE

Resolving gel	Composition
10%	1.25 mL 4X resolving buffer, 1.68 mL 30% (w/v) acrylamide, 2.07 mL ddH_2O, 50 µL 5 mM Phos-tag™, 50 µL 10 mM $MnCl_2$, 50 µL APS, 5 µL TEMED
Stacking gel	Composition
3.5%	2.5 mL 4X stacking buffer, 1.5 mL 30% (w/v) acrylamide, 6 mL ddH_2O, 100 µL APS, 10 µL TEMED

2.4 Immunolabeling and confocal microscopy

For microscopy studies ARVM were cultured in 28 mm single cell culture wells, as described in section 2.1.2. The culture medium was removed and the cells were washed with 2 mL of phosphate-buffered saline (PBS). The cells were fixed in 1 mL 4% paraformaldehyde (diluted in PBS from a 16% stock) for 10 min at RT; washed with 2 mL of PBS; permeabilized with 1 mL 0.2% Triton-X100 (diluted in PBS from a 10% stock) for 5 min at RT and washed again with 2 mL of PBS. A cotton bud was used to dry the internal edges of the well and a wax pen was used to create a liquid-repellant barrier. To block non-specific binding of secondary antibodies, the cells were incubated in 5% normal goat serum (diluted in BSA gold buffer) for 20 min at RT. Primary antibodies were diluted in BSA gold buffer and the cells were incubated overnight, in a humid chamber at 4^{o}C. The cells were washed three times with PBS (5 min per washes). Secondary antibodies were diluted in BSA gold buffer and the cells were incubated for 3 h, in a humid chamber at RT. The cells were washed with PBS (5 min wash) after which, a drop of Lisbeth's mounting medium was applied and a glass cover slip was positioned on top of the cells. The edges of the plastic well were removed by using of a hot metal wire and the edge-free base was glued onto a glass microscope slide. These were stored at 4^{o}C until viewing on the confocal microscope. Samples were viewed on an inverted microscope (Leica SP5 System, Mannheim, Germany) equipped with UV-diode, argon lasers and helium-neon lasers, using a 63X/1.4 oil immersion lens. Details of primary and secondary antibodies and fluorescent dyes are provided in Table 2.7 and Table 2.8, respectively.

Table 2.7 Primary antibodies used for confocal microscopy

Primary antibody	Supplier and catalogue no.	Working dilution
α-Actinin	Sigma Aldrich, A7732	1:100
B56δ	Bethyl Laboratories, A301-100A	1:200

Table 2.8 Secondary antibodies and fluorescent dyes used for confocal microscopy

Secondary antibody/ dye	Supplier and catalogue no.	Working dilution
DAPI	Sigma Aldrich, 32670	1:100
Cy3-conjugated anti-mouse IgG	Jackson ImmunoResearch, 115-165-146	1:500
Cy5-conjugated anti-rabbit IgG	Jackson ImmunoResearch, 111-175-144	1:500

2.5 Construction of adenoviral vectors

2.5.1 Plasmids

pEGFP-C1 (Figure 2.2) was a kind gift from Veerle Janssens (KU Leuven, Belgium). The plasmid, carrying the cDNA of human B56δ (UniProt entry Q14738), was used as the template plasmid from which the green fluorescent protein (GFP)-fusion gene was derived. pShuttle-CMV (Stratagene, Figure 2.3) was used as the shuttle vector into which the gene of interest (GOI) was subcloned. The kanamycin cassette present within this plasmid provides bacterial resistance to the antibiotic kanamycin. pAdEasy-1 (Stratagene, Figure 2.3) was used to generate recombinant adenoviral DNA. The plasmid, which contains most of the human adenovirus serotype 5 (AdV) genome, lacks the E1 and E3 genes and as such, is replication-deficient.

2.5.2 DNA gel electrophoresis

DNA was resolved by electrophoresis in 0.8% or 1% agarose TAE gels containing the nucleic acid stain GelRed (Cambridge Biosciences). The composition of the gels is indicated in Table 2.1. The Gels were run at 100 volts and the DNA was visualized by exposure to UV light in a G:BOX Chemi XT16 Gel Documentation and Analysis System (Syngene).

Table 2.9 Composition of agarose TAE gels used for DNA electrophoresis

Agarose TAE gel	Composition
0.8%	2 mL 50X TAE, 198 mL ddH_2O , 0.8 g agarose, 10 µL GelRed
1%	2 mL 50X TAE, 198 mL ddH_2O , 0.8 g agarose, 10 µL GelRed

2.5.3 Site-directed mutagenesis

A single point mutation was introduced into the cDNA of human B56δ using the QuikChange II Site-Directed Mutagenesis Kit (Agilent), to replace the Ser residue at position 573 with alanine (Ala, A). The sequences of the forward (Fwd) and reverse (Rev) mutagenic primers are shown in Table 2.10. Mutated bases are underlined. pEGFP-C1 was used as template DNA. A site-directed mutagenesis reaction comprised: 5 µL 10X Reaction Buffer; 10 ng template DNA; 125 ng S573A Fwd primer; 125 ng S573A Rev primer; 1 µL dNTP mix; 3 µL QuikSolution and 2.5 U *PfuUltra* HF DNA Polymerase, in a final volume of 50 µL. Reactions were cycled as indicated in Table 2.11. Following site-directed mutagenesis, the DNA was treated with 10 U of *Dpn*I for 1 hour at 37°C, to digest methylated and hemimethylated template DNA. Plasmid DNA was sent to Eurofins MWG Operon (Ebersberg, Germany) for sequencing, to confirm successful site-directed mutagenesis.

Table 2.10 Site-directed mutagenesis primers

Primer	Sequence
S573A Fwd	5'ggggcagctccgccttcctccgcag3'
S573A Rev	5'ctgcggaggaaggcggagctgcccc3'

Table 2.11 Site-directed mutagenesis cycling parameters

Segment	Number of cycles	Temperature	Time
1	1	95°C - denaturation	1 min
2	18	94°C - denaturation	50 s
		60°C - primer annealing	50 s
		68°C - extension	7 min 30 s
3	1	68°C - final extension	7 min 30 s

2.5.4 Polymerase chain reaction

The cDNA encoding GFP-B56δ-WT and GFP-B56δ-S573A was amplified from the original pEGFP-C1 plasmid and the mutated pEGFP-C1 plasmid, respectively, by polymerase chain reaction (PCR). To enable subcloning of the GOI into pShuttle-CMV, PCR primers were designed such that restriction sites for *Kpn*I and *Not*I were introduced at the 5' and 3' end of the GOI, respectively. The sequences of the Fwd and Rev PCR primers are shown in Table 2.12. Restriction sites are underlined. A PCR reaction comprised: 1X Phusion HF buffer; 200 µM dNTP mix; 0.2 µM *Kpn*I Fwd primer; 0.2 µM *Not*I Rev primer; 10 ng template plasmid and 1 U Phusion DNA polymerase, in a final volume of 50 µL. Reactions were cycled as indicated in Table 2.13. PCR reaction products were purified as described in section 2.5.5.

Table 2.12 PCR primers

Primer	Sequence
*Kpn*I Fwd	5'atggtacccaccatggtgagcaagggcgag3'
*Not*I Rev	5'gactgcggccgctcagagagcctcctggct3'

Table 2.13 PCR cycling parameters

Segment	Number of cycles	Temperature	Time
1	1	95°C - denaturation	30 s
2	30	94°C - denaturation	1 min
		55°C - primer annealing	1 min
		72°C - extension	2 min
3	1	72°C - final extension	10 min

2.5.5 Purification of PCR products

DNA was purified using the High Pure PCR Product Purification Kit (Roche). All centrifugation steps were performed at 13000 rpm in a bench-top microcentrifuge. The volume of the reaction was adjusted to 100 µL with ddH_2O. 500 µL of Binding Buffer was added and the resulting solution was transferred to a High Pure Filter Tube. This was centrifuged for 1 min. The flowthrough was discarded and 500 µL of Wash Buffer was added to the upper reservoir of the filter tube. This was centrifuged for 1 min and the process was repeated. DNA was eluted from the filter by centrifugation, following addition of 50 µL Elution Buffer.

2.5.6 DNA restriction digest

The GOI and pShuttle-CMV were digested (in separate reactions) with 10 U of both *Kpn*I and *Not*I in 1X NEBuffer 4 and BSA (100 µg/mL), in a total volume of 60 µL for 1 hour at 37°C. The GOI and shuttle vector were purified as described in section 2.1.5. The DNA concentration was determined using a NanoDrop 2000 UV-Vis Spectrophotometer (Thermo Scientific).

2.5.7 DNA ligation

The amount of insert (GOI) required for ligation with 50 ng of pShuttle-CMV shuttle vector, for a 3:1 insert-to-vector mole ratio, was calculated using the following equation.

Insert (ng) = [vector (ng) x size of insert (kb) x 3] ÷ Size of vector (kb)

The GOI and shuttle vector were ligated with T4 DNA ligase in 1X T4 DNA Ligase buffer, in a total volume of 20 µL for 2 h at RT. 5 µL of the ligation reaction were transformed into DH5α competent cells as described in section 2.5.8.

2.5.8 Transformation of *E.coli* DH5α competent cells

Subcloning efficiency DH5α competent cells (Invitrogen) were stored at -80°C and thawed on ice prior to the transformation. 5 µL of plasmid DNA was added to 50 µL of cells. These were maintained on ice for 30 min and were heat-shocked at 42°C for 30 s. The cells were incubated on ice for 2 min and resuspended in 500 µL of pre-warmed SOC medium. Finally, the cells were incubated in a bench-top shaker (37°C, 500 rpm) for 1 hour. The cultures were spread on LB-kanamycin agar plates and the inverted plates were incubated overnight at 37°C.

2.5.9 Transformation of *E.coli* BJ5183 electrocompetent cells

Clones of pShuttle-CMV that contained the GOI were digested with 10 U of *Pme*I in 1X NEBuffer 4 and BSA (100 µg/mL), in a total volume of 30 µL for 1 hour at 37°C. To generate recombinant adenoviral DNA (rAd5-GOI) homologous recombination between pShuttle-CMV-GOI pAdEasy-1 was performed in *E.coli* BJ5183-AD-1 electrocompetent cells (Stratagene). The cells were stored at -80°C and thawed on ice prior to the transformation. 40 µL of cells were added to 100ng (1 µL) of *Pme*I-digested pShuttle-CMV-GOI and transferred to a chilled electroporation cuvette for electroporation (200 Ω, 2.5 kV, 25 µF). The cells were resuspended in 200 µL of pre-warmed SOC medium and incubated in a bench-top shaker (37°C, 500 rpm) for 1 hour. The cultures were spread on LB-kanamycin agar plates and the inverted were incubated overnight at 37°C.

2.5.10 Amplification of bacterial colonies

Colonies of bacterial cells (DH5α or BJ5183), grown on LB-kanamycin agar plates overnight, were inoculated into 3 mL of LB-kanamycin for overnight incubation in an orbital shaker (37°C, 225 rpm). Plasmid DNA was isolated and purified as described in section 2.5.11.

2.5.11 Isolation and purification of plasmid DNA

Plasmid DNA was isolated from bacteria using the QIAprep Spin Miniprep Kit (Qiagen). All centrifugation steps were performed at 13000 rpm in a bench-top microcentrifuge. Bacterial cells were pelleted in microcentrifuge tubes from 1.5 mL of the overnight culture and resuspended in 250 µL of Buffer P1. 250 µL of Buffer P2 and 350 µL Buffer N3 was added sequentially and the tubes were inverted several times after each addition. The samples were centrifuged for 10 min, which resulted in the formation of a white precipitate that contained cell debris. The supernatant was transferred to a QIAprep spin column and centrifuged for 1 min. The flowthrough was discarded. 750 µL of Buffer PE was added to the upper reservoir of the tube and the column was centrifuged for 1 min. The flowthrough was discarded and the empty column was centrifuged again for 1 min to remove any residual buffer. The column was transferred to a clean microcentrifuge tube and 50 µL of Buffer EB was added. The column was left to stand for 1 min and plasmid DNA was eluted by centrifugation.

2.5.12 Culture of HEK293 cells

HEK293 cells in modified DMEM culture medium were maintained in T75 flasks at 37^{o}C and were passaged twice a week (or when 90% confluent). The culture medium was removed and the cells were incubated with 1 mL of 0.5% (w/v) Trypsin-EDTA (Invitrogen), to detach the cells from the surface of the flask. 10 mL of modified DMEM was added to the detached cells and 1.5 mL of the resulting suspension was transferred to a new T75 flask that contained 13.5 mL of modified DMEM culture medium.

2.5.13 Transfection of HEK293 cells

10 µg of rAd5-GOI was linearized by digestion with 100 U of *Pac*I in 1X NEBuffer 1 and BSA (100 µg/mL) in a total volume of 100 µL, for 2 h at 37^{o}C. For the transfection, HEK293 cells were seeded in wells of a 6-well cell culture plate (at a density of 6 x 10^5 cells per well) and incubated overnight at 37^{o}C. The cells were transfected when 50-60% confluent. The transfection solution consisted of 20 µL PolyFect Transfection Reagent (Qiagen), 80µL

Opti-MEM (Life Technologies) and 20 µL of linearized rAd5-GOI. The solution was incubated for 10 min at RT (with gentle flicking) and diluted with 600 µL of DMEM. Finally, the solution was added drop-wise to the cells in one well. The transfected cells were maintained at 37°C and harvested when cytopathic effects, including the rounding up of cells and their detachment from the surface of well, were observed. The expression of GFP was determined by fluorescence microscopy, to monitor the course of the transfection.

2.5.14 Amplification of adenoviruses

Transfected HEK293 cells were harvested 2-3 weeks post-transfection, when approximately 50% of the cells showed evidence of a cytopathic effect. The cells were collected in culture medium and transferred to a 50 mL conical centrifuge tube. Virus particles were released from the cells by subjecting these to three freeze/thaw cycles, alternating the tube between liquid nitrogen and a 37°C water bath. Cellular debris was collected by centrifugation (10 min, 800 g) and the supernatant, containing the primary adenoviral stock, was added to the culture medium of HEK293 cells in a T75 flask. When approximately 50% of the cells showed evidence of a cytopathic effect (2 or 3 days post-infection), the next round of amplification was initiated. In the final round, HEK293 cells seeded in ten T175 flasks were infected. At the end of this final round the cells were collected in media, transferred to 50 mL conical centrifuge flasks and pelleted by centrifugation (10 min, 800 g). The supernatants were removed and the pellets were combined in 2 mL of phosphate buffered saline (PBS). Virus particles were released by subjecting the cells to three freeze/thaw cycles, as previously described. Cellular debris was collected by centrifugation (10 min, 800 g) and the adenovirus, contained in the supernatant, was purified by cesium chloride (CsCl) density gradient ultracentrifugation, as described in section 2.5.15.

2.5.15 Purification of adenoviruses

A discontinuous CsCl gradient was prepared in an ultracentrifuge tube. This consisted of 4 mL heavy (1.4 g/mL) CsCl and 4 mL light (1.25 g/mL) CsCl. The adenovirus suspension

was overlaid onto the gradient and PBS was added so that the total liquid volume was within a short distance from the rim of the tube (Figure 2.5). The tube was centrifuged at 20000 rpm for 2 h at 20°C in a Beckman SW41 Ti swingout rotor with slow acceleration and no brake. The adenovirus (at the interphase between the heavy and light CsCl) was collected in a 5 mL syringe, by piercing the tube with an 18-gauge needle. To further purify the adenovirus and remove the cesium chloride, the solution was dialyzed against a virus dialysis buffer for 24 h at 4°C. The dialysis buffer was changed 3-4 times after which, the purified adenovirus was aliquoted in sterile microcentrifuge tubes and stored at -80°C.

2.5.16 $TCID_{50}$ assay

The infectious titer of the purified adenovirus was determined by performing the tissue culture infectivity dose 50 ($TCID_{50}$) assay. 90 µL of HEK293 cells in modified DMEM were seeded in each well of a 96-well cell culture plate. The plate was incubated at 37°C for 24 h, until the cells were 70-80% confluent. The purified adenovirus was serially diluted in modified DMEM from 10^{-5} to 10^{-11}. The cells in the same row of the plate were inoculated with 10 µL of the same dilution. 10 µL of modified DMEM (without adenovirus) were added to the cells in the last row, as a negative control. The plate was maintained at 37°C. On day 5, the culture medium was replaced in all wells where signs of infection were not apparent. On day 8, the plate was scored for infection and the titer of the purified adenovirus was determined. To visualize GFP and therefore determine the number of wells infected, the plate was inspected on a fluorescence microscope. The wells containing GFP-expressing cells were scored as positive. The titer of the adenovirus was determined as follows, using the method described by Nicklin and Baker.[181]

Proportionate distance, PD = (A – 50) ÷ (A – B)

A = % response greater than 50% and B = % response less than 50%

Log_{10} ($TCID_{50}$) = log of dilution giving a response > 50% – PD

For example, the $TCID_{50}$ assay results for AdV.GFP-B56δ-WT were as follows:

Dilution	Positive wells	
10^{-5}	12 out of 12	100%
10^{-6}	12 out of 12	100%
10^{-7}	12 out of 12	100%
10^{-8}	3 out of 12	25%
10^{-9}	0 out of 12	0%
10^{-10}	0 out of 12	0%
10^{-11}	0 out of 12	0%

PD = (100 – 50) ÷ (100 – 25) = 0.67

Log_{10} ($TCID_{50}$) = -7 – 0.67 = -7.67

$TCID_{50} = 10^{-7.67}$

The virus titer is equivalent to the reciprocal of the $TCID_{50}$ per mL of virus dilution added.

Virus titer = $(1 \div 10^{-7.67}) \div 0.01$
= 4.67×10^{-9} $TCID_{50}$ / mL

Based on the Poisson distribution the $TCID_{50}$ can be converted to plaque forming units (PFU) by multiplying the value by 0.69.

Virus titer = 4.67×10^{-9} $TCID_{50}$ x 0.69
Virus titer = 3.23×10^{9} PFU/mL

2.6 Measurement of PP2A activity

PP2A activity was measured using the PP2A Immunoprecipitation Phosphatase Assay Kit (Millipore). Malachite green solution, malachite green additive, phosphate standard, Thr phospho-peptide (K-T-pT-I-R-R), PP2A catalytic subunit antibody (clone 1D6) and protein A agarose beads, which are provided in the kit, were used as described in the following sections.

2.6.1 Preparation of malachite green phosphate detection solution

Malachite green phosphate detection solution was prepared with malachite green additive (solution B) and malachite green solution (solution A). 10 µL of solution B was used per 1 mL of solution A. 100 µL of mixed solution AB was used per well of a 96-well ½ volume microtitre plate.

2.6.2 Preparation of phosphate standards

Phosphate standards containing between 0 and 2000 pmol phosphate per 25 µL were prepared in microcentrifuge tubes using the phosphate standard, as shown in Table 2.14. 25 µL of each standard was transferred to wells of a 96-well ½ volume microtiter plate. 100 µL of malachite green phosphate detection solution was added to each well and colour was allowed to develop for 10 min at RT. Absorbance was measured at 650 nm in a BioTek ELx808 Plate Reader. The absorbance of the blank solution was subtracted from the absorbance of the standards and the resulting values were plotted against the corresponding phosphate concentration. Representative images of phosphate standards and the phosphate standard curve is shown in Chapter 6 (Figure 6.1).

Table 2.14 Preparation of phosphate standards

Standard	Phosphate standard (µL)	ddH_2O (µL)
1	0	250
2	20	230
3	40	210
4	60	190
5	80	170
6	100	150
7	120	130
8	140	110
9	160	90
10	180	70
11	200	50

2.6.3 Preparation of the Thr phospho-peptide

A 1 mM solution of the Thr phospho-peptide was prepared by dissolving 1 mg of the supplied powder in 1.10 mL ddH_2O. The solution was aliquoted and stored at -20°C, until required.

2.6.4 PP2A immunoprecipitation and phosphatase assay

2.6.4.1 **Immunoprecipitation of PP2A catalytic subunits**

ARVM were washed in TBS and lysed in cold immunoprecipitation lysis buffer (IP lysis buffer, 150 µL per well). Lysates were collected in microcentrifuge tubes and clarified by centrifugation (14000 g, 5 min, 4°C). The protein concentration in the supernatant was determined as described in section 2.3.1. 100-200 µg of protein was transferred to a microcentrifuge tube and the volume was adjusted to 500 µL with IP lysis buffer. For immunoblot analysis of protein expression in the pre-IP lysate, 50 µL was transferred to a microcentrifuge tube and 50 µL of 2X Laemmli sample buffer was added. PP2A catalytic subunits were immunoprecipitated from the remaining 450 µL of lysate with 5 µg of PP2A catalytic subunit antibody and 40 µl of protein A agarose beads. Microcentrifuge tubes were placed on a rotating wheel for 2 h at 4°C. Immunocomplexes were collected by centrifugation. For immunoblot analysis of protein expression in the post-IP supernatant,

50 µL of the supernatant was transferred to a microcentrifuge tube and 50 µL of 2X Laemmli sample buffer was added. The immunocomplexes were washed three times in immunocomplex wash buffer (IC wash buffer) then two times in PP2A reaction buffer.

2.6.4.2 **Phosphatase assay**

Immunocomplexes were incubated with 60 µl of 1 mM Thr phospho-peptide and 20 µl of PP2A reaction buffer in a bench-top shaker for 10 min (30^{o}C, 900 rpm). 25 µl of the reaction end-product product was transferred to wells of a 96-well ½ volume microtitre plate. 100 µl of malachite green phosphate detection solution was added and colour was allowed to develop for 10 min at RT. Absorbance was measured at 650 nm. If necessary, the reaction end-product product was diluted with ddH_2O so that a less-intense colour response was obtained and the absorbance of the sample was within the linear range of the phosphate standard curve. A schematic overview of the assay is shown in Figure 2.6. For immunoblot analysis of immunoprecipitated PP2A catalytic subunits, 40 µl of 2X Laemmli sample buffer was added to the pelleted beads.

2.6.4.3 **Calculating phosphatase activity**

Phosphatase activity is expressed as pmol phosphate released from the Thr phospho-peptide per min. For example, as interpolated from the phosphate standard curve, the phosphate concentration of a sample whose absorbance was 0.24 was 528 pmol per 25 µL. Given that dephosphorylation reactions proceeded for 10 min in a volume of 80 µL, the phosphate concentration in this volume at the end of the reaction was 1689.6 pmol. Therefore, 168.96 pmol phosphate were released from the Thr phospho-peptide per min. If the reaction end-product was diluted so that the absorbance was within the linear range of the standard curve, the dilution factor was accounted for.

2.7 Solutions

10X Reservoir buffer	25 mM Tris, 192 mM glycine, 0.35 mM SDS
3X Laemmli sample buffer	187.5 mM Tris (pH 8.6), 6% SDS; 30% glycerol, 15% β-mercaptoethanol, 0.015% bromophenol blue
4X Resolving buffer	1.5 M Tris (pH 8.7), 14 mM SDS
4X Stacking buffer	0.5 M Tris (pH 6.8), 14 mM SDS
50X TAE	2 M Tris, 64 mM EDTA, 17.5% (v/v) acetic acid
ARVM lysis buffer	50 mM Tris (pH 7.5), 5 mM EGTA, 2 mM EDTA, 100 mM NaF, 1% (v/v) Triton-X100, 1 complete mini protease inhibitor tablet (Roche) per 10 ml
BSA gold buffer	20 mM Tris-base, 155 mM NaCl, 2 mM EGTA, 2mM $MgCl_2$, 1% w/v BSA (pH 7.5)
IC wash buffer	20 mM Imidazole-HCl (pH 7)
IP lysis buffer	20 mM Imidazole-HCl (pH 7), 2 mM EGTA, 2 mM EDTA, 1% (v/v) Triton-X100, 1 complete mini protease inhibitor tablet (Roche) per 10 ml
LB-kanamycin	10 g/L NaCl, 10 g/L tryptone, 5 g/L yeast extract, 50 µg/ml kanamycin
LB-kanamycin agar	10 g/L NaCl, 10 g/L tryptone, 5 g/L yeast extract, 50 µg/ml kanamycin, 15 g/L agar
Lisbeth's mounting medium	30 mM Tris (pH 9.5), 70% (v/v) glycerol, 5% (w/v) n-propyl gallate
Modified DMEM	Dulbecco's modified Eagles media, 10% (v/v) fetal calf serum, 50 U penicillin, 100 µg streptomycin
Modified M199 medium	M199 Hanks media, 2 mM creatine, 2 mM carnitine, 5 mM taurine, 100 IU/ml penicillin/streptomycin

Modified Tyrode solution	130 mM NaCl, 5.4 mM KCl, 1.4 mM $MgCl_2$, 0.4 mM NaH_2PO_4, 4.2 mM HEPES, 10 mM glucose, 20 mM taurine, 10 mM creatine (pH 7.3 at 37°C)
PP2A reaction buffer	20 mM HEPES (pH 7.4), 150 mM NaCl, 5 mM $MgCl_2$, 0.01% (v/v) Triton-X100
Semi-dry transfer buffer	20 mM Tris (pH 8.3), 120 mM glycine, 1.3 mM SDS, 20% (v/v) methanol
SOC medium	8.5 mM NaCl, 2.5 mM KCl, 20 g/L tryptone, 5 g/L yeast extract, 20 mM glucose (pH 7)
TBS	20 mM Tris-base (pH 7.6), 140 mM NaCl
Tissue lysis buffer	Sterile PBS, 1 complete mini protease inhibitor tablet (Roche) per 10 mL, 100 µL phosphatase inhibitor cocktail 3 (Sigma) per 10 mL
Urea sample buffer	3.7 M Urea, 134.6 mM Tris (pH 6.8), 5.4% SDS, 2.3% NP-40, 4.45% β-mercaptoethanol, 4% glycerol, 6 mg/100 mL bromophenol blue
Virus dialysis buffer	10% (w/v) glycerol, 1 mM $MgCl_2$, 10 mM Tris (pH 7.4)
Wet transfer buffer	25 mM Tris, 192 mM, 20% (v/v) methanol

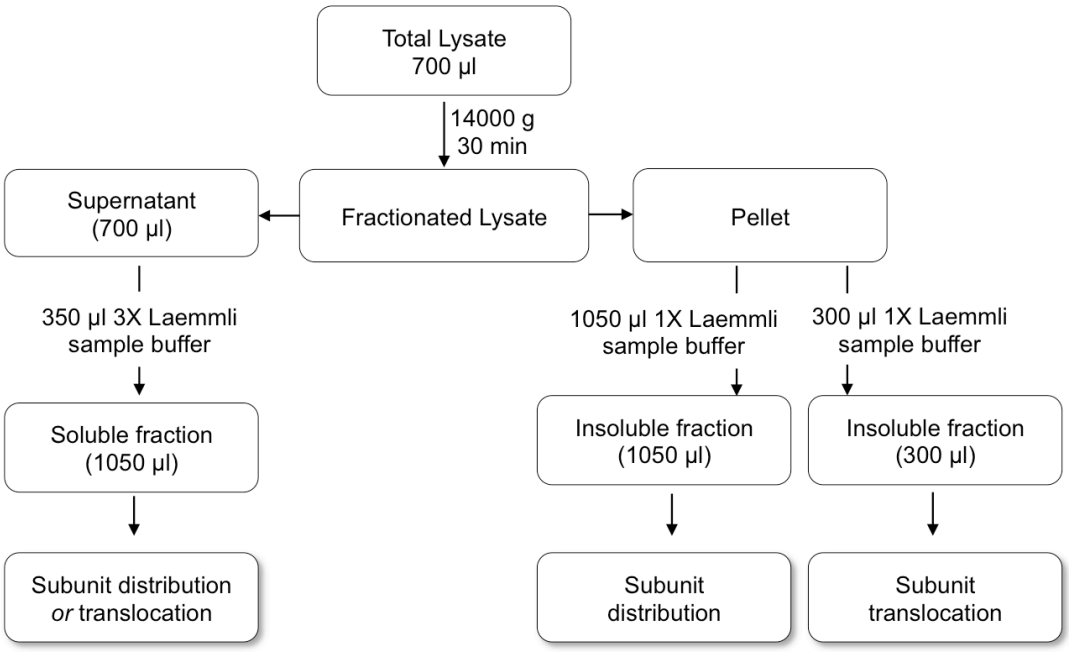

Figure 2.1 Subcellular fractionation protocol

ARVM, lysed in a lysis buffer that contained 1% Triton-X100, were subjected to fractionation by centrifugation (14000g, 30 min, 4^{o}C). A supernatant (containing soluble proteins) and a pellet (containing insoluble proteins) were obtained. The supernatant was transferred to a microcentrifuge tube and was diluted to 1050 µl with 350 µl of 3X Laemmli sample buffer. The pellet was solubilized in 1X Laemmli sample buffer (1050 µl to study subunit distribution or 300 µl to study subunit translocation).

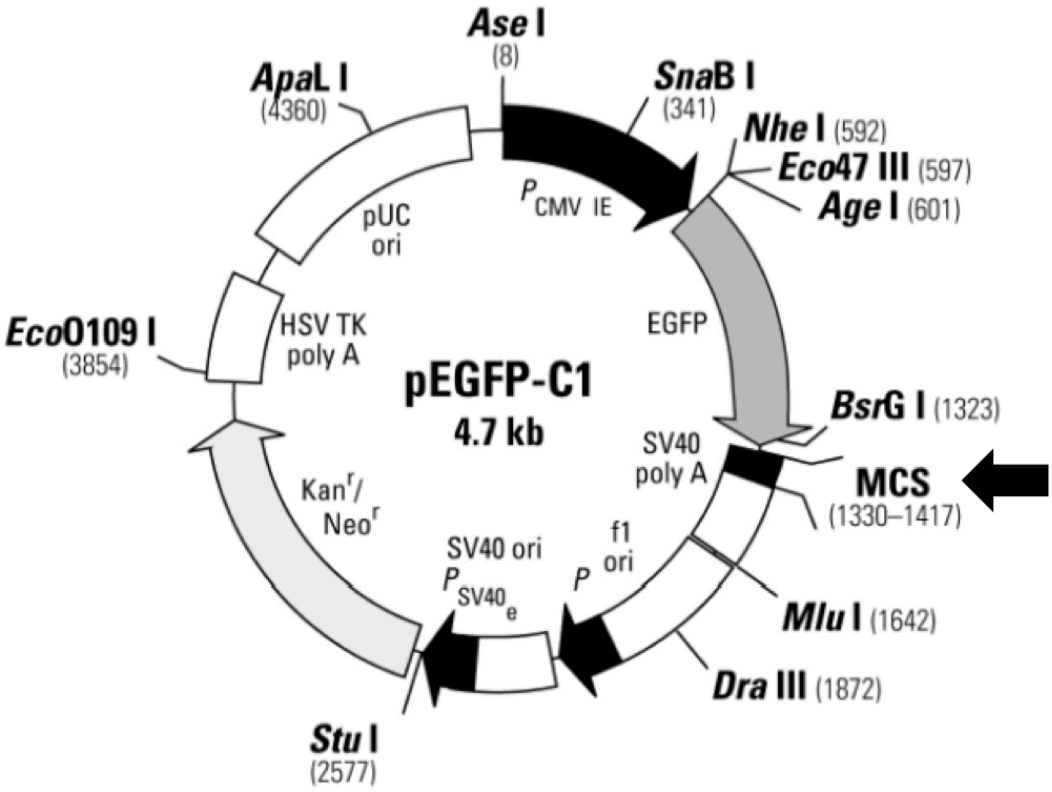

Figure 2.2 pEGFP-C1 plasmid map

The human gene for B56δ is cloned at the multiple cloning site (MCS), indicated by the arrow.

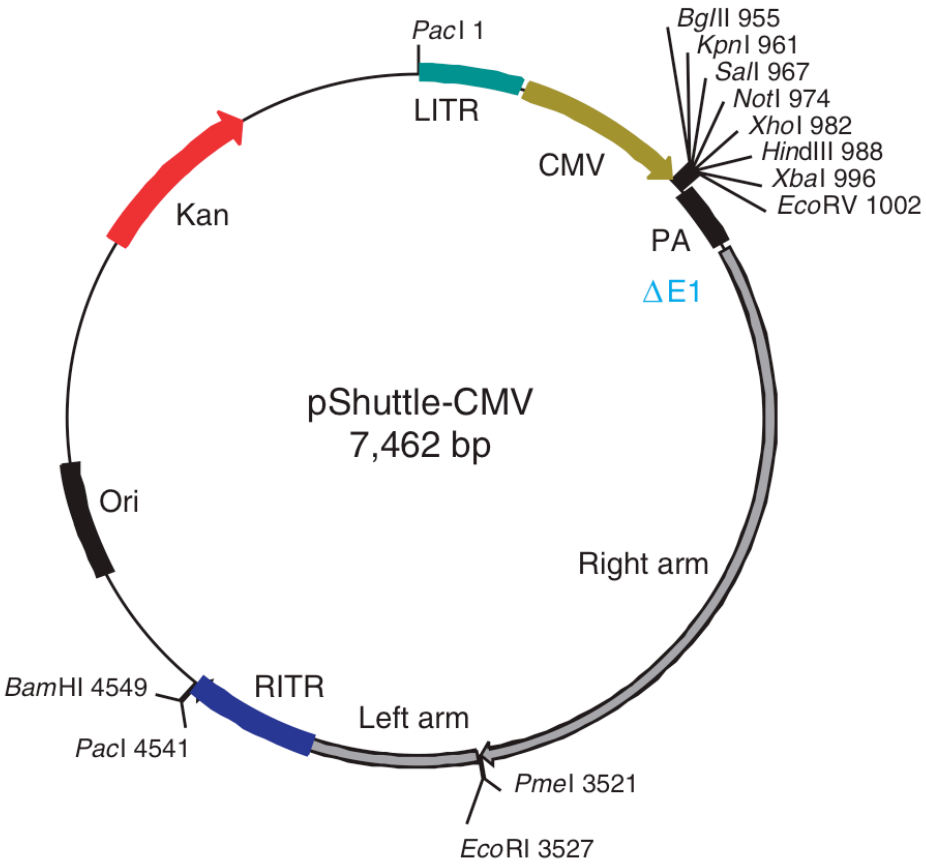

Figure 2.3 pShuttle-CMV plasmid map

The GOI was subcloned at the multiple cloning site, at the *Kpn*I and *Not*I sites. The kanamycin (Kan) cassette provides resistance to the antibiotic kanamycin, enabling selection of transformed bacterial cells.

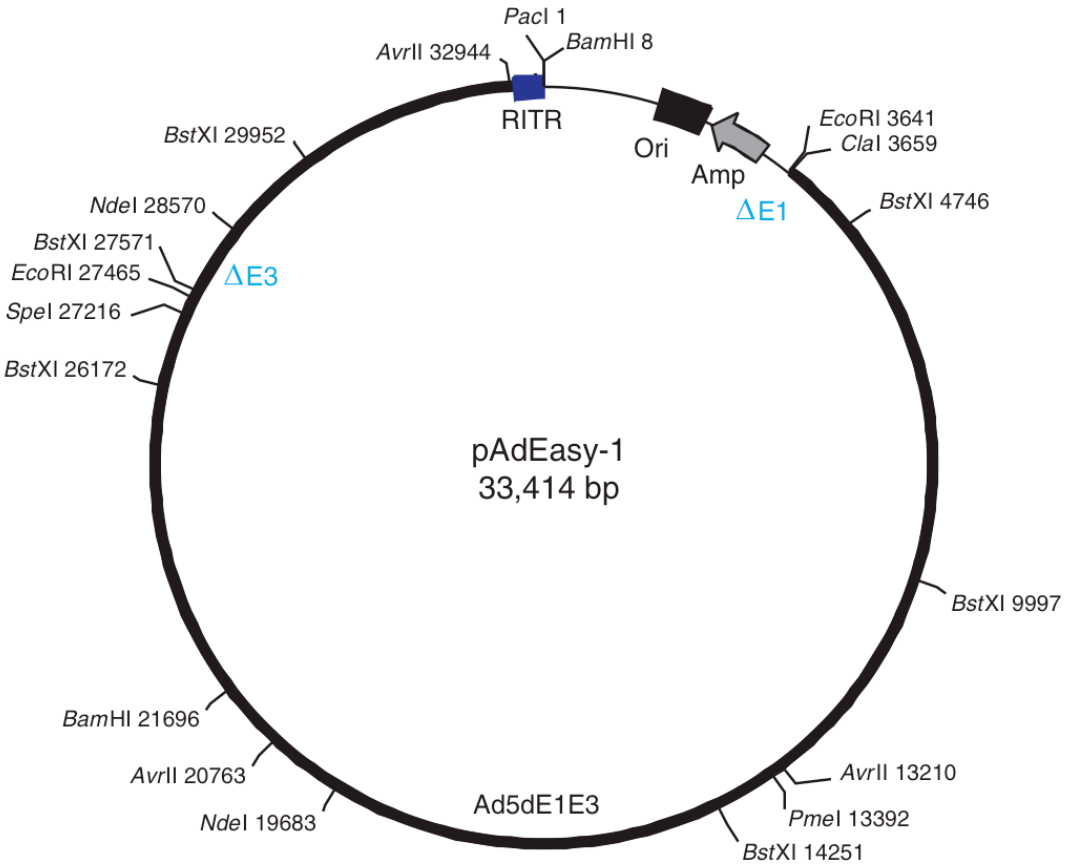

Figure 2.4 pAdEasy-1 plasmid map

Recombinant adenoviral DNA was obtained by homologous recombination between pShuttle-CMV-GOI and pAdEasy-1 in bacterial cells.

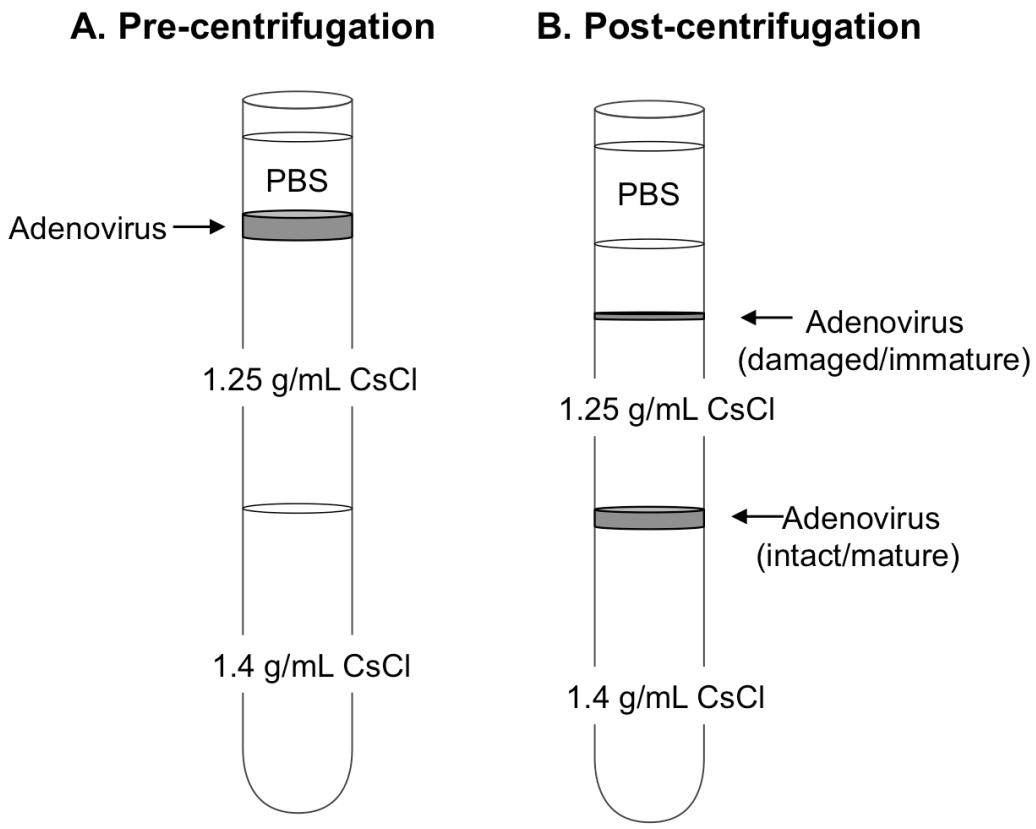

Figure 2.5 Purification of adenoviruses

A. A discontinuous CsCl gradient consists in 4 mL of heavy (1.4 g/mL) CsCl and 4 mL of light (1.25 g/mL) CsCl. The adenovirus is overlaid on top of the gradient and PBS is added until just below the rim of the tube. **B.** After centrifugation, intact and mature adenovirus particles are found at the interface between the heavy and light CsCl gradient. Damaged or immature adenovirus particles are found within the light CsCl gradient.

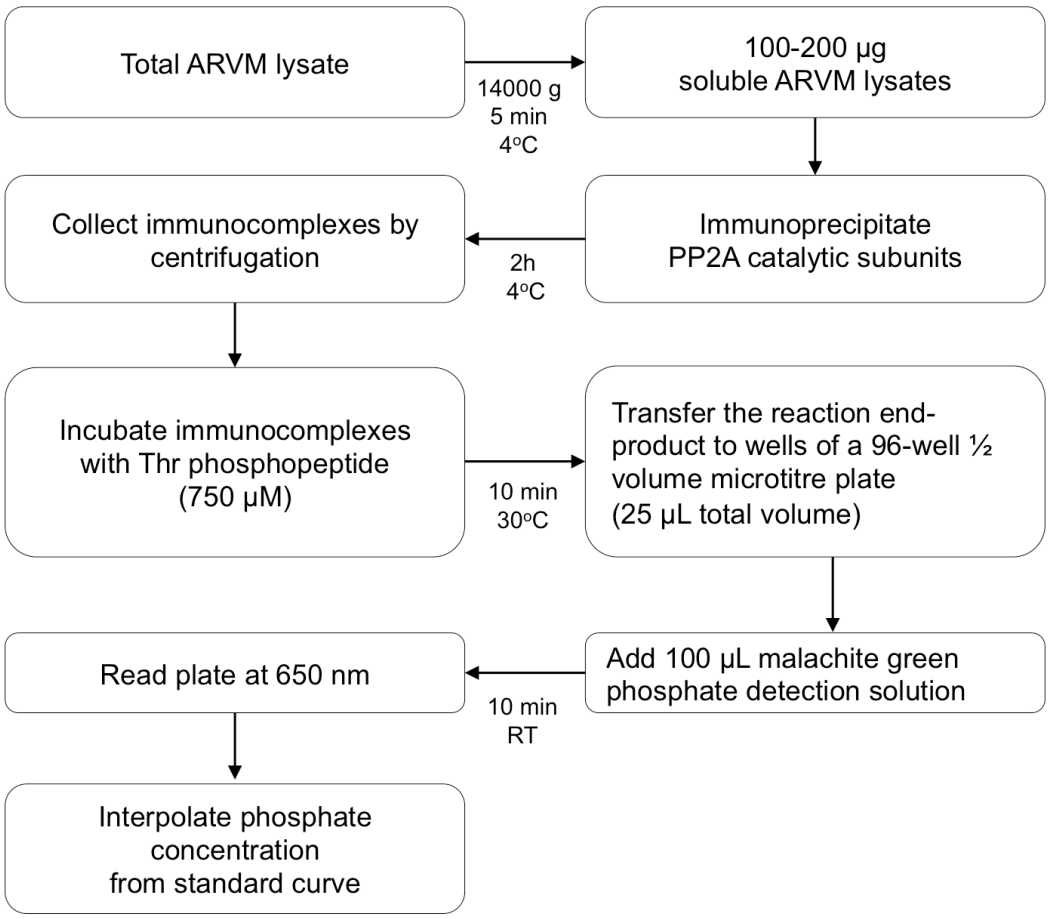

Figure 2.6 PP2A immunoprecipitation phosphatase assay

The catalytic subunits of PP2A were immunoprecipitated from 100-200 µg of soluble ARVM lysates. The immunocomplexes were collected and incubated with a substrate Thr phospho-peptide. Inorganic phosphates in the reaction end-product were detected with malachite green phosphate detection solution. The absorbance of the sample was measured at 650 nm and the phosphate concentration was interpolated from the phosphate standard curve.

3 Expression and Subcellular Distribution of PP2A Subunits in ARVM

3.1 Introduction

The subcellular distribution of PP2A holoenzymes is governed by regulatory B-type subunits.[65] The B56 family comprises five isoforms (α, β, γ, δ and ε); γ and δ isoforms each have three splice variants and thus, B56 subunits are the largest family of B-type subunits. Given that B56 subunits are stable only when bound to the PP2A core enzyme,[182] the subcellular distribution of these subunits reflects the distribution of specific holoenzymes.

The subcellular distribution of B56α and B56γ_1 was studied in neonatal and ARVM with heterologous expression of HA-tagged proteins.[111] Whereas immunolabeled HA-B56α exhibited a cytosolic distribution with a striated pattern, immunolabeled HA-B56γ_1 was primarily localized in nuclear speckles.[111] These differences in subcellular targeting result from small domains present at the N- and C-terminus of B56 proteins. In this context, the nuclear compartmentalization of B56γ_1 is likely to result from a nuclear localization signal at its C-terminus.[111] In contrast, the localization of B56α at the Z-disc and M-line regions is mediated by a C-terminal residue that interacts with the spectrin-binding domain in ankyrin-B.[119]

The subcellular distribution of endogenous PP2A subunits (including scaffold, catalytic and regulatory B56γ and B56ε subunits) was recently studied in adult mouse ventricular myocytes.[183] Whereas immunolabeled PP2A scaffold and catalytic subunits were distributed throughout the cytosol and nucleus, the immunolabeled regulatory subunits were localized to discrete regions;[183] B56γ was primarily localized to the nucleus and B56ε was localized to the Z-disc.[183]

Studies in isolated cardiac myocytes suggest that the subcellular distribution of selected PP2A subunits is altered in response to external stimuli. For example, the catalytic subunit is recruited to the sarcolemma in response to adenosine A1 receptor stimulation.[162] The

findings that are particularly relevant to the work described in this chapter, however, are those reported by Yin *et al*.[166] The studies were performed in isolated "skinned" ARVM and showed that B56α is depleted from the myofilaments following ISO stimulation (Figure 3.1). Thus, altered PP2A localization in response to β-AR stimulation, might contribute to the regulation of protein phosphorylation and function in β-adrenergic signaling.

3.2 Objectives

The objectives of the studies described in this chapter were to:

- Determine the expression of PP2A scaffold, catalytic and regulatory B56 subunits in ARVM, at protein level.
- Investigate the subcellular distribution of PP2A scaffold, catalytic and regulatory B56 subunits in unstimulated ARVM, by immunoblot analysis of subcellular fractions.
- Investigate potential changes in the subcellular distribution of PP2A scaffold, catalytic and regulatory B56 subunits in ARVM in response to β-adrenergic stimulation, by immunoblot analysis of subcellular fractions.

3.3 Methods

3.3.1 ARVM isolation, culture, stimulation and subcellular fractionation

For the experiments described in this chapter, ARVM were isolated from the hearts of adult male Wistar rats and cultured as described in the Methods (sections 2.1.1 and 2.1.2). In some experiments the cells were exposed to vehicle or 10 nM ISO for 10 min. The cells were incubated at 37^{o}C for the duration of the experiment. Subcellular fractionation was performed as described in the Methods (section 2.1.5).

3.3.2 Immunoblot analysis

SDS-PAGE and immunoblot analysis were performed as described in the Methods (sections 2.3.2 to 2.3.4). For the experiments described in this chapter, proteins were transferred to the support membrane by the semi-dry transfer method. Details of the antibodies used are provided in the Methods (Tables 2.4 and 2.5).

3.4 Results

3.4.1 Validation of ARVM subcellular fractionation

The method used for the fractionation of ARVM was adapted from a previously described protocol.[166] The cultured cells were lysed in a buffer that contained 1% Triton-X100, to solubilize membranes and release cytosolic proteins. The separation of soluble and insoluble proteins was achieved by centrifugation. To validate the fractionation, soluble and insoluble fractions were subjected to immunoblot analysis of proteins with known subcellular compartmentalization. Glyceraldehyde 3-phophate dehydrogenase (GAPDH) and the α_1 subunit of the NKA were selected as markers for the cytosolic and the membrane compartment, respectively. cTnI and histone 2B (H2B) were selected as markers for the myofilament and the nuclear compartment, respectively. As expected, GAPDH and α_1NKA were present exclusively in the soluble fraction whereas cTnI and H2B appeared only in the insoluble fraction (Figure 3.2). These results confirmed the successful capture of cytosolic/membrane and myofilament/nuclear proteins in the soluble and insoluble fraction, respectively.

3.4.2 Expression and subcellular distribution of PP2A subunits

Expression and subcellular distribution of scaffold, catalytic and regulatory B56α, -γ and δ subunits were determined by immunoblot analysis of total ARVM lysates and ARVM subcellular fractions, respectively (Figure 3.3). For these experiments, proteins in the soluble and insoluble fraction were diluted in the same volume and equal volumes of each sample were subjected to electrophoresis. Therefore, the intensity of signals from the two fractions provides information on the relative abundance of each subunit in different subcellular compartments. B56γ subunits, which are expressed in ARVM, appeared only in the insoluble fraction (Figure 3.3, panel D). Scaffold, catalytic and regulatory B56α and -δ subunits, which are also expressed in ARVM, were detected in both fractions and were most abundant in the soluble fraction (Figure 3.3, panels A-C and E). Coomassie staining of the membranes revealed that global protein abundance was highest in the soluble fraction and lowest in the insoluble fraction (Figure 3.3, panel F). Therefore, according to the

fractionation method that was used, it appears that soluble proteins account for a larger proportion of the ARVM proteome. Taken together, these results suggest that like most ARVM proteins, B56α-PP2A and B56δ-PP2A holoenzymes are relatively more abundant in cytosolic/membrane (soluble) compartments. In contrast, B56γ-PP2A holoenzymes are likely to exist only in myofilament/nuclear (insoluble) compartments.

3.4.3 ISO-induced translocation of B56α-PP2A holoenzymes

As described in section 3.1, previous studies in our laboratory showed subcellular redistribution of B56α in ARVM exposed to the β-adrenergic agonist ISO.[166] As also described in section 3.1, B56 subunits are stable only when they are part of holoenzymes. Thus, the distribution of PP2A scaffold and catalytic subunits in subcellular fractions of vehicle and ISO-stimulated ARVM was investigated. To improve detection of all subunits in the insoluble fraction and thereby enable quantitative analysis of subunit abundance, more concentrated insoluble fractions were prepared. The capture of cytosolic/membrane proteins (in the soluble fractions) and myofilament/nuclear proteins (in the insoluble fractions) was confirmed as described in section 3.4.1. Consistent with previous findings, the abundance of B56α was reduced in the insoluble fraction and increased in the soluble fraction of ISO-stimulated ARVM (Figure 3.4). Furthermore, as also shown in Figure 3.4, the abundance of scaffold and catalytic subunits was also altered. Specifically, the abundance of both subunits was reduced in the insoluble fraction and increased in the soluble fraction of ISO stimulated ARVM. These results therefore suggest that β-adrenergic stimulation induces the redistribution of PP2A *complexes*. To determine whether ISO-induced redistribution is exclusive to B56α-PP2A holoenzymes, the distribution of B56γ and B56δ was also investigated (Figure 3.4). The abundance of neither subunit, in soluble and insoluble fractions, was altered by ISO stimulation. These results suggest therefore that B56γ and B56δ are not subject to translocation from insoluble to soluble subcellular compartments upon β-adrenergic stimulation. Nevertheless, the possibility that the localization of either subunit may be altered *within* a compartment cannot be excluded.

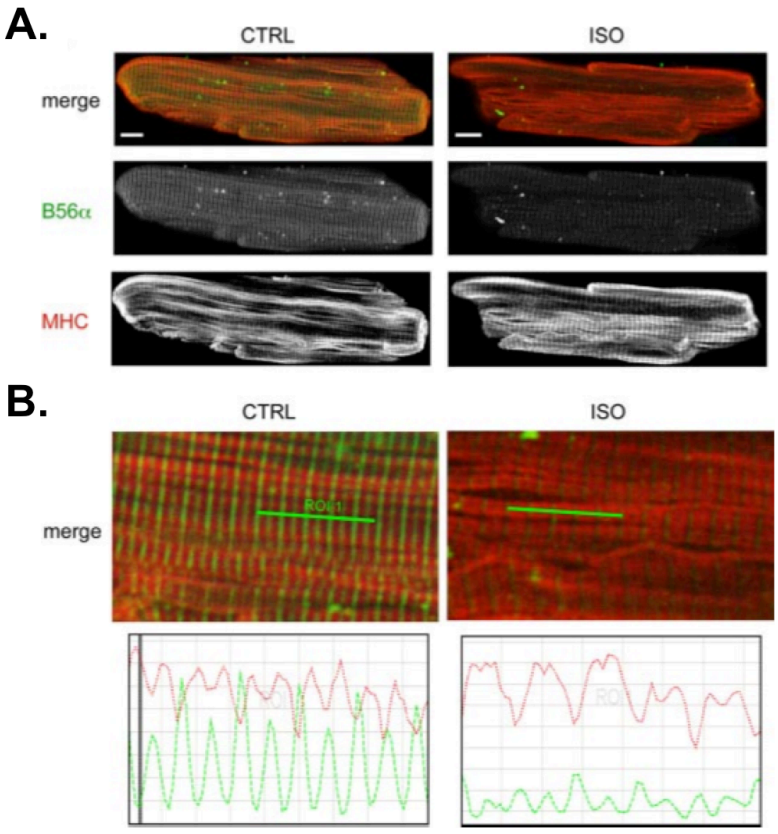

Figure 3.1 Localization of B56α in sarcomere

A. Images of isolated "skinned" ARVM after a 10 min exposure to vehicle (CTRL) or 10 nM ISO. B56α and sarcomeric myosin heavy chain (MHC) are labelled in green and red, respectively. Scale bar = 10 μm. **B.** Top panels show high magnification sections of merged images from A and bottom panels show fluorescence intensity histograms taken from the indicated region of interest (ROI). Note the localization of B56α in Z-disc and M-line regions and between the A-band regions populated by sarcomeric MHC under basal conditions, and the reduced intensity of the signal for B56α in both these regions after β-adrenergic stimulation. Figure taken from Yin et al.[166]

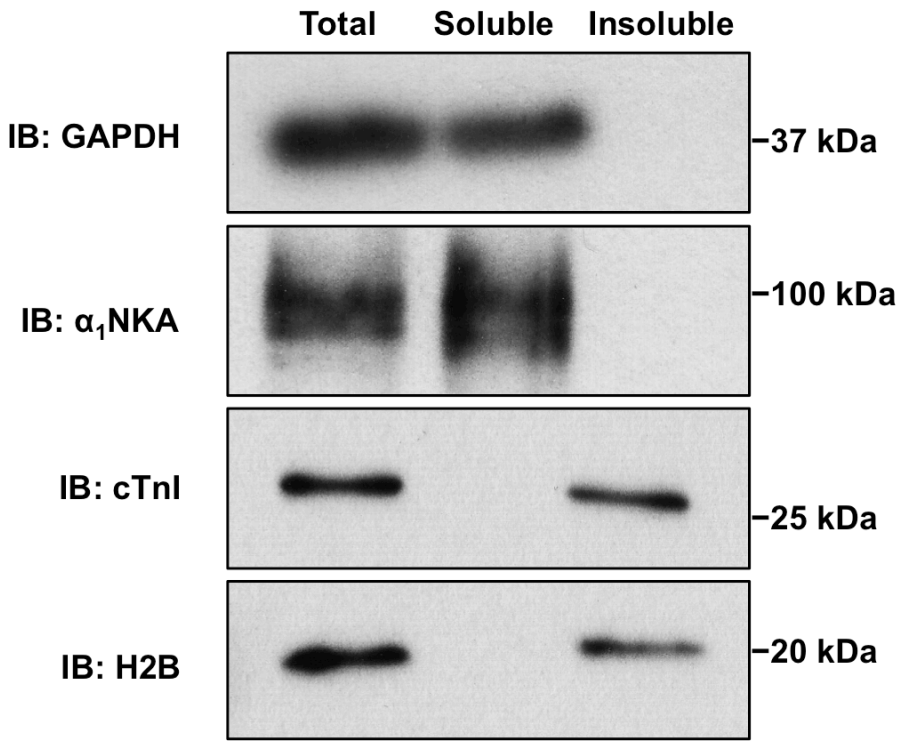

Figure 3.2 Validation of the subcellular fractionation method

ARVM were lysed in a lysis buffer containing 1% Triton-X100 and cell lysates were fractionated by centrifugation. Figure shows the distribution of GAPDH (cytosolic), α_1NKA (membrane), cTnI (myofilament) and H2B (nuclear) in soluble and insoluble subcellular fractions. Results are representative of three independent experiments.

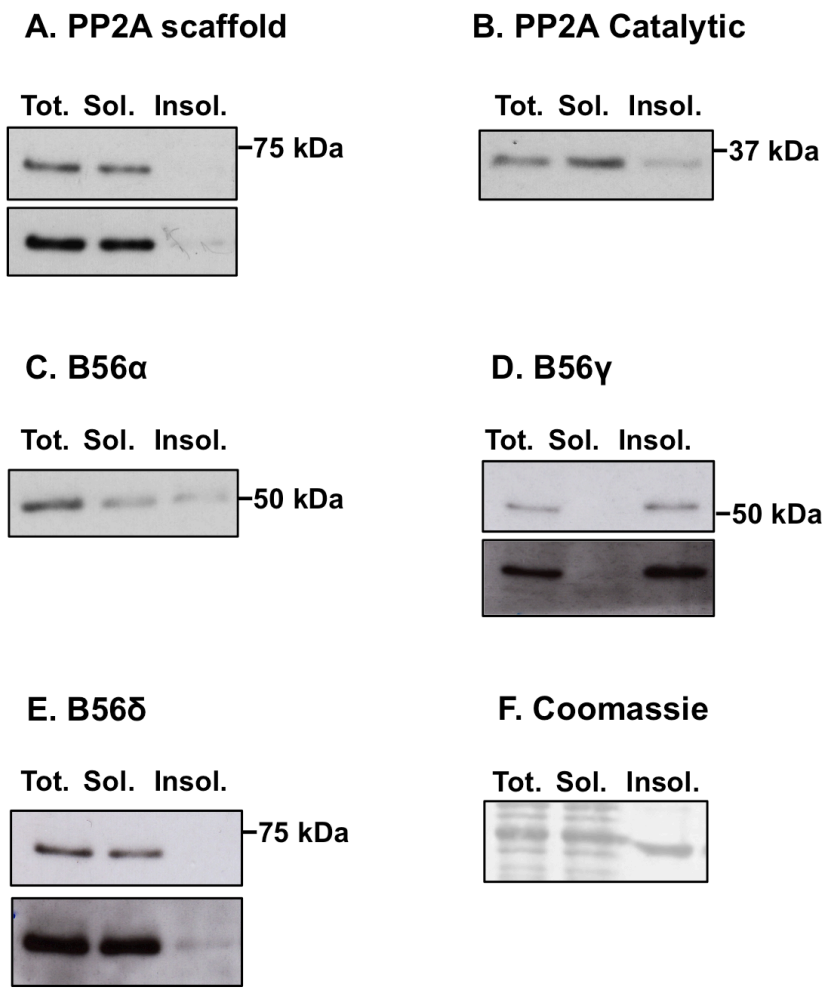

Figure 3.3 Expression and distribution of PP2A subunits in ARVM

The expression and the subcellular distribution of PP2A subunits were determined by immunoblot analysis of total and fractionated ARVM lysates, respectively. Figure shows the expression and distribution of **A.** PP2A scaffold **B.** PP2A catalytic **C.** B56α **D.** B56γ and **E.** B56δ subunits. In A, D and E, short and long exposure autoradiograms are shown. **F.** Coomassie staining of the membrane revealed global protein abundance in each lane. (n=3)

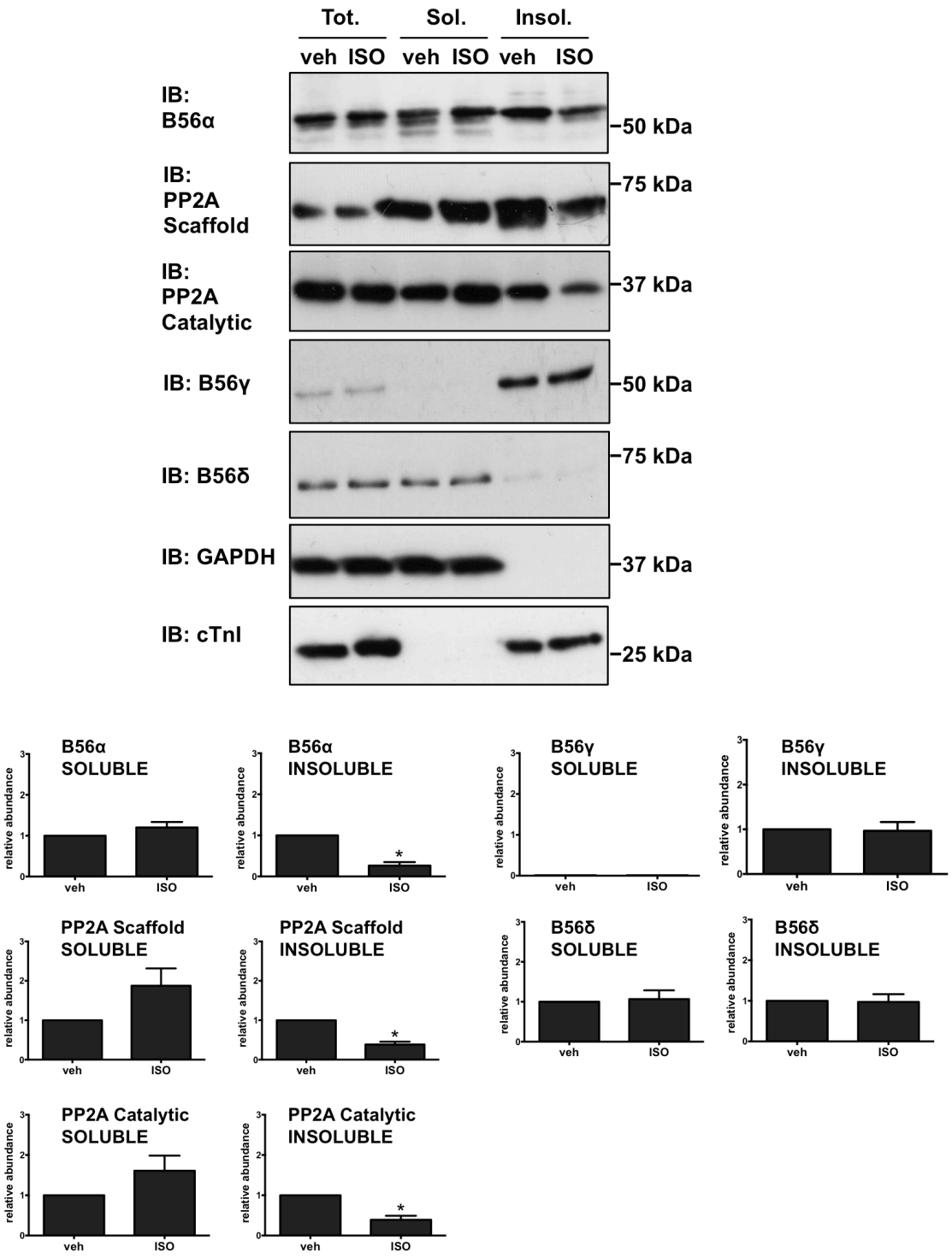
Tot.
Sol.
Insol.
veh ISO veh ISO veh ISO
IB: B56α
50 kDa
IB: PP2A Scaffold
75 kDa
IB: PP2A Catalytic
37 kDa
IB: B56γ
50 kDa
IB: B56δ
75 kDa
IB: GAPDH
37 kDa
IB: cTnI
25 kDa
B56α SOLUBLE
B56α INSOLUBLE
B56γ SOLUBLE
B56γ INSOLUBLE
PP2A Scaffold SOLUBLE
PP2A Scaffold INSOLUBLE
B56δ SOLUBLE
B56δ INSOLUBLE
PP2A Catalytic SOLUBLE
PP2A Catalytic INSOLUBLE
relative abundance
veh
ISO
*

Figure 3.4 ISO-induced translocation of PP2A subunits in ARVM

ARVM were exposed to vehicle (veh) or ISO (10 nM) for 10 min. Figure shows representative immunoblots and quantitative data for abundance of B56α, PP2A scaffold subunits, PP2A catalytic subunits, B56γ and B56δ in soluble (sol.) and insoluble (insol.) fractions of veh- and ISO-stimulated ARVM. Immunoblots of GAPDH and cTnI indicate protein loading in the soluble and insoluble fractions, respectively. Quantitative data are given as mean ± SEM. In each experiment, PP2A subunit abundance in the ISO-treated group was expressed relative to that in the corresponding veh-treated group. **P* < 0.05 versus veh (n=6).

3.5 Discussion

The work presented in this chapter reveals the protein expression and subcellular distribution of native PP2A scaffold, catalytic and regulatory B56α, -γ and -δ subunits in ARVM. The expression and subcellular distribution were determined by immunoblot analysis of total and fractionated ARVM lysates, respectively. The cells were lysed in a buffer that contained 1% Triton-X100 and fractionated by centrifugation. Using this methodology, cytosolic and membrane proteins were extracted in the soluble fraction whereas myofilament and nuclear proteins were contained in the insoluble fraction.

Under the initial experimental conditions, in which soluble and insoluble proteins were diluted in equal volumes, the relative abundance of PP2A subunits in cytosolic/membrane and myofilament/nuclear compartments was inferred. B56γ was detected exclusively in the insoluble fraction and thus, consistent with the evidence in the literature,[111,183] in ARVM this regulatory subunit is likely to target PP2A holoenzymes to myofilament and/or nuclear compartments. Scaffold, catalytic and regulatory B56α and B56δ subunits were present in both the soluble (cytosolic/membrane) and the insoluble (myofilament/nuclear) fraction (Figure 3.3). In ARVM, PP2A holoenzymes are thus widely distributed across multiple subcellular compartments, where they may be targeted to specific substrates by distinct regulatory B56 subunits.

According to the fractionation method used, ARVM appeared to comprise relatively smaller amounts of insoluble proteins. Whilst this did not impede detection of PP2A subunits in the insoluble fraction, it impaired the detection of their potential ISO-induced depletion from this fraction. To expand on previous findings and explore ISO-induced changes in abundance of PP2A subunits in the insoluble fraction, more concentrated samples were therefore prepared. In these experiments there was no significant contamination of the soluble fraction with myofilament/nuclear proteins (cTnI and H2B) or of the insoluble fraction with cytosolic/membrane proteins (GAPDH and α_1NKA). Thus, any change in the relative abundance of a given protein in these fractions could be used as a reasonable indicator of translocation between subcellular compartments. Consistent with previously published findings,[166] ISO induced the redistribution of B56α. Specifically,

this subunit was depleted from the insoluble fraction and enriched in the soluble fraction of ISO-stimulated ARVM. A novel observation in these studies was the concomitant redistribution of PP2A scaffold and catalytic subunits, suggesting that localization of B56α-containing PP2A *holoenzymes* is subject to β-adrenergic regulation (Figure 3.4).

Surprising at first, the depletion of subunits from the insoluble fraction was significant whilst the enrichment in the soluble fraction was not significant. Nevertheless, these results can be justified by considering the basal subcellular distribution of these subunits. Scaffold, catalytic and B56α subunits were markedly more abundant in the soluble fraction relative to the insoluble fraction. Therefore, what appears to be a small (not significant) proportional increase in the soluble fraction may represent a large (significant) proportional decrease in the insoluble fraction.

A recent study in which the cardiac phenotype of transgenic mice with cardiac-specific overexpression of B56α is relevant to the work described in this chapter.[172] Under basal conditions, the phosphorylation of myofilament proteins (cTnI at S23/24 and cMyBP-C at S282) was reduced in the TG hearts relative to the WT hearts. Following β-adrenergic stimulation, however, whilst the phosphorylation of these proteins was comparable in WT and TG hearts, the phosphorylation of PLB at S16 was attenuated in the latter. In light of these recent data, it is possible to speculate that ISO-induced translocation of B56α-containing PP2A may increase phosphorylation of substrates in the myofilament compartment and simultaneously reduce the phosphorylation of substrates in the cytosolic compartment

4 β-Adrenergic Regulation of B56δ Phosphorylation in ARVM

4.1 Introduction

The human gene encoding the PP2A regulatory B56δ subunit (i.e. *PPP2R5D*) is localized on chromosome region 6p21.1 and gives rise to three N-terminal splice variants through alternative splicing.[117,184,185] With 602 amino acids and a predicted molecular weight of 69,999 Da (i.e. 70 kDa) δ_1 is the longest splice variant. Relative to this splice variant, δ_2 and δ_3 lack amino acids 84-115 and 1-115, respectively.

Five consensus PKA phosphorylation sites were identified in the amino acid sequence of δ_1.[12] *In vitro,* PKA phosphorylates only four sites (S60, S75, S88 and S573) and the phosphorylation of these stimulates the dephosphorylation of substrate proteins by the pertinent holoenzyme.[114,186] In HEK293 cells, the heterologously-expressed protein is phosphorylated primarily at S573 (and only slightly at S88) following the incubation of the cells with the cAMP analogue dibutyryl cAMP.[114] Importantly, *in vitro* and in cells, the phosphorylation at S573 is necessary and sufficient to activate the holoenzyme.[114]

The phosphorylation of B56δ by PKA *in vivo* was first reported by Ahn *et al*., in isolated mouse striatal neurons.[114] In these cells PKA, activated downstream of dopamine D1 receptors, phosphorylates B56δ at S573. In contrast, in rat ovarian granulosa cells PKA phosphorylates the protein downstream of luteinizing hormone (LH) receptors.[187] The functional consequences of PKA-mediated B56δ phosphorylation at S573 in striatal neurons and ovarian cells differ and are described in the introduction to Chapter 7. The important aspect to consider in *this* chapter is the evidence that, at least in some cells, PKA, activated downstream of $G\alpha_s$ GPCRs, stimulates protein *dephosphorylation* through phosphorylation of B56δ and activation of PP2A.

4.2 Objectives

The objectives of the studies described in this chapter were to:

- Determine if stimulation with ISO induces the phosphorylation of B56δ in ARVM and the dose- and time-dependence of the response.
- Determine the relative contribution of β_1- and β_2-ARs to ISO-induced phosphorylation of B56δ.
- Determine the role of PKA, as a downstream mediator of B56δ phosphorylation.
- Investigate the subcellular distribution of B56δ in unstimulated and ISO-stimulated ARVM, by immunofluorescence.

4.3 Methods

4.3.1 ARVM isolation, culture and pharmacological treatment

For the experiments described in this chapter, ARVM were isolated from the hearts of adult male Wistar rats and cultured as described in the Methods (sections 2.1.1 and 2.1.2). The cells were exposed to vehicle or ISO (1-100 nM) for 2-60 min. Propranolol (100 nM), CGP 20712A (100 nM), ICI 118,551 (100 nM) or the appropriate vehicle was added 10 min before incubation with ISO. H89 (2-10 μM), myr-PKI (10 μM) or the appropriate vehicle was added 30 min before incubation with ISO. The cells were exposed to N^6-Benz-cAMP (100-500 μM) for 30 min. Details of the compounds used are provided in the Methods (Table 2.1). The cells were maintained at 37°C for the duration of the treatment(s). For immunoblot analysis, the cells were harvested in 2X Laemmli sample buffer (200 μl per well).

4.3.2 Mouse heart samples

Flash-frozen hearts from homozygous B56δ KO and WT littermate mice were a kind gift from Veerle Janssens (KU Leuven, Belgium).[120] Heart samples were prepared as described in the Methods (section 2.2). Samples of unstimulated and ISO-stimulated WT C57/BL6 mouse hearts were kindly provided by Dr. Karen Aughton (King's College, London). The hearts were perfused in the Langendorff mode with Krebs solution for 10 min, then with Krebs solution ± 10 nM ISO for a further 10 min.

4.3.3 Immunoblot analysis

SDS-PAGE and immunoblot analysis were performed as described in the Methods (sections 2.3.2 to 2.2.4). Phos-tag™ SDS-PAGE and immunoblot analysis was performed as described in the Methods (section 2.3.5). Details of the antibodies used are provided in the Methods (Tables 2.4 and 2.5).

4.3.3.1 **Principles of Phos-tag™ SDS-PAGE**

The principles of Phos-tag™ SDS-PAGE are shown schematically in Figure 4.1. When associated with two divalent manganese ions (Mn^{2+}), the acrylamide-pendant Phos-tag™ reagent binds phospho-monoester dianions on Ser, Thr and Tyr residues.[188] The migration of a protein through a Phos-tag™ gel therefore depends on its phosphorylation status; the more phosphorylated a protein is, the slower it will migrate through the gel. If multiple phospho-species of a particular protein are present within a sample, immunoblot analysis will reveal bands with distinct migration profiles. The slower migrating bands will contain the more-phosphorylated species whereas the faster migrating bands will contain the less-phosphorylated species.

4.3.4 Immunolabeling and confocal microscopy

For confocal microscopy studies ARVM were seeded in 28 mm dishes, as described in the Methods (section 2.1.2). The cells were fixed with 4% paraformaldehyde and were permeabilized with 0.2% Triton-X100, following a 10 min exposure to vehicle or 10 nM ISO. Immunolabeling and imaging of the cells were performed as described in the Methods (section 2.4). Details of the antibodies and fluorescent dyes used are provided in the Methods (Table 2.7 and 2.8).

4.4 Results

4.4.1 Validation of a B56δ antibody

Immunoblot analysis of cardiac B56δ was performed with an affinity-purified rabbit polyclonal antibody raised against a peptide comprising residues 552 and 602 of human B56δ (UniProt entry Q14738). Importantly, as shown in Figure 4.2, the sequence of this peptide is conserved in rat and mouse isoforms. To confirm the specificity of the antibody, ARVM samples were probed in parallel with heart samples of littermate WT and global B56δ KO mice. As shown in Figure 4.3, in both ARVM and WT mouse heart samples the antibody primarily detected a protein whose apparent molecular weight was ~70-kDa (band A). Additional weaker bands (B in ARVM; B and C in WT mouse heart) were observed at smaller molecular weights. Relative to A, the intensity of bands B and C was markedly lower and in ARVM, band B was detected only when the largest volume of sample was loaded and the film was exposed to the ECL signal for longer. None of the proteins detected by the antibody in ARVM and in the WT mouse heart were detected in the KO mouse heart. This indicated that in the former samples the antibody specifically and exclusively detected B56δ, whose full-length variant is predicted to have a molecular weight of 72-kDa in the rat.

4.4.2 Investigating ISO-induced phosphorylation of B56δ by Phos-tag™ SDS-PAGE and immunoblot analysis

As described in section 4.1, *in vitro* PKA phosphorylates B56δ at S60, S75, S88 and S573.[114,186] In primary (non-cardiac) cells, however, the kinase phosphorylates only S573.[114] ISO is an agonist at the β-ARs and thus stimulates the cAMP and PKA signaling pathway. Having shown that B56δ is expressed in ARVM at protein level, potential ISO-induced phosphorylation was explored. In the absence of phospho-specific antibodies, the Phos-tag™ SDS-PAGE and immunoblot analysis methodology (described in section 4.3.3.1) was used. Samples of ARVM exposed to vehicle or 10 nM ISO were subjected to Phos-tag™ SDS-PAGE and immunoblot analysis of B56δ was performed with the antibody described

in section 4.4.1. As shown in Figure 4.4 (panel A), in ISO-stimulated cells the predominant B56δ species migrated more slowly than in cells exposed to vehicle. These results thus indicated that ISO increased the phosphorylation of B56δ. Samples were additionally resolved by standard SDS-PAGE. As shown in Figure 4.4 (panel B), in the absence of the Phos-tag™ reagent and using the same antibody for detection, B56δ protein displayed an identical migration profile in both treatment groups and no additional bands were observed.

4.4.3 ISO-induced phosphorylation of B56δ at S573

Based on the evidence that in primary (non-cardiac) cells B56δ is phosphorylated by PKA at S573,[114] the phosphorylation of this site was investigated by immunoblot analysis with a phospho-specific antibody that recognizes B56δ phosphorylated at S573, a kind gift from Angus Nairn (The Rockefeller University, NY).[114] This corresponds to S593 in the rat sequence (Figure 4.2). To get an indication as to whether the antibody detected B56δ in ARVM, in the first experiment samples of unstimulated and ISO-stimulated ARVM were loaded in duplicate on one gel and proteins were transferred to a single membrane that was cut into two halves before immunoblot analysis. One half was probed with the total B56δ antibody and the other half was probed with the phospho-specific antibody. As shown in Figure 4.5 (panel A), the latter antibody detected a protein at the same molecular weight as the protein that was detected by the total B56δ antibody (~70-kDa, indicated by the arrow), suggesting that it recognized B56δ. Furthermore, the affinity of the phospho-specific antibody for B56δ was increased dramatically following stimulation of ARVM with ISO, as shown by the increased intensity of the signal in this sample. These results thus indicated that in ARVM B56δ is phosphorylated at S573 in response to ISO stimulation.

An additional prominent band was observed in samples of vehicle- and ISO-treated ARVM probed with the pS573 antibody. This appeared above the 75-kDa marker and the intensity of the signal did not vary with ISO stimulation. Given that the B56δ antibody did not detect this protein, it is unlikely to be an isoform of B56δ. Nevertheless, this was investigated further by probing samples of unstimulated and ISO-stimulated ARVM in parallel with samples of WT and B56δ KO mouse hearts. As shown in Figure 4.5 (panel B),

the ~70 kDa protein that was detected in ARVM by the pS573 antibody (and whose phosphorylation was increased by treatment with ISO) was detected also in the WT mouse heart, but not in the KO mouse heart. This provided confirmation that in ARVM the antibody detected B56δ phosphorylated at S573. The protein that was detected by the antibody above the 75-kDa marker in ARVM was detected in both the WT and in the B56δ KO mouse heart. This confirmed that it was not an isoform of B56δ and that the signal resulted from non-specific binding of the antibody to an unidentified cardiac protein.

In further studies B56δ phosphorylation was determined at S573 in samples of unstimulated and ISO-stimulated WT mouse hearts perfused in the Langendorff mode. These samples were probed in parallel with samples of unstimulated and ISO-stimulated ARVM; the results showed that ISO induces B56δ phosphorylation at S573 in isolated cardiac cells and hearts (Figure 4.5, panel C).

4.4.4 Dose- and time-response profiles of ISO-induced phosphorylation of B56δ at S573

Having shown that the phosphorylation of B56δ was increased at S573 in ARVM exposed to 10 nM ISO for 10 min, in subsequent studies the dose- and time-response profiles were determined. In dose-response studies, the cells were stimulated with 1, 10 or 100 nM ISO. As shown in Figure 4.6 (panel A), the ISO-induced phosphorylation of S573 was dose-dependent and was increased significantly by stimulation with a concentration of ISO that was ≥ 10 nM. In time-response studies the cells were exposed to 10 nM ISO for 2-60 min. As shown in Figure 4.6 (panel B), maximal phosphorylation of S573 occurred within 2 min and the response was sustained for at least 60 min.

4.4.5 The role of β-ARs in ISO-induced phosphorylation of B56δ at S573

To confirm that ISO-induced phosphorylation of S573 was mediated by β-ARs, the response to ISO was determined in the absence and presence of the non-selective β-AR antagonist propranolol. As shown in Figure 4.7 (panel A), in the presence of this

antagonist ISO did not cause an increase in phosphorylation of S573, confirming that ISO induced the phosphorylation of the site by stimulating β-ARs. To determine the relative contributions of β_1- and β_2-ARs, ISO-induced phosphorylation of S573 was determined in the absence and presence of the selective β_1-AR antagonist CGP 20712A (CGP)[189] or the selective β_2-AR antagonist ICI 118,551 (ICI).[190] As shown in Figure 4.7 (panel A), CGP abolished ISO-induced phosphorylation of S573. In contrast, ICI partially attenuated the response. In complementary work, the phosphorylation of cTnI at S23/24 was determined by immunoblot analysis in the same samples. As shown in Figure 4.7 (panel B), ISO induced the phosphorylation of cTnI at S23/24. As expected, the response was abolished by propranolol. The response was abolished also by CGP but was unchanged by ICI.

4.4.6 The role of PKA in ISO-induced phosphorylation of B56δ at S573

In mouse striatal neurons PKA phosphorylates B56δ at S573 downstream of dopamine D1 receptors.[114] Given that in cardiac myocytes the stimulation of β_1-AR leads to an increase in PKA activity, the role of this kinase as a potential mediator of ISO-induced phosphorylation of S573 was investigated. In initial studies, the ISO-induced change (increase) in B56δ phosphorylation at S573 was determined in the absence and presence of H89. This is a pharmacological inhibitor of PKA that competes with ATP at its binding site on PKA catalytic subunits.[191] As shown in Figure 4.8 (panel A), the ISO-induced increase in S573 phosphorylation was attenuated in the presence of H89, with a significant reduction in the magnitude of the response observed in myocytes pre-treated with 10 μM of the inhibitor. In complementary studies the ISO-induced increase in B56δ S573 phosphorylation was determined in the absence and presence of myristoylated PKI 14-22 amide (myr-PKI). This cell-permeant synthetic peptide mimics the endogenous protein kinase inhibitor peptide (PKI) and inhibits PKA by sequestering its free catalytic subunit.[191] As shown in Figure 4.8 (panel B), pre-treatment with 10 μM myr-14-22-PKI attenuated the ISO-induced increase in phosphorylation of S573. As also shown in Figure 4.8 (panel B), the ISO-induced increase in phosphorylation of cTnI at its established PKA sites (S23/24) was attenuated by a similar magnitude. Together, these data show that ISO-induced phosphorylation of S573 was reduced by compounds that inhibit PKA activity

through different mechanisms, suggesting therefore that PKA activity is necessary for the response. To determine if PKA activation is sufficient for the response, the phosphorylation of the site was determined in ARVM exposed to N^6-Benz-cAMP, a membrane-permeant PKA-selective cAMP analog.[192] As shown in Figure 4.8 (panel C), with increasing concentrations of N^6-Benz-cAMP (100, 250 or 500 μM) a dose-dependent increase in the phosphorylation of S573 was observed. As also shown in Figure 4.8 (panel C), similar increases in phosphorylation of cTnI at S23/24 were observed.

4.4.7 Subcellular distribution of B56δ in ARVM

The subcellular distribution of endogenous B56δ was determined in unstimulated and ISO-stimulated ARVM by confocal microscopy. In these studies B56δ was immunolabeled with the subunit-specific antibody that was described in section 4.4.1. To determine the integrity of the cells sarcomeric Z-discs were immunolabeled with a mouse α-actinin antibody. Nuclei were stained with DAPI. As shown in Figure 4.9 (panel A), in unstimulated ARVM B56δ is distributed throughout the cytosol and is present in nuclei. The images of ISO-stimulated cells suggest that this subcellular distribution is not altered in response to β-adrenergic stimulation (Figure 4.9, panel B). To determine the specificity of the B56δ antibody, unstimulated myocytes were incubated with an equivalent amount of non-immune (control) rabbit IgG. The Cy5 fluorescence in these cells was determined using identical microscope settings. As shown in Figure 4.9 (panel C), although some fluorescence was detected, this was minimal. The possibility that B56δ fluorescence resulted from a non-specific interaction between rabbit IgG domains and cellular proteins was therefore excluded.

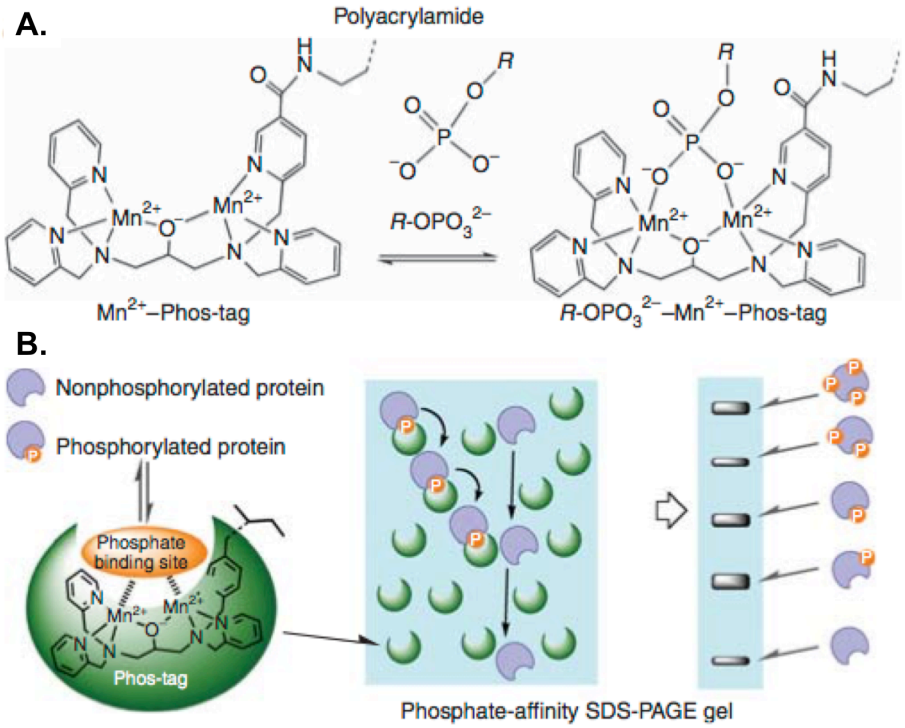

Figure 4.1 Principles of Phos-tag™ SDS-PAGE

A. Structure of the polyacrylamide-bound Mn^{2+}-Phos-tag complex and the reversible trapping of phospho-monoester dianions ($R\text{-}OPO_3^{2-}$). **B.** Mn^{2+}-Phos-tag traps phospho-proteins in polyacrylamide gels and thereby retards their migration. The more phosphorylated a protein is, the slower it will migrate through the gel. Figure taken from Kinoshita *et al.*[188]

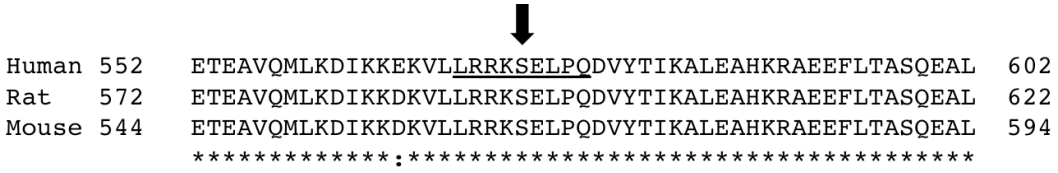

Figure 4.2 Amino acids at the C-terminus of human, mouse and rat B56δ

The B56δ antibody is raised against a peptide comprising residues 552 and 602 of human B56δ. The phospho-specific (pS573) B56δ antibody is raised against a phospho-peptide comprising residues 569 and 577 of human B56δ (underlined). Arrow indicates the Ser residue phosphorylated by PKA in cells. Asterisks indicate identical amino acids. UniProt entries: human (Q14738), mouse (Q91V89), rat (Q499R1).

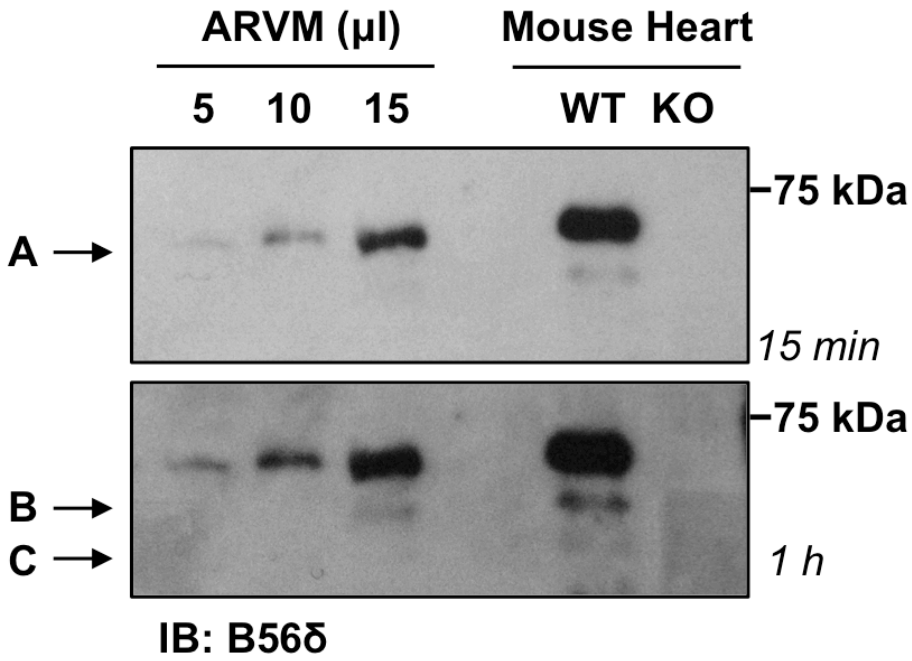

Figure 4.3 Validation of a B56δ antibody

Increasing volumes (5, 10 or 15 µl) of an ARVM sample and equal volumes of WT and B56δ KO heart samples were subjected to SDS-PAGE. Immunoblot analysis of B56δ was performed with an affinity-purified rabbit polyclonal antibody. Figure shows detection of proteins by this antibody in ARVM and in the WT mouse heart. In both species the antibody primarily detected a protein whose apparent molecular weight was ~70-kDa (band A). Additional, less-abundant proteins were also detected at lower molecular weights (bands B and C). The absence of these from the KO mouse heart confirmed that in ARVM and in the WT mouse heart the antibody specifically and exclusively detected B56δ. (n=1)

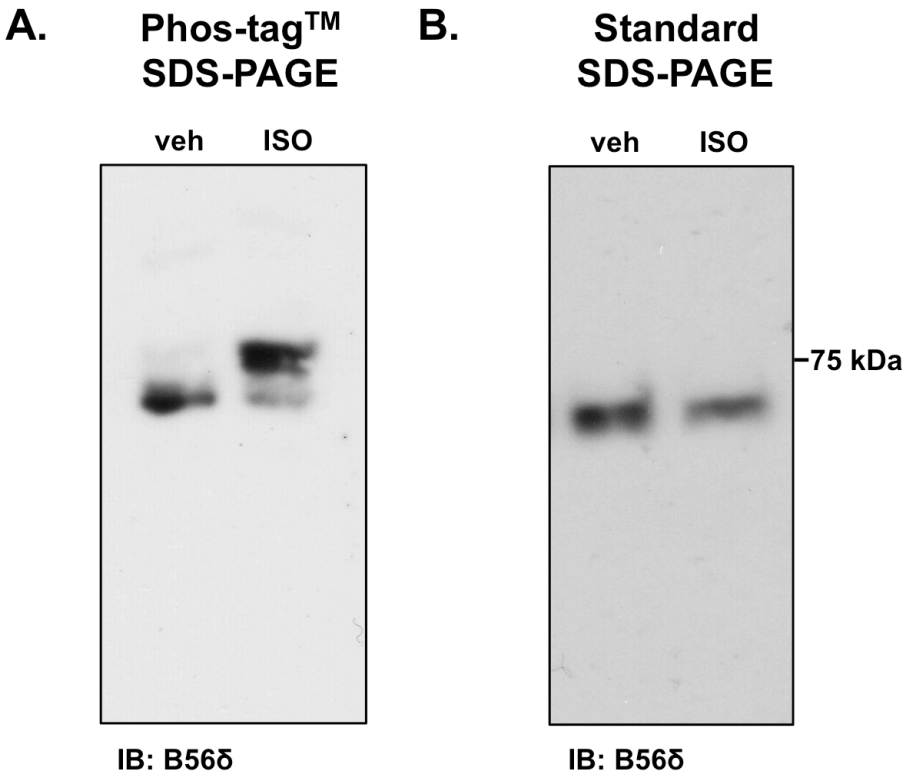

Figure 4.4 Investigating ISO-induced phosphorylation of B56δ by Phos-tag™ SDS-PAGE and immunoblot analysis

ARVM were exposed to vehicle (veh) or ISO (10 nM) for 10 min. Figure shows B56δ detected by immunoblot analysis in samples resolved by **A**. Phos-tag™ SDS-PAGE and **B.** Standard SDS-PAGE. (n=1)

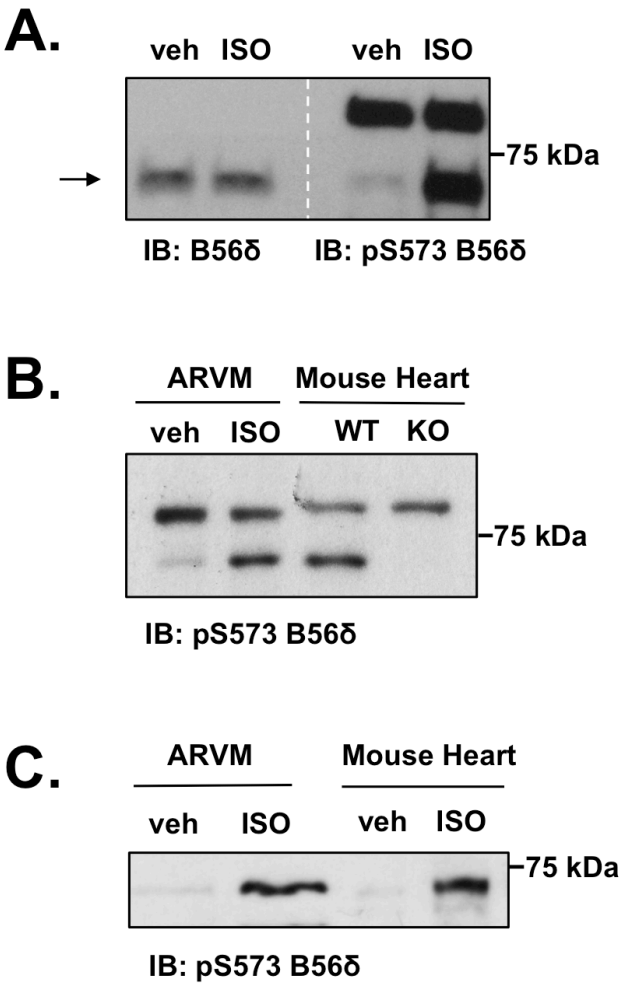

Figure 4.5 ISO-induced phosphorylation of B56δ at S573

ARVM were exposed to vehicle (veh) or ISO (10 nM) for 10 min. A. Samples were resolved on one gel and proteins were transferred to a single membrane that was cut into two halves before immunoblot analysis. Figure shows B56δ and B56δ phosphorylated at S573, as detected by immunoblot analysis with the B56δ antibody (left) and pS573 B56δ antibody (right), respectively. Arrow indicates ~70-kDa protein detected by both antibodies. B. Detection of proteins by the pS573 B56δ antibody in ARVM and in WT and B56δ KO mouse hearts. C. ISO-induced phosphorylation of B56δ at S573 in ARVM and in the Langendorff-perfused mouse heart.

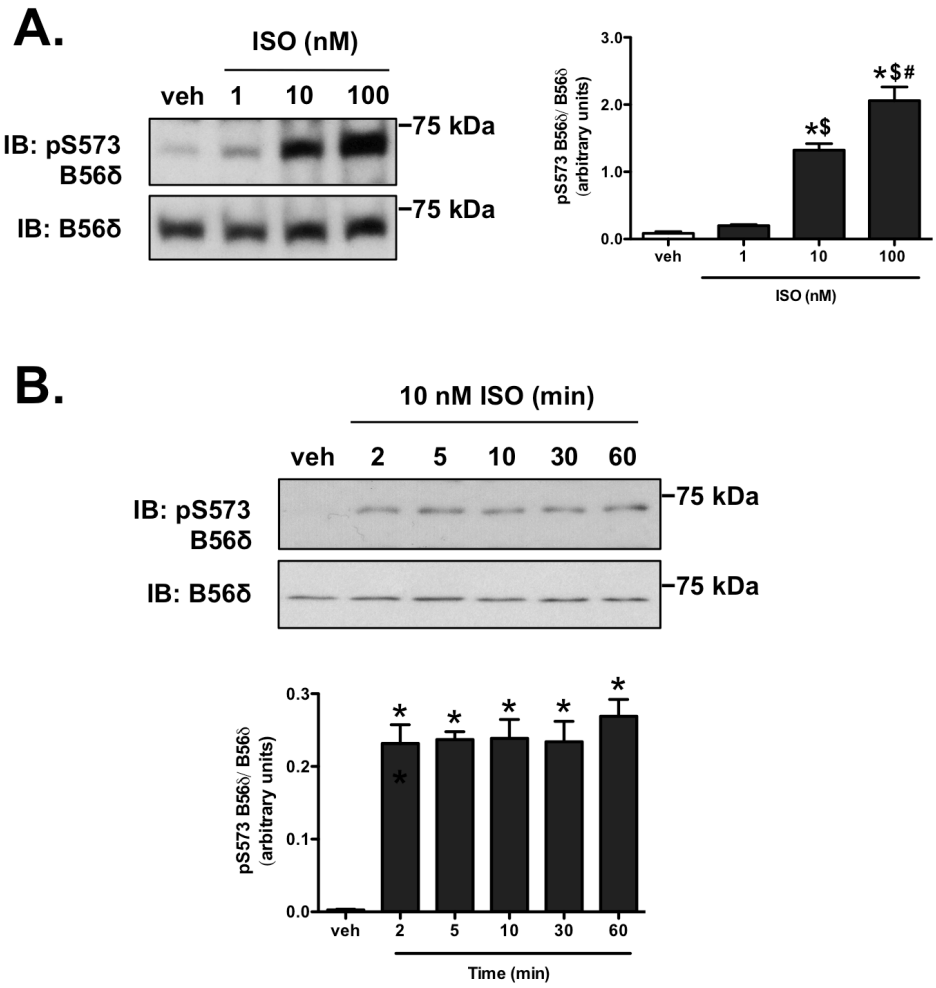

Figure 4.6 Dose- and time-response profiles of ISO-induced phosphorylation of B56δ at S573

A. ARVM were exposed to vehicle (veh) or ISO (1-100 nM) for 10 min. Figure shows representative immunoblot and quantitative data for B56δ phosphorylation at S573. **P*<0.05 versus veh, $^{\$}$*P*<0.05 versus 1 nM ISO, $^{\#}$*P*<0.05 versus 10 nM ISO (n=3). **B.** ARVM were exposed to veh for 60 min or ISO (10 nM) for 2-60 min. Figure shows representative immunoblots and quantitative data (mean ± SEM) for B56δ phosphorylation at S573. **P*<0.05 versus veh (n=3). In A and B, the signal generated by the phospho-specific antibody was normalized to the signal generated by the antibody detecting the total protein.

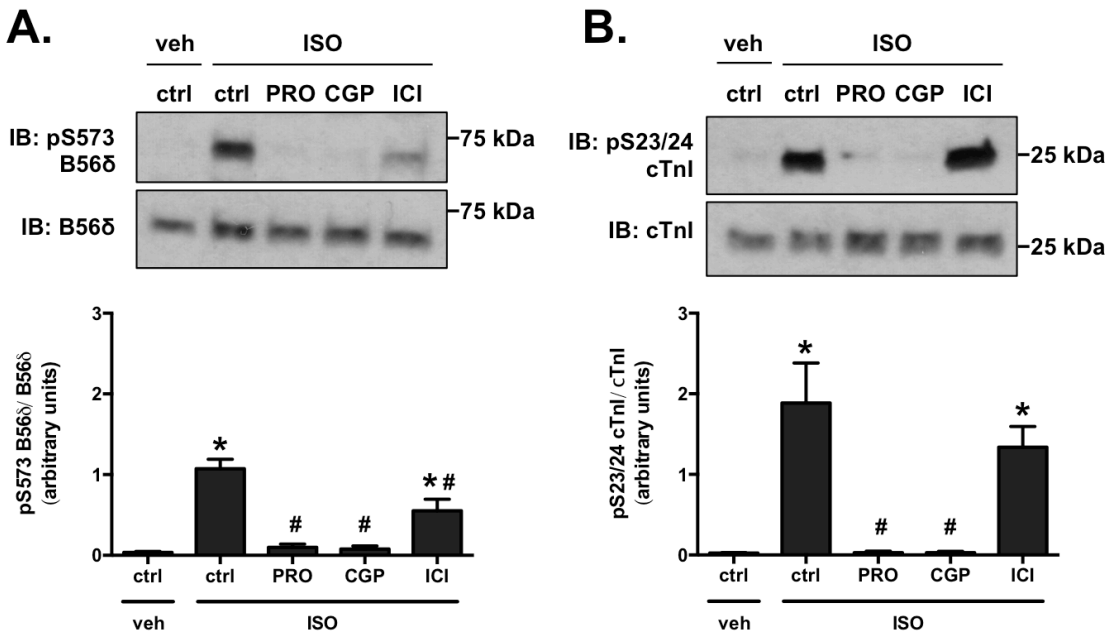

Figure 4.7 The role of β-ARs in ISO-induced phosphorylation of B56δ at S573

ARVM were exposed to vehicle (veh) or ISO (10 nM) for 10 min, following a 10 min pre-treatment with a β-AR antagonist or control (ctrl). Data show the effect of the non-selective β-AR antagonist propranolol (PRO, 100 nM), the β_1-selective antagonist CGP 20712A (CGP, 100 nM) and the β_2-selective antagonist ICI 118,551 (ICI, 100 nM) on ISO-induced phosphorylation of **A.** B56δ at S573 and **B.** cTnI at S23/24. Figures show representative immunoblots and quantitative data (mean ± SEM) for protein phosphorylation. *P<0.05 versus ctrl and vehicle, #P<0.05 versus ctrl and ISO (n=7). In A and B, the signal generated by the phospho-specific antibody was normalized to the signal generated by the antibody detecting the total protein.

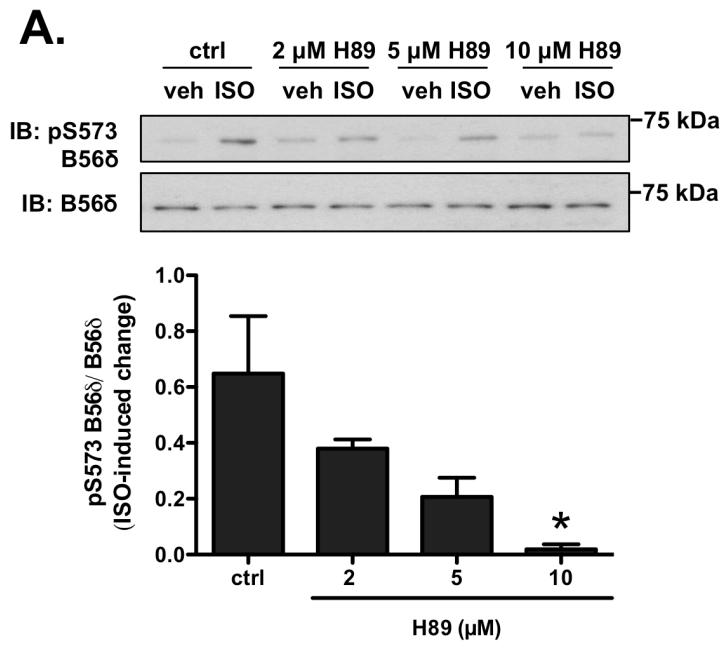
A.
ctrl
2 μM H89
5 μM H89
10 μM H89
veh ISO
veh ISO
veh ISO
veh ISO
IB: pS573 B56δ
75 kDa
IB: B56δ
75 kDa
pS573 B56δ/ B56δ (ISO-induced change)
1.0
0.8
0.6
0.4
0.2
0.0
*
ctrl
2
5
10
H89 (μM)

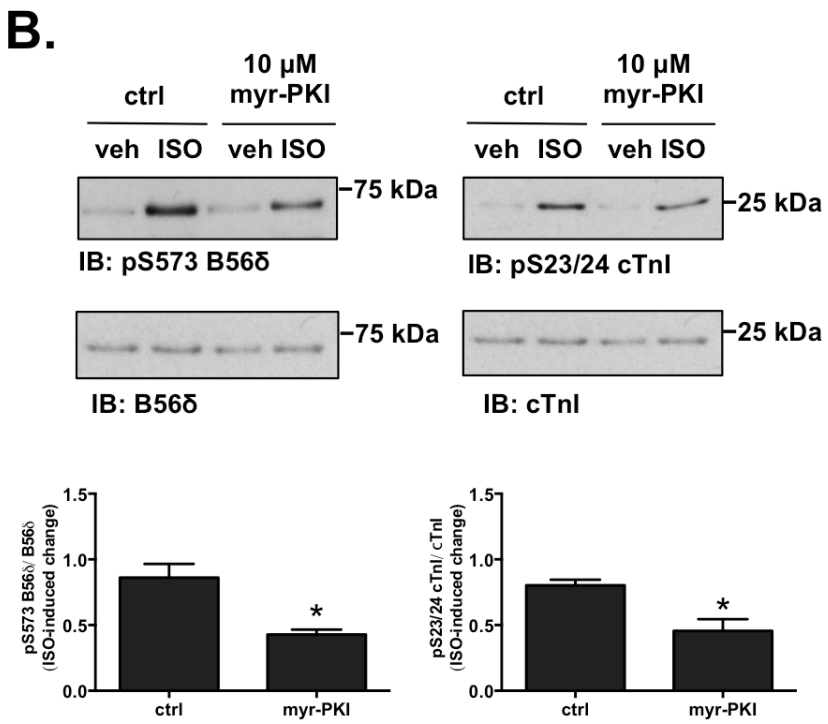
B.
ctrl
10 μM myr-PKI
veh ISO
veh ISO
75 kDa
IB: pS573 B56δ
75 kDa
IB: B56δ
ctrl
10 μM myr-PKI
veh ISO
veh ISO
25 kDa
IB: pS23/24 cTnI
25 kDa
IB: cTnI
pS573 B56δ/ B56δ (ISO-induced change)
1.5
1.0
0.5
0.0
*
ctrl
myr-PKI
pS23/24 cTnI/ cTnI (ISO-induced change)
1.5
1.0
0.5
0.0
*
ctrl
myr-PKI

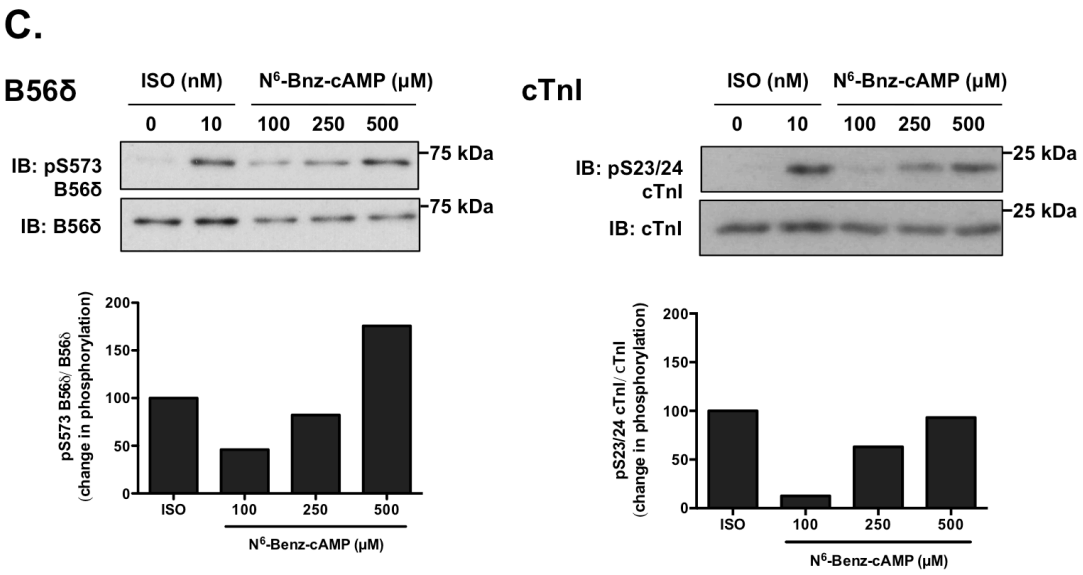

Figure 4.8 The role of PKA in ISO-induced phosphorylation of B56δ at S573

In A and B, ARVM were exposed to vehicle (veh) or ISO (10 nM) for 10min, following a 30 min pre-treatment with an inhibitor of PKA or control (ctrl). In C, ARVM were exposed to ISO (10 nM) for 10 min or to an activator of PKA or ctrl for 30 min. **A.** Effect of the PKA inhibitor H89 (2, 5 or 10 μM) on ISO-induced change in B56δ phosphorylation at S573. **B.** Effect of the PKA inhibitor myr-PKI (10 μM) on ISO-induced change in phosphorylation of B56δ at S573 and cTnI at S23/24. **C.** Effect of the PKA activator N^6-Benz-cAMP (100, 250 or 500 μM) on phosphorylation of B56δ at S573 and cTnI at S23/24. Bar charts show the change in phosphorylation induced by ISO or N^6-Benz-cAMP (n=1). In A and B, figures show representative immunoblots and quantitative data (mean ± SEM) for ISO-induced change in phosphorylation. $P<0.05$ versus ctrl (n = 4).

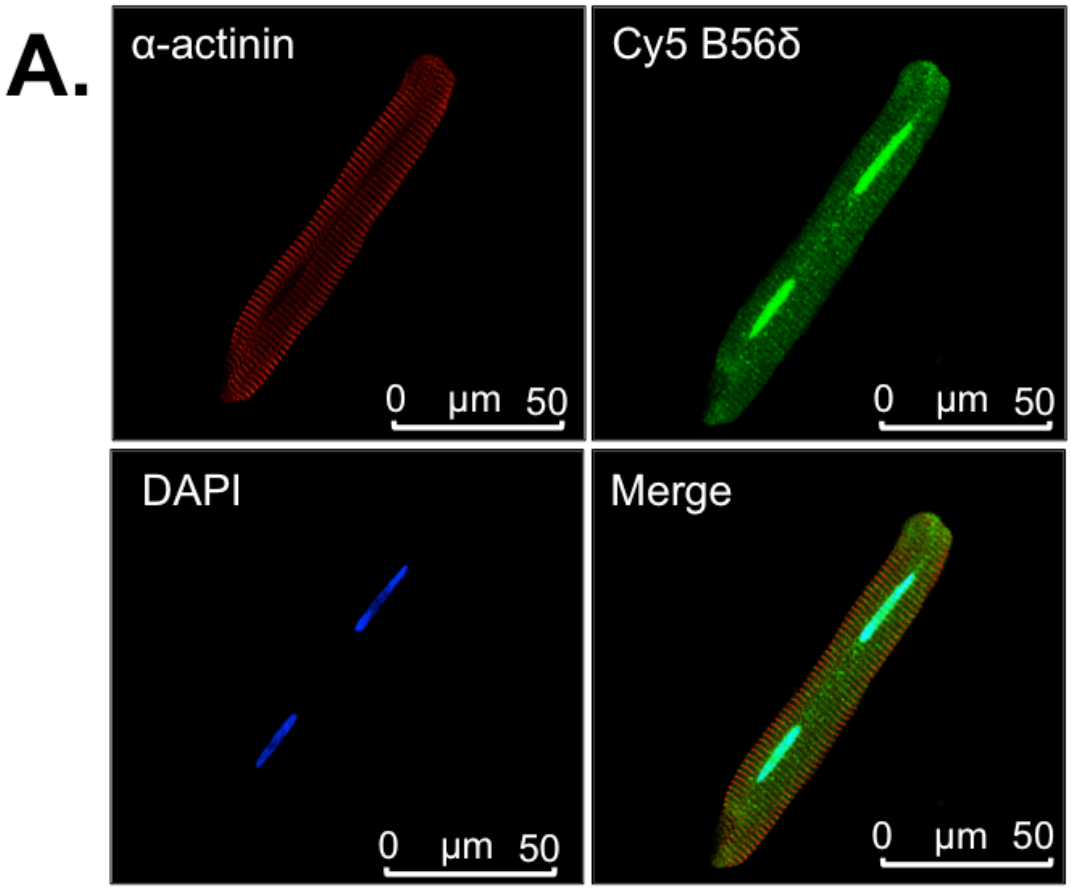
A.
α-actinin
0 µm 50
Cy5 B56δ
0 µm 50
DAPI
0 µm 50
Merge
0 µm 50

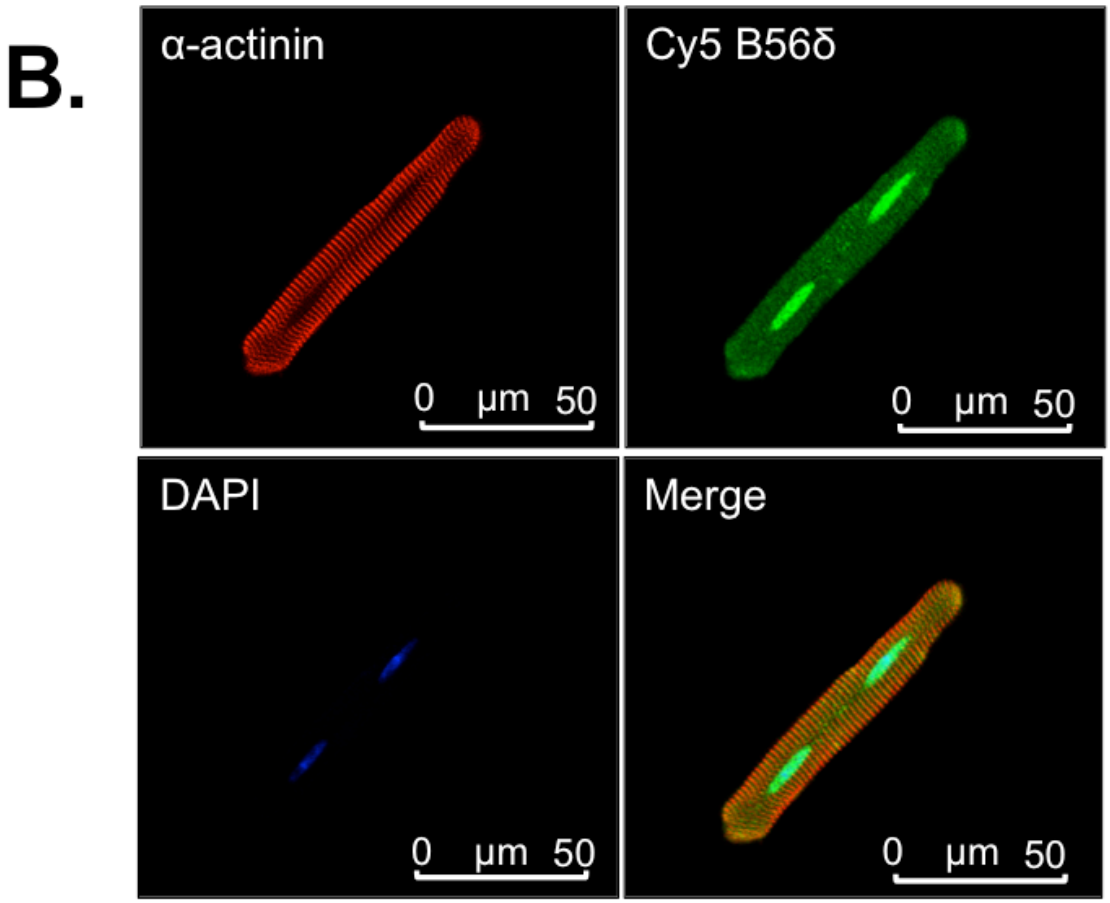
B.
α-actinin
0 µm 50
Cy5 B56δ
0 µm 50
DAPI
0 µm 50
Merge
0 µm 50

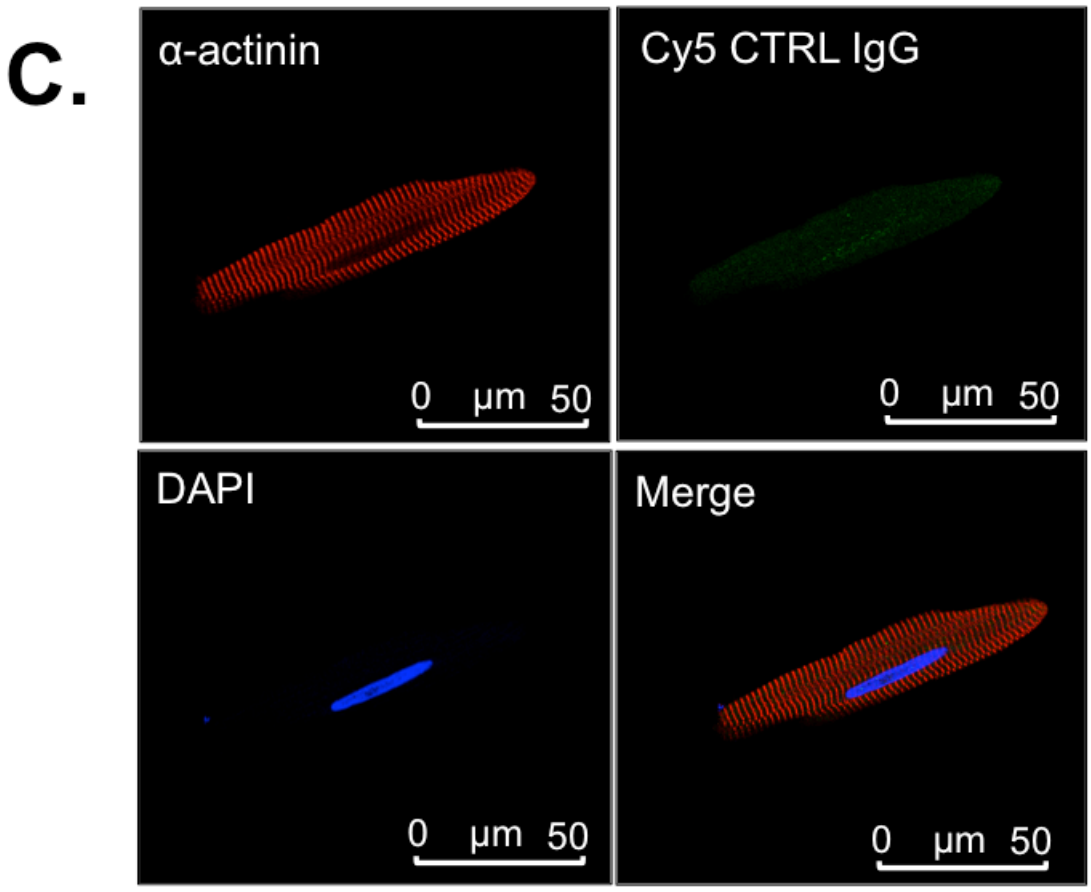

Figure 4.9 Localization of B56δ in ARVM

Representative images of ARVM after a 10 min exposure to **A.** Vehicle or **B.** ISO (10 nM). Fixed and permeabilized cells were immunolabeled with mouse α-actinin and rabbit B56δ primary antibodies and Cy3-anti-mouse and Cy5-anti-rabbit secondary antibodies. Nuclei were stained with DAPI. DAPI-stained nuclei (blue), Cy3-labeled α-actinin (red) and Cy5-labelled B56δ (green) are shown in separate channels. A merged imaged is also shown. **C.** Fixed and permeabilized (unstimulated) cells were immunolabeled as described above, with the exception that the rabbit anti-B56δ primary antibody was replaced with an equivalent amount of non-immune (control, CTRL) rabbit IgG.

4.5 Discussion

The work presented in this chapter shows β-adrenergic regulation of B56δ phosphorylation in ARVM and mouse heart. The expression of B56δ was determined by immunoblot analysis with an antibody that recognizes a sequence at the C-terminus of the human protein, which is also present in rat and mouse isoforms. In ARVM this antibody detected a protein whose apparent molecular weight corresponded to the predicted molecular weight of full-length rat B56δ (i.e. 72-kDa). Importantly, all proteins that were detected in ARVM and in the WT mouse heart were not detected in the B56δ KO mouse heart, indicating that the antibody specifically and exclusively detected B56δ (Figure 4.3).

The three splice variants of human B56δ differ at the N-terminus.[184,185] The sequence that is recognized by the B56δ antibody, at the C-terminus of δ_1, is conserved in δ_2 and δ_3. Therefore, if additional (N-terminal) splice variants of B56δ had been expressed in ARVM, these would have been detected. However, immunoblots of B56δ suggest that only the full-length (72-kDa) variant is expressed in ARVM at protein level. Nevertheless, the possibility that additional splice variants are expressed at levels that are below the antibody's limit of detection cannot be excluded. Related to this, in the sample of WT mouse heart, which contained more protein, multiple proteins, likely to have been splice variants of B56δ, were detected.

The stimulation of β-ARs drives cAMP and PKA signaling in cardiac myocytes.[7] Based on this principle and on evidence that in non-cardiac cells PKA phosphorylates B56δ,[114,187] the phosphorylation of B56δ was explored in ARVM exposed to the β-AR agonist ISO. To initially determine whether B56δ was phosphorylated in response to ISO stimulation the Phos-tag™ SDS-PAGE and immunoblot analysis method was used. The results of these studies showed that the migration of B56δ was reduced in ISO-treated myocytes, indicating that its phosphorylation was increased (Figure 4.4). Although in primary cells (mouse neurons) PKA phosphorylates B56δ only at S573, in HEK293 incubated with a cAMP analog a small increase in S88 phosphorylation was reported.[114] By using the Phos-tag™ methodology it is possible to determine the existence of multiple phospho-species of

a particular protein.[193] In this instance, due to a lack of better sample resolution, it was not possible to determine whether B56δ is phosphorylated at multiple sites in ARVM.

Further studies of the specific site of phosphorylation were guided by evidence that in primary cells PKA, activated downstream of $G\alpha_s$ GPCRs, phosphorylates B56δ at S573.[114] By using an antibody that detects B56δ phosphorylated at S573, increased phosphorylation of this site was observed in ARVM exposed to physiologically relevant concentrations of the β-AR agonist ISO (Figure 4.5). Although its relevance is beyond the scope of this discussion, the phospho-specific antibody (raised against the phospho-peptide LRRKpSELPQ, Figure 4.2) recognized an additional protein in ARVM and mouse hearts. Based on the strong intensity of the signal that resulted from its detection, this protein is likely to be maximally phosphorylated under basal conditions.

The ISO-induced phosphorylation of B56δ at S573 was characterized using tools to interfere with elements of the β-adrenergic signaling pathway. By using propranolol to block all β-ARs, the phosphorylation of B56δ at S573 was shown to depend on activation of these receptors. By using CGP and ICI to selectively block β_1- or β_2-ARs, respectively, the phosphorylation was shown to depend primarily on stimulation of β_1-ARs, with a small contribution made by β_2-ARs (Figure 4.7). In our dose-response studies in ARVM, we found that 100 nM CGP was sufficient to abolish the increase in cTnI phosphorylation that is induced by 10 nM ISO. Since increased phosphorylation of myofilament proteins (including cTnI) occurs primarily downstream of β_1-AR stimulation,[40] this finding indicates that 100 nM CGP is sufficient to block β_1-AR stimulation by 10 nM ISO in ARVM. Previous work has shown that isoprenaline has comparable affinity for β_1- or β_2-ARs when expressed at comparable abundance in a given cell type.[194] Furthermore, the affinity of CGP for the β_1-AR subtype (pK$_i$ 8.5-9.3) is comparable to that of ICI for the β_2-AR subtype (pK$_i$ 8.3-9.2).[195] Thus, we reasoned that a 100 nM concentration of ICI should be sufficient to block β_2-AR stimulation by 10 nM ISO in ARVM, particularly since the density of β_2-ARs is markedly lower than that of β_1-ARs in this cell type.[41] Nevertheless, in the absence of direct evidence from a robust readout of β_2-AR activity in ARVM, we cannot be certain that a 100 nM concentration of each subtype-selective antagonist achieved comparable antagonism of ISO effects at β_1- versus β_2-ARs.

To study the role of PKA in ISO-induced phosphorylation of B56δ at S573 this response was determined in the absence and presence of the PKA inhibitor H89. The concentration of H89 that has been used to inhibit PKA in ARVM is 10 μM[196,197] and indeed, a significant reduction in phosphorylation of B56δ at S573 was attained by using the inhibitor at such concentration. However, H89 is non-selective and many off-targeted effects have been described.[198,199] Importantly, antagonistic activity at β_1- and β_2-ARs has been reported.[200] Therefore, an alternative inhibitor of PKA (myr-PKI) was used. The results from these complementary studies showed that by inhibiting PKA, the increase in B56δ phosphorylation at S573 was attenuated. The phosphorylation of cTnI at the sites that are phosphorylated by PKA in β-adrenergic signaling (S23/24)[47] was determined as readout of PKA activity. As expected, the ISO-induced increase in cTnI phosphorylation was blunted in the presence of myr-PKI. Importantly, the increase in phosphorylation of cTnI (S23/24) and B56δ (S573) was blunted by a similar magnitude, indicating that the observed reduction in phosphorylation of B56δ reflected maximal PKA inhibition. In parallel studies the effect of direct PKA activation on B56δ S573 phosphorylation was explored. By using N^6-Benz-cAMP to activate PKA, phosphorylation of B56δ at S573 was increased. Taken together, these data showed that in ARVM PKA is necessary and sufficient for the phosphorylation of B56δ at S573 downstream of stimulated β-ARs (Figure 4.8).

Dynamic changes in the subcellular distribution of PP2A subunits occur in ARVM in response to stimulation of different receptors. For example, PP2A catalytic subunits are enriched at the intercalated disk regions in response to stimulation of adenosine A1 receptors.[162] More relevant to this thesis, the subcellular localization of the regulatory B56α subunit is altered in response to stimulation of β-ARs (Chapter 3).[166] Immunolabeled B56δ appeared to be distributed throughout the myocyte and was enriched in nuclei (Figure 4.9). This widespread distribution, which has been observed also in rat brain cells[201] and in neuronally differentiated PC12 cells,[120] may suggest that in ARVM B56δ-PP2A regulates the phosphorylation of proteins in different subcellular compartments. Furthermore, in the absence of apparent differences in distribution of B56δ in ISO-stimulated ARVM, it is likely that in these cells PKA-mediated phosphorylation of B56δ at

S573 alters the activity of its associated catalytic subunit, without a change in its subcellular localization.

5 Construction and Characterization of Novel Adenoviral Vectors

5.1 Introduction

The studies in the previous chapter revealed that in cardiac cells endogenous B56δ is phosphorylated at S573 by PKA, primarily downstream of stimulated β_1-ARs. *In vitro* and in transfected HEK293 cells, the phosphorylation of B56δ at S573 by PKA stimulates the activity of the associated catalytic subunit, inducing dephosphorylation of substrate proteins.[114,186] Although it may be predicted that also in cardiac cells the phosphorylation of B56δ at S573 would lead to increased activity of B56δ-containing PP2A, the impact of such phosphorylation on the subcellular localization of the holoenzyme, protein phosphorylation and function in β-adrenergic signaling is unknown.

The functional role of B56δ S573 phosphorylation *in vivo* has thus far been determined only in the mouse striatum.[114] In these studies flag-tagged B56δ in WT or quad-mutant (non-phosphorylatable form) was heterologously expressed in striatal neurons by adeno-associated virus-mediated gene transfer.[114] *In vivo* endogenous B56δ is phosphorylated by PKA only at S573;[114] nevertheless, in the heterologous non-phosphorylatable protein S60, S75 and S88, which are phosphorylated by PKA *in vitro*, were also rendered non-phosphorylatable.[114]

Determination of the role of B56δ phosphorylation at S573 in cardiac cells requires the expression of a B56δ variant that has been rendered non-phosphorylatable through a single amino acid substitution (S573A). The work described in this chapter describes the construction and characterization of novel adenoviral vectors to allow the heterologous expression of B56δ in WT or non-phosphorylatable form in ARVM.

5.2 Objectives

The objectives of the studies described in this chapter were to:

- Construct adenoviral vectors that express GFP-tagged human B56δ in WT or non-phosphorylatable (S573A) form, referred to as AdV.GFP-B56δ-WT and AdV.GFP-B56δ-SA, respectively.
- Determine expression and ISO-induced phosphorylation of GFP-B56δ-WT and GFP-B56δ-SA at S573A in ARVM.
- Determine the impact of heterologous expression of GFP-tagged WT and S573A B56δ on protein expression profiles of selected PP2A subunits in ARVM.

5.3 Methods

5.3.1 Construction of adenoviral vectors

5.3.1.1 **Principles of the AdEasy system**

The construction of replication-defective adenoviral vectors using the AdEasy system involves (i) cloning a GOI into one of four shuttle vectors and (ii) transferring the GOI into the adenovirus genome; typically the human AdV genome, lacking the E1 and E3 genes.[202] The recombinant shuttle vector is linearized with *Pme*I and transformed into *E. coli* BJ5183 cells, which contain the adenoviral backbone plasmid pAdEasy-1. In these cells, recombinant adenoviral DNA (rAd-GOI) is generated by homologous recombination. The transformed cells are selected for kanamycin resistance (provided by the shuttle vector DNA) and recombinants are identified by digestion with appropriate restriction enzymes. rAd-GOI is linearized with *Pac*I, to expose the inverted terminal repeats (ITR), and transfected into HEK293 cells. These express recombinant adenovirus E1 and can thus amplify adenoviral DNA that lacks the E1 gene.[202] A schematic overview of the AdEasy system is provided in Figure 5.1.

5.3.1.2 **Methodology**

Adenoviral vectors were constructed as described in the Methods (section 2.5). In brief, pEGFP-C1, carrying the human gene for B56δ in WT form (UniProt entry Q14738), was used as template DNA for site-directed mutagenesis, to substitute the Ser at position 573 with Ala. GFP-B56δ-WT and GFP-B56δ-SA cDNA was amplified by PCR from the original pEGFP-C1 plasmid and the mutated pEGFP-C1 plasmid, respectively. Amplification was confirmed by DNA electrophoresis (Figure 5.2). The amplified cDNA (also referred to as GOI) and pShuttle-CMV, both digested with *Kpn*I and *Not*I, were ligated by T4 DNA ligase. Subcloning efficiency DH5α competent cells were transformed with 5 µl of the ligation product after and mini-preps were performed to isolate plasmid DNA from bacterial cells. To identify clones that contained pShuttle-CMV-GOI, 5 µl of plasmid DNA was digested with *Bgl*II and products of the digestion were resolved by electrophoresis. Positive clones, whose digestion with *Bgl*II yielded a 750 bp fragment (Figure 5.3), were linearized with

*Pme*I and transformed into *E.coli* BJ5183-AD-1 electrocompetent cells, for homologous recombination with pAdEasy-1. Well-isolated small colonies, which are most likely to contain recombinant adenoviral DNA (rAd-GOI), were inoculated into LB-kanamycin and mini-preps were performed to isolate plasmid DNA. To confirm that homologous recombination had occurred, the size of the supercoiled DNA was checked by electrophoresis on a 0.8% TAE gel. Candidate recombinants, which yielded a product that was larger than the 12 kb marker, were validated by digestion with *Pac*I. True recombinants, which yielded a 4.5 or 3 kb product and a product > 30 kb (Figure 5.4), were transformed into DH5α cells and mini-preps were performed to isolate plasmid DNA. For packaging of the adenovirus particles, *Pac*I-digested rAd5-GOI was transfected into HEK293 cells. These were maintained at 37^{o}C and harvested when significant cytopathic effects (and expression of GFP) were observed. The adenovirus was amplified in the same cell line and purified by CsCl density gradient ultracentrifugation. The infectious titer of the purified adenoviruses was determined by performing the $TCID_{50}$ assay. Titers of 3.2 x 10^{9} and 2.18 x 10^{10} PFU/mL were obtained for AdV.GFP-B56δ-WT and AdV.GFP-B56δ-SA, respectively.

5.3.2 ARVM isolation, culture, infection with adenoviruses and stimulation

For the experiments described in this chapter, ARVM were isolated from the hearts of adult male Wistar rats and cultured as described in the Methods (sections 2.1.1 and 2.1.2). However, in some experiments the cells were maintained in culture for 42 h. Infection with adenoviral vectors was performed as described in the Methods (section 2.1.3). ARVM were exposed to vehicle or 10 nM ISO (10 min, 37^{o}C) 18 h post-infection. For immunoblot analysis of protein expression and phosphorylation the cells were harvested in 2X Laemmli sample buffer (200 µl per well).

5.3.3 Immunoblot analysis

SDS-PAGE and immunoblot analysis were performed as described in the Methods (sections 2.3.2 to 2.3.4). For the experiments described in this chapter, proteins were

transferred to the support membrane by the semi-dry transfer method. Details of the antibodies used are provided in the Methods (Tables 2.4 and 2.5).

5.4 Results

Although the initial objective was to characterize expression of GFP-tagged WT and S573A B56δ in parallel, this was prevented by difficulties encountered in constructing AdV.GFP-B56δ-SA. Thus, whilst the construction of this adenoviral vector was re-attempted, studies were begun with AdV.GFP-B56δ-WT.

5.4.1 Characterization of AdV.GFP-B56δ-WT

Heterologous expression of GFP-tagged WT B56δ in ARVM was achieved by infection with the adenoviral vector that encodes human B56δ fused to GFP at the N-terminus (AdV.GFP-B56δ-WT). In a first experiment, ARVM were infected with an increasing dose of the adenovirus (MOI 0-500); the cells were harvested at either 18 or 42 h post-infection and the protein expression was determined by immunoblot analysis. To confirm that the full-length epitope-tagged protein was expressed and determine its abundance relative to that of endogenous B56δ, the samples were subjected to immunoblot analysis with the B56δ antibody. As shown in Figure 5.5 (panel A), the antibody detected faster-migrating (endogenous) B56δ at ~70-kDa, and slower-migrating (heterologous) B56δ at ~100-kDa. The latter corresponds to the predicted molecular weight of GFP-B56δ, indicating that the full-length fusion protein is expressed in ARVM. The results showed that the expression of heterologous B56δ increased with increasing dose of adenovirus in the first 18 h of infection, and was comparable in abundance to the endogenous protein at MOI 30-50. Furthermore, the expression of endogenous B56δ was similar in all samples, including uninfected cells. At the 42-hour time point the expression of heterologous B56δ was increased further and some apparent degradation products were observed. As an alternative and complementary way to monitor the expression of the heterologous protein the cells were imaged on a fluorescence microscope. As shown in Figure 5.5 (panel B), GFP fluorescence was negligible with a MOI of 30 at 18 h post-infection and a robust fluorescence was observed 42 h post-infection only in myocytes infected with a MOI of 500.

To further characterize the adenoviral vector the expression of non-B56δ PP2A subunits (i.e. scaffold, catalytic and regulatory B56α and -γ subunits) was determined. As shown in Figure 5.6 (panel A), the expression of scaffold subunits was similar in all samples, including uninfected cells. The expression of catalytic subunits, however, increased with increasing MOI in the first 18 h of infection. At the 42-hour time point, their expression was similarly elevated in all samples of infected cells. As also shown in Figure 5.6 (panel C), the expression of B56α was reduced at 42 h post-infection with a MOI that was ≥ 30. The expression of B56γ, however, was unchanged (Figure 5.6, panel D).

To determine whether the increased expression of catalytic subunits is driven by the heterologous expression of B56δ, the expression of catalytic subunits was compared between ARVM that expressed either GFP-B56δ-WT or GFP. The adenovirus that expresses GFP (i.e. AdV.GFP) was used at MOI 10 and the reason for this is explained in Chapter 7. As shown in Figure 5.7, the relative increase in catalytic subunit expression in cells infected with AdV.GFP-B56δ-WT was almost identical to the relative increase in B56δ expression (~11 fold). These results suggest therefore that the increase in the expression of PP2A catalytic subunits is a consequence of the increased expression of B56δ regulatory subunits.

5.4.2 Characterization of AdV.GFP-B56δ-SA

Heterologous expression of GFP-tagged S573A B56δ in ARVM was achieved by infection with the adenoviral vector that encodes mutated human B56δ fused to GFP at the N-terminus (AdV.GFP-B56δ-SA). In a first experiment the cells were infected with increasing dose of the adenovirus (MOI 0-200). The cells were harvested 18 h post-infection and protein expression was determined by immunoblot analysis. Again, to confirm that the full-length heterologous protein was expressed in ARVM, the samples were subjected to immunoblot analysis with the B56δ antibody. A sample of ARVM that expressed GFP-B56δ-WT was included in the last lane, as a positive control. As shown in Figure 5.8, the antibody detected faster-migrating (endogenous) B56δ at ~70-kDa, and slower-migrating heterologous S573A and WT B56δ at ~100-kDa. These results confirmed that full-length GFP-B56δ-SA is also expressed in ARVM. As also shown in Figure 5.8, whilst the

expression of heterologous B56δ increased with increasing dose of adenovirus, the expression of endogenous B56δ was similar in all samples, including uninfected cells. Furthermore, the expression profile suggested that a comparable abundance of heterologous and endogenous B56δ would be achieved with a MOI of 20-50. As shown in Figure 5.9, the expression of PP2A catalytic subunits was again increased with increasing dose of adenovirus.

Further studies were performed to confirm the dose of AdV.GFP-B56δ-SA that produces expression of GFP-B56δ-SA at an abundance comparable to that of GFP-B56δ-WT, achieved by infection of myocytes with AdV.GFP-B56δ-WT at MOI 30. The expression of heterologous proteins was determined by using both the B56δ antibody and the GFP antibody. As shown in Figure 5.10 (panels A and B), immunoblot analysis of the samples with either antibody revealed that comparable expression of each heterologous protein could be achieved by infecting myocytes with either adenoviral vector at MOI 30. Furthermore, under these conditions the expression of catalytic subunits was also comparable (Figure 5.10, panel C).

5.4.3 ISO-induced phosphorylation of heterologously expressed B56δ at S573

To determine whether heterologously expressed WT B56δ is phosphorylated at S573 in response to β-adrenergic stimulation and confirm that heterologously expressed S573A B56δ is not phosphorylated at this site, ARVM with heterologous expression of B56δ proteins were subjected to stimulation with ISO. Expression of B56δ and phosphorylation at S573 were determined by immunoblot analysis with the B56δ and pS573 B56δ antibody, respectively. As shown in Figure 5.11, the B56δ antibody detected heterologous B56δ in all samples. The pS573 B56δ antibody, however, detected ISO-induced phosphorylation of S573 only in endogenous and heterologous WT B56δ. Thus, heterologously expressed GFP-B56δ-WT is phosphorylated at S573 in response to stimulation with ISO.

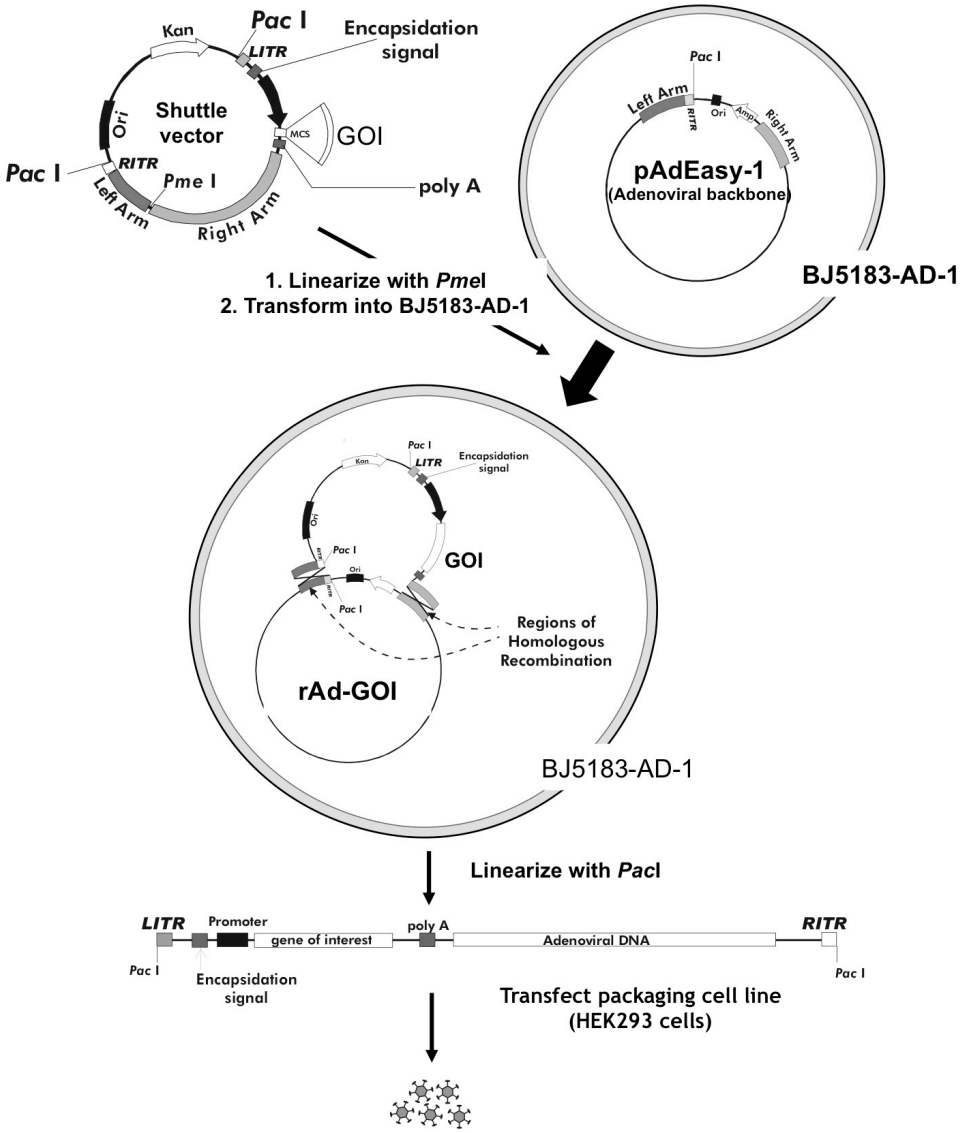

Figure 5.1 Schematic representation of the AdEasy system

The shuttle vector, which contains the GOI, is linearized with *Pme*I and transformed into BJ5183-AD-1 cells, for homologous recombination with pAdEasy-1, which contains the adenoviral backbone. Recombinant adenoviral DNA (rAd-GOI) is linearized with *Pac*I and transfected into HEK293 cells, for packaging of adenovirus particles. Adapted from He *et al*.[203]

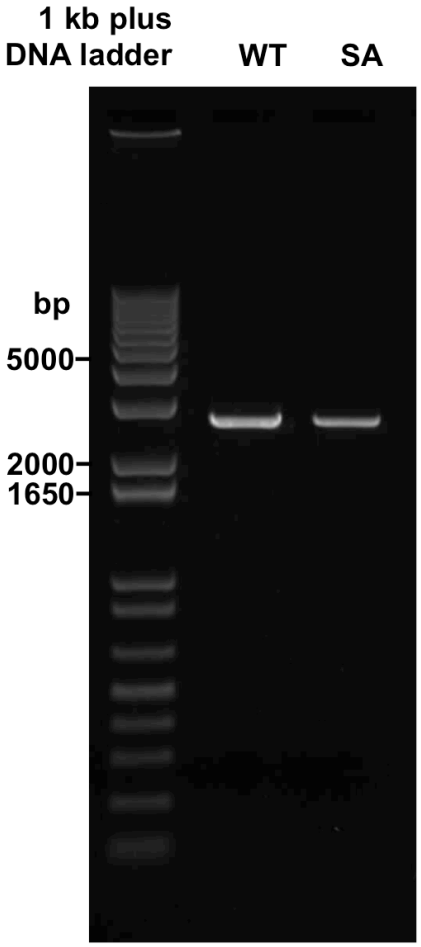

Figure 5.2 DNA electrophoresis to confirm amplification of GOI by PCR

GFP-B56δ-WT (WT) and GFP-B56δ-SA (SA) cDNA was amplified by PCR from the original pEGFP-C1 plasmid and the mutated pEGFP-C1 plasmid, respectively. Restriction sites for *Kpn*I and *Not*I were introduced at the 5' and 3' end of the PCR product, respectively. The expected size of GFP-B56δ is 2607 base pairs (bp).

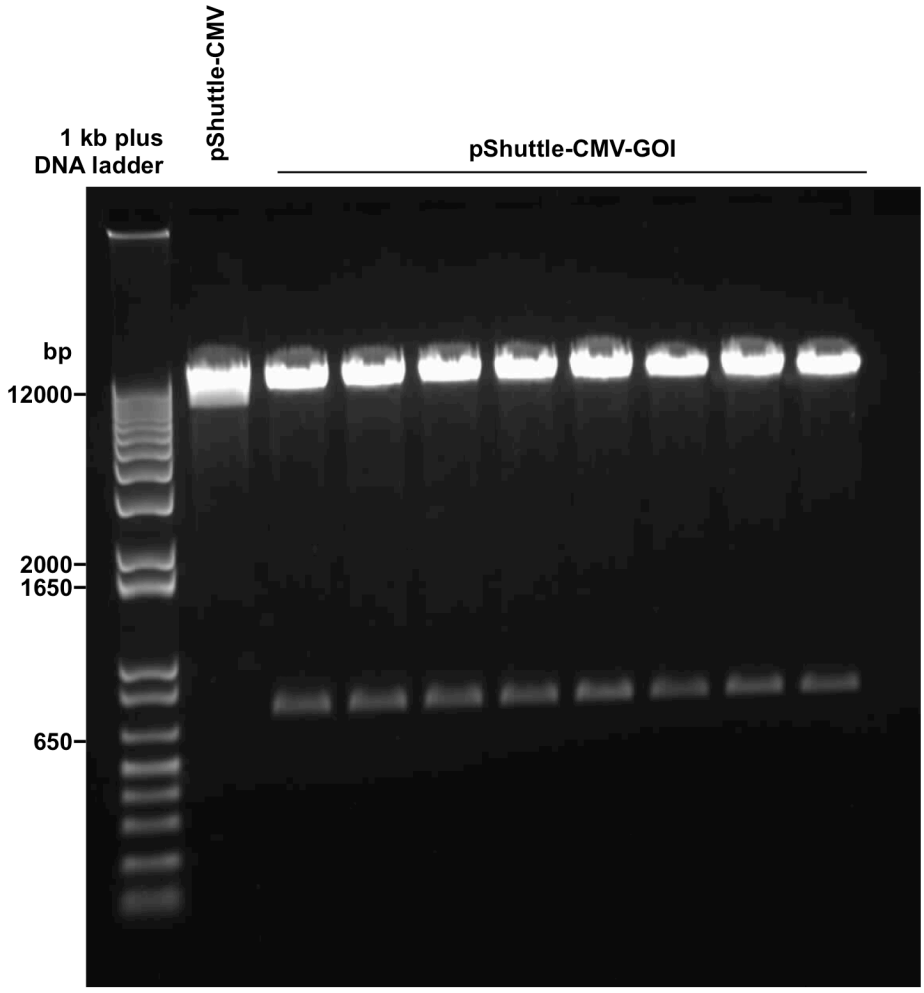

Figure 5.3 DNA electrophoresis to confirm ligation of pShuttle-CMV with GOI

The GOI (GFP-B56δ-WT or GFP-B56δ-SA) was digested with *Kpn*I and *Not*I and ligated with pShuttle-CMV, digested with the same enzymes. The ligation products were transformed into *E. coli* DH5α cells. Isolated plasmid DNA was digested with *Bgl*II, which cuts within both the GOI and shuttle vector. The digestion products were resolved by electrophoresis. The appearance of a 750 bp fragment confirms the presence of GOI in pShuttle-CMV.

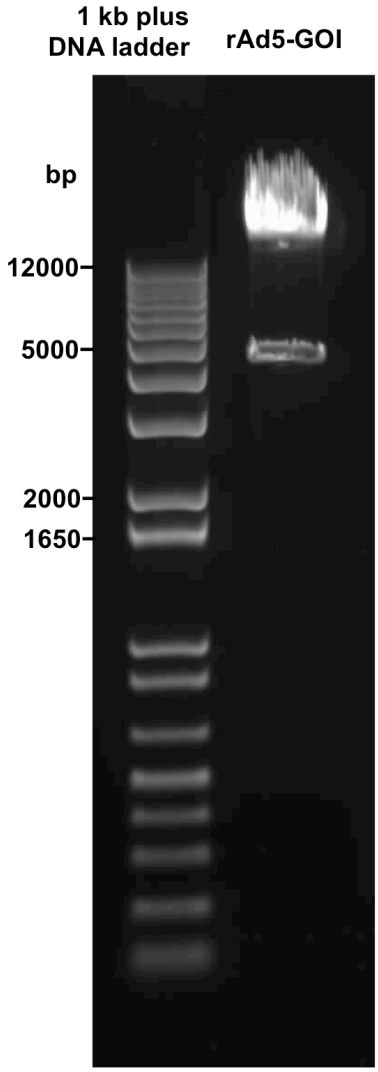

Figure 5.4 DNA electrophoresis to confirm recombination between pShuttle-CMV-GOI and pAdEasy-1

Homologous recombination between pShuttle-CMV-GOI and pAdEasy-1, containing the human AdV genome, was performed in *E.coli* BJ5183-AD-1 cells. Candidate recombinants were validated by digestion with *Pac*I. Digestion of recombinant adenoviral DNA (rAD5-GOI) yielded a 4.5 kb product and a product > 30 kb.

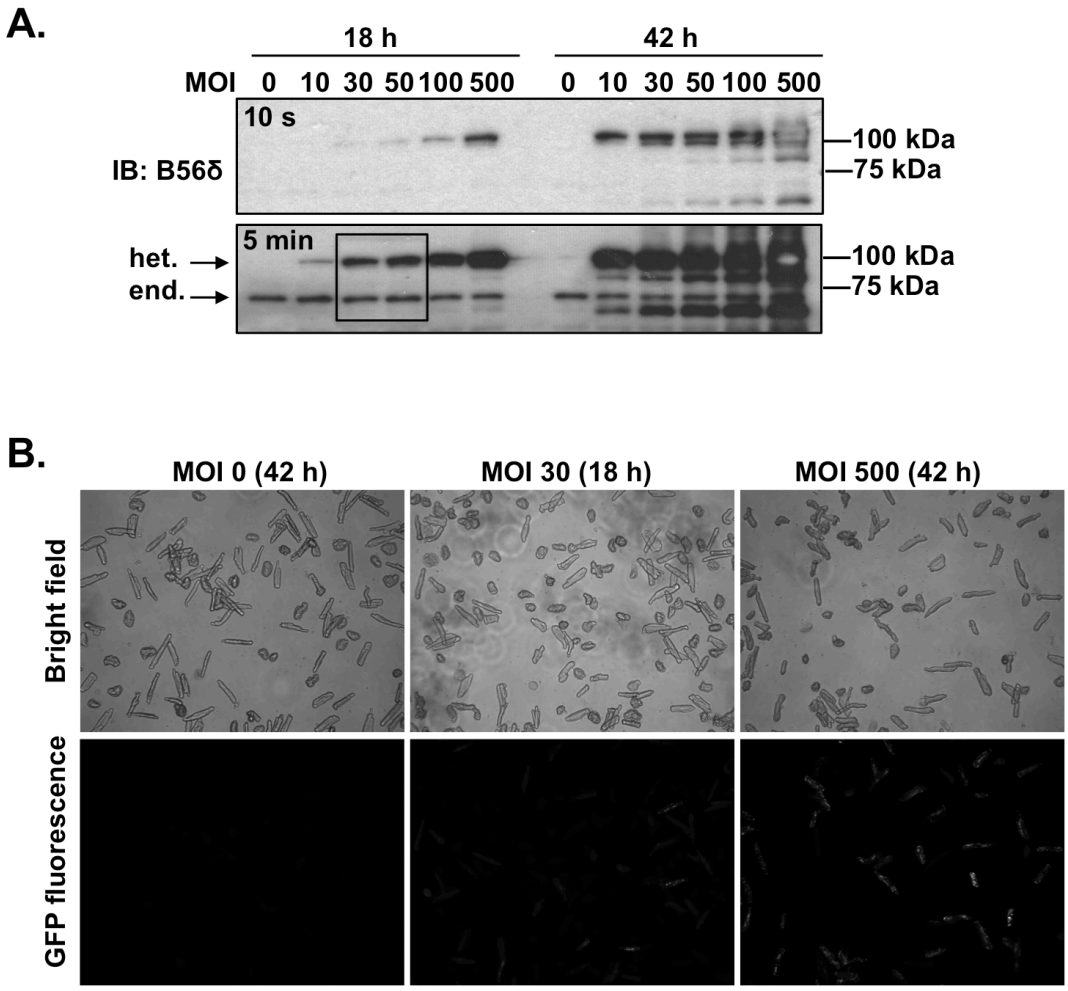

Figure 5.5 Expression of GFP-B56δ-WT in ARVM

ARVM were infected with an increasing dose of AdV.GFP-B56δ-WT (MOI 0-500) and were harvested 18 or 42 h post-infection. **A.** Expression of heterologous (het.) and endogenous (end.) B56δ. Shorter (10 s) and longer (5 min) exposure autoradiograms are shown. Samples in which heterologous B56δ is expressed at an abundance that is similar to the endogenous protein are indicated by a rectangle. **B.** Representative bright field and fluorescence images of myocytes at 18 and 42 h post-infection with AdV.GFP-B56δ-WT at MOI 30 or 500, respectively.

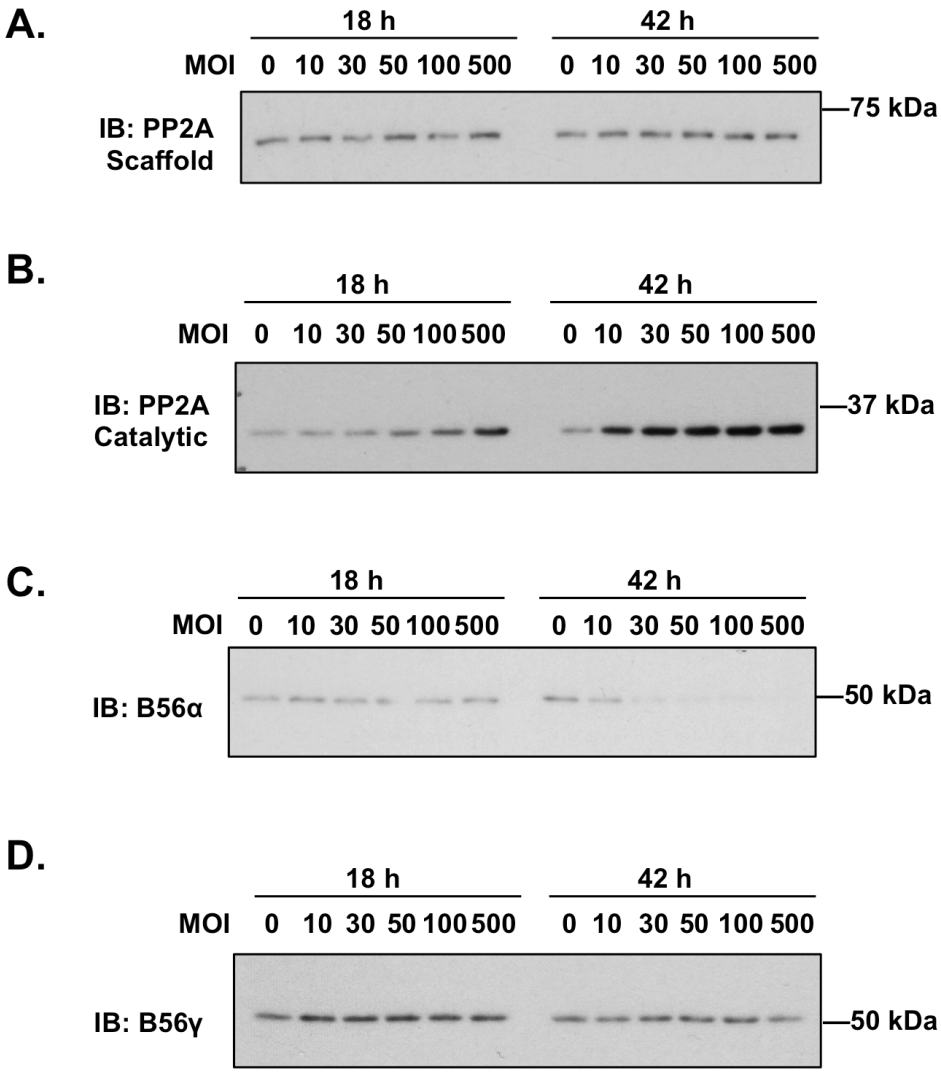

Figure 5.6 PP2A subunit expression profile in ARVM infected with AdV.GFP-B56δ-WT

ARVM were infected with an increasing dose of AdV.GFP-B56δ-WT (MOI 0-500) and were harvested 18 or 42 h post-infection. Figure shows expression of **A.** PP2A scaffold subunits; **B.** PP2A catalytic subunits; **C.** B56α and **D.** B56γ, as determined by immunoblot analysis with subunit-specific antibodies.

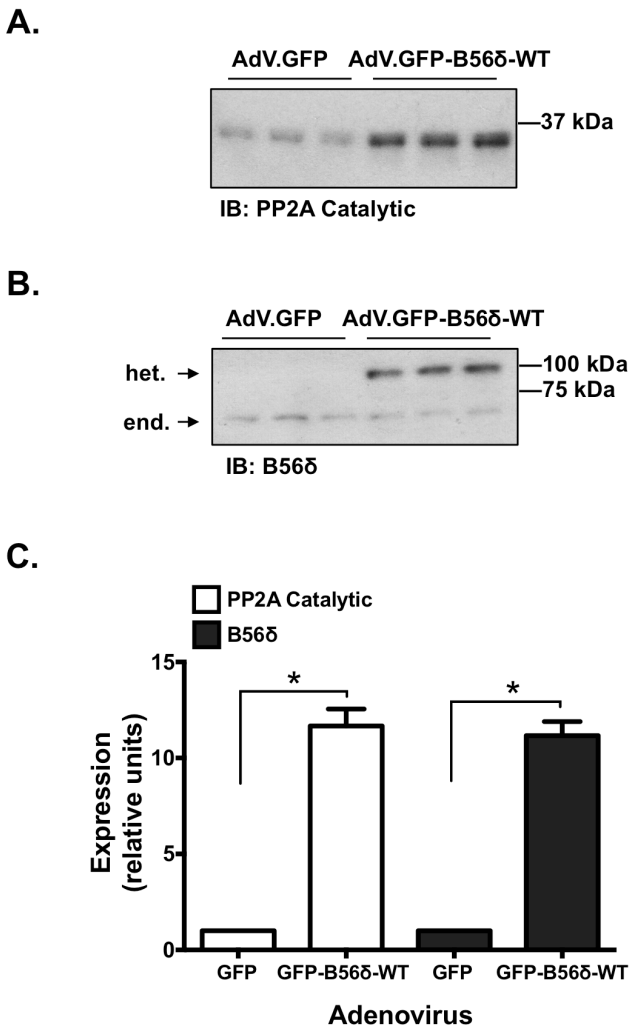

Figure 5.7 Effect of heterologous expression of WT B56δ on PP2A catalytic subunit expression

ARVM were infected with AdV.GFP (MOI 10) or AdV.GFP-B56δ-WT (MOI 30) and were harvested 18 h post-infection. **A.** Expression of PP2A catalytic subunits. **B.** Expression of heterologous (het.) and endogenous (end.) B56δ. **C.** Quantitative data (mean ± SEM) for the relative expression of PP2A catalytic and B56δ (end. or end. plus het.) subunits in myocytes infected with AdV.GFP or AdV.GFP-B56δ-WT. **P*<0.05 between indicated groups (n=3).

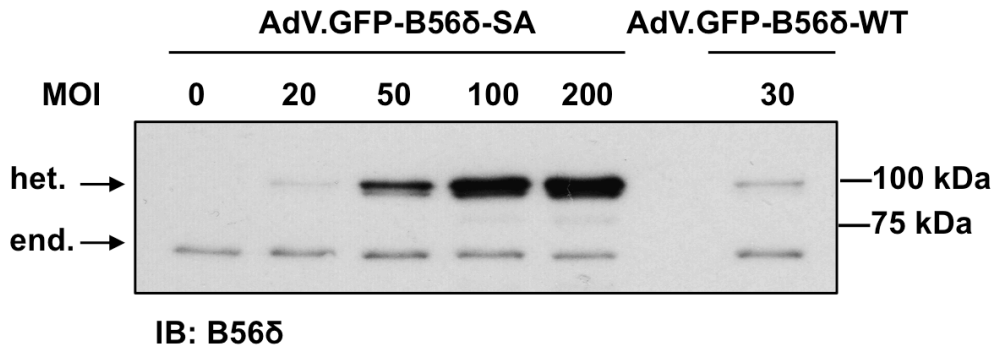

Figure 5.8 Expression of GFP-B56δ-SA in ARVM

ARVM were infected with an increasing dose of AdV.GFP-B56δ-SA (MOI 0-200) and were harvested 18 h post-infection. Figure shows the expression of heterologous (het.) and endogenous (end.) B56δ. A sample of ARVM infected with AdV.GFP-B56δ-WT was included in the last lane as a positive control.

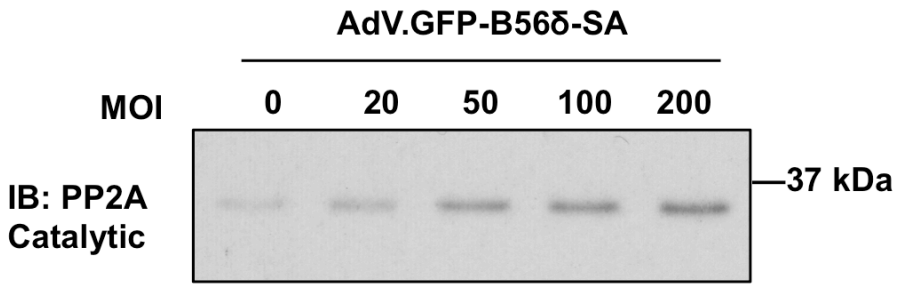

Figure 5.9 Effect of heterologous expression of S573A B56δ on the expression of PP2A catalytic subunits

ARVM were infected with an increasing dose of AdV.GFP-B56δ-SA (MOI 0-200) and were harvested 18 h post-infection. Immunoblot shows the expression of PP2A catalytic subunits.

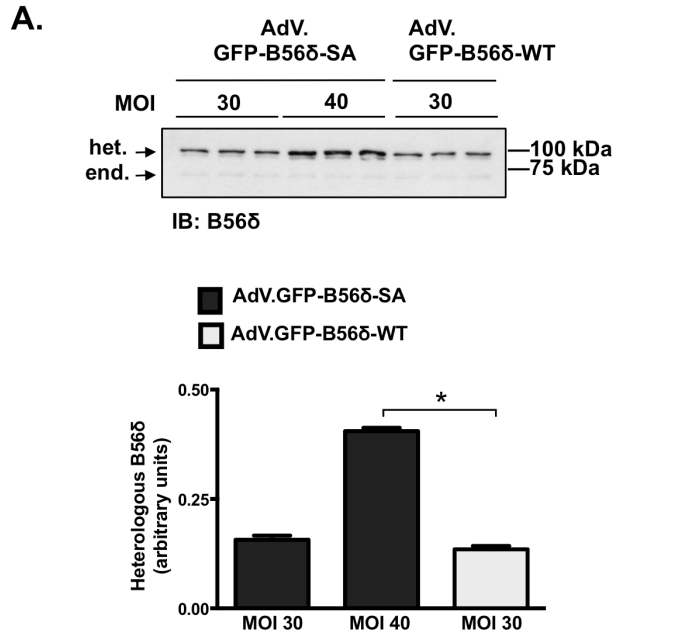
A.
AdV.
GFP-B56δ-SA
AdV.
GFP-B56δ-WT
MOI
30
40
30
het.
end.
100 kDa
75 kDa
IB: B56δ
AdV.GFP-B56δ-SA
AdV.GFP-B56δ-WT
Heterologous B56δ
(arbitrary units)
0.50
0.25
0.00
*
MOI 30
MOI 40
MOI 30

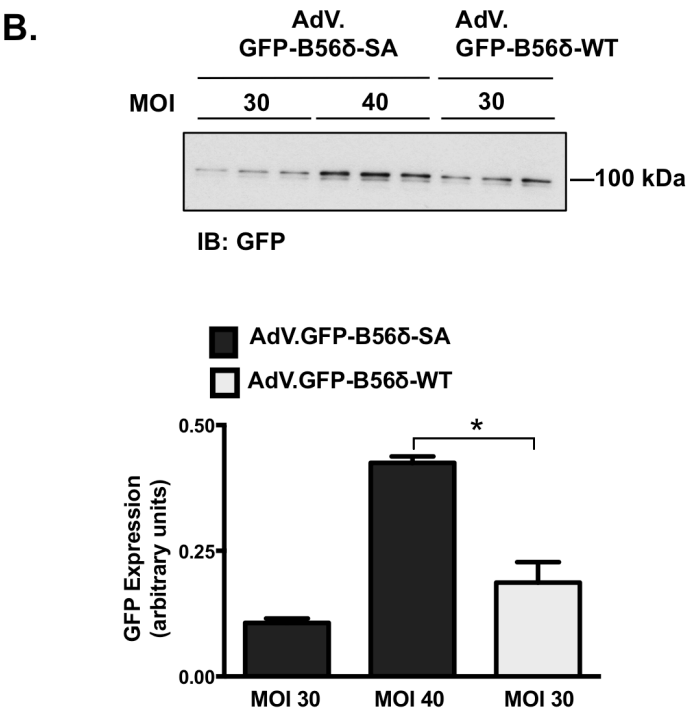
B.
AdV.
GFP-B56δ-SA
AdV.
GFP-B56δ-WT
MOI
30
40
30
100 kDa
IB: GFP
AdV.GFP-B56δ-SA
AdV.GFP-B56δ-WT
GFP Expression
(arbitrary units)
0.50
0.25
0.00
*
MOI 30
MOI 40
MOI 30

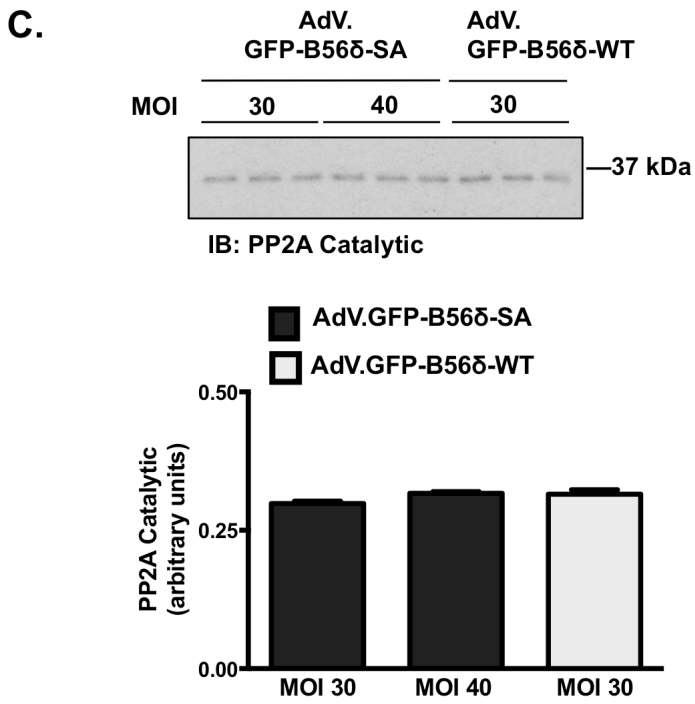

Figure 5.10 Selecting a MOI for AdV.GFP-B56δ-SA

ARVM were infected with AdV.GFP-B56δ-SA (MOI 30 or 40) or AdV.GFP-B56δ-WT (MOI 30) and were harvested 18 h post-infection. Figure shows immunoblots and quantitative data (mean ± SEM) for expression of **A.** heterologous (het.) and endogenous (end.) B56δ; **B.** GFP and **C.** PP2A catalytic subunits. **P*<0.05 vs. AdV.GFP-B56δ-WT (n=3).

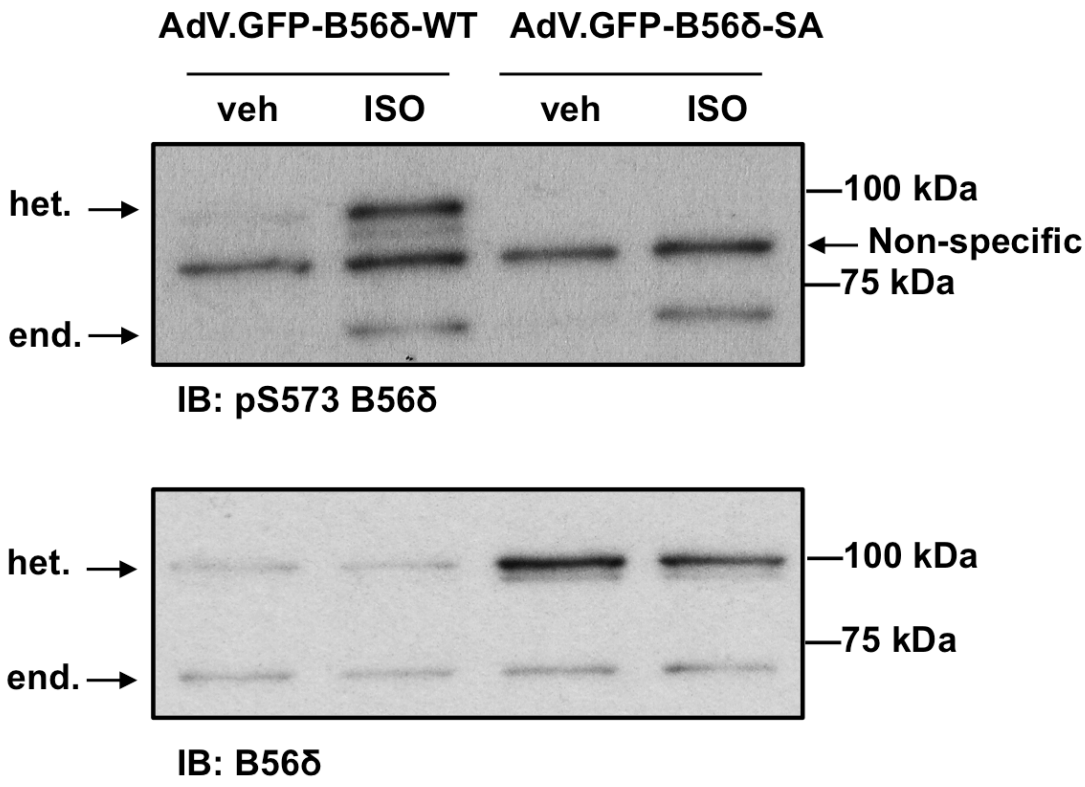

Figure 5.11 ISO-induced phosphorylation of heterologously expressed B56δ at S573

ARVM infected with AdV.GFP-B56δ-WT or AdV.GFP-B56δ-SA were exposed to vehicle (veh) or ISO (10 nM) for 10 min at 18 h post-infection. Top panel shows ISO-induced phosphorylation of S573 in endogenous (end.) and heterologous (het.) WT B56δ. A non-specific signal is indicated. Bottom panel shows the expression of het. and end. B56δ.

5.5 Discussion

To study the role of B56δ phosphorylation at S573 in β-adrenergic regulation of cardiac PP2A activity, protein phosphorylation and function, adenoviral vectors encoding GFP-tagged human B56δ in WT or non-phosphorylatable (S573A) form were constructed. The objective of the studies presented in this chapter was to characterize the use of these adenoviral vectors in ARVM.

The first studies were performed with AdV.GFP-B56δ-WT. On a fluorescence microscope GFP was not detected at 18 h post-infection. Immunoblot analysis of infected cells with the B56δ antibody, however, revealed that at this time point heterologous B56δ *was* expressed. Furthermore, the results showed that expression at an abundance similar to that of endogenous B56δ was achieved by infection with a relatively small dose (MOI 30) of the adenovirus (Figure 5.5). The disparity in detection of the heterologous protein by the two methods may be explained by the fact that expression of heterologous B56δ, at a level that is similar to the expression of endogenous B56δ, is not sufficient to produce a detectable level of GFP fluorescence.

An interesting observation was that heterologous expression of GFP-B56δ-WT is accompanied by a proportional increase in expression of PP2A catalytic subunits (Figure 5.7). It appears that increased expression of the catalytic subunits in response to increased expression of a B56 regulatory subunit is not an uncommon event and was reported in transgenic mice with cardiac-specific overexpression of B56α.[172] Besides suggesting that in the cellular environment GFP-B56δ-WT may interact with the catalytic subunits of PP2A, these results suggest that rather than displacing endogenous B56δ from existing PP2A holoenzymes, GFP-B56δ-WT may be incorporated into new PP2A holoenzymes. In mammalian cells B56 subunits are stable only when bound to the PP2A core dimer.[182,204] Thus, the fact that the expression of endogenous B56δ was unchanged in the presence of the heterologous B56δ further suggests that the endogenous regulatory subunit was not displaced from holoenzymes.

The unchanged expression of PP2A scaffold subunits may at first seem inconsistent with the increased expression of catalytic subunits, given that these are not stable in the absence of scaffold subunits. A possible explanation for these results may be that in ARVM there is an existing pool of scaffold subunits, whereas the expression of catalytic subunits is subject to up-regulation (transcriptional or translational) when necessary.

Interestingly, at 42 h post-infection with AdV.GFP-B56δ-WT at MOI ≥ 30 the expression of endogenous B56α was reduced (Figure 5.6). Further studies would be required to establish the underlying mechanism(s) for this response. However, a possible explanation for it may be that the response is compensatory; if in ARVM B56α and B56δ have redundant roles, to accommodate increased B56δ-PP2A (and phosphatase activity), B56α-PP2A (and phosphatase activity) is reduced. It has been reported that the expression of B56α is reduced, in isolated cardiac cells, in response to activation of stress pathways.[171] An alternative explanation for the loss of protein expression in the present studies may be that the response is stress-induced. Specifically, it may be caused by the presence of excess amounts of the adenovirus and/or the prolonged incubation of the cells with the adenovirus.

With regards to characterization of GFP-B56δ-SA expression in ARVM, besides loss of basal- and ISO-induced phosphorylation at S573, differences from GFP-B56δ-WT were not observed. The full-length protein was expressed, indicating that B56δ protein stability is not dependent on its phosphorylation at S573. Furthermore, the expression of PP2A catalytic subunits in cells that expressed GFP-B56δ-SA was not different from cells that expressed GFP-B56δ-WT at a comparable level, suggesting that the apparent interaction between the catalytic and heterologous B56δ subunits is also not dependent on S573 phosphorylation (Figures 5.8 and 5.9).

In conclusion, at 18 h post-infection and MOI 30 of either adenoviral vector, the abundance of GFP-B56δ-WT-PP2A and GFP-B56δ-SA-PP2A is similar. These vectors may thus be used to investigate the role of B56δ phosphorylation at S573 in cardiac myocytes, particularly in response to β-AR stimulation, with good confidence that any differences in

cellular PP2A activity, protein phosphorylation and function can be attributed to B56δ phosphorylation at S573.

6 The Role of B56δ Phosphorylation at S573 in β-Adrenergic Regulation of Cardiac PP2A Activity

6.1 Introduction

The studies presented in Chapter 4 established that in cardiac cells endogenous B56δ is phosphorylated by PKA at S573 in β-adrenergic signaling. The role of the phosphorylation in β-adrenergic regulation of cardiac PP2A activity, however, is unknown. *In vitro* and in non-cardiac cells, the phosphorylation of B56δ at S573 is necessary and sufficient to stimulate the activity of the associated catalytic subunit, increasing both the rate of substrate dephosphorylation and substrate affinity.[114,186] In these published studies the activity of B56δ-PP2A was determined *in vitro* by measuring the radioactivity released from radiolabeled phospho-proteins. These were either standard phospho-proteins used in *in vitro* phosphatase assays (i.e. histone 2B, histone 1 and phosphorylase a),[186] or the purified substrate phospho-protein of B56δ-PP2A identified in mouse striatum (i.e. DARPP-32, dopamine- and cAMP-regulated neuronal phosphorotein).[114]

An alternative assay to determine phosphatase activity, which does not involve radioactivity, is the colorimetric assay in which malachite green reagent is used to detect inorganic phosphates released from a synthetic substrate phospho-peptide *in vitro*.[205] In acidic conditions inorganic phosphates form a complex with ammonium molybdate and malachite green. The absorbance of the complex, which can be measured at wavelengths between 620 and 660 nm, is proportional to the inorganic phosphate concentration and is correlated to enzyme activity. The short peptides used in this assay are poor PP1 substrates and their use thus provides some degree of assay specificity.[205] Nevertheless, it has been reported that a contribution from PP1 cannot be fully excluded.[206] Therefore, in the studies described in this chapter, the utility of a PP2A immunoprecipitation phosphatase assay to determine the specific activity of cardiac PP2A was explored. This

assay utilizes malachite green reagent to determine the activity of the PP2A catalytic subunit isolated from cells by immunoprecipitation.

6.2 Objectives

The objectives of the studies described in this chapter were to:

- Determine the suitability of a PP2A immunoprecipitation phosphatase assay for assessment of PP2A activity in ARVM.
- Determine PP2A activity in ARVM expressing heterologous B56δ in WT or S573A form, in the absence and presence of ISO stimulation.

6.3 Methods

6.3.1 ARVM isolation, culture, adenoviral gene transfer and stimulation

For the experiments described in this chapter, ARVM were isolated from the hearts of adult male Wistar rats and cultured as described in the Methods (sections 2.1.1 and 2.1.2). Where indicated, infection with adenoviral vectors was performed as described in the Methods (section 2.1.3). The cells were exposed to vehicle or 10 nM ISO (10 min, 37^{o}C) 18 h post-infection.

6.3.2 Measurament of PP2A activity

PP2A phosphatase activity was determined as described in the methods (section 2.6). In brief, the catalytic subunits of PP2A were immunoprecipitated from clarified ARVM lysates with a mouse monoclonal subunit-specific antibody. The immunoprecipitates were incubated with the substrate Thr phospho-peptide (750 μM, 10 min). 25 μL of the reaction end-product was assayed with malachite green phosphate detection solution in wells of a 96-well ½ volume microtiter plate. The absorbance of the sample was measured at 650 nm and the phosphate concentration was interpolated from the phosphate standard curve. Phosphatase activity, expressed as pmol phosphate released from the Thr phospho-peptide per min (pmol Pi/min), was calculated as described in the Methods (section 2.6.4.3).

6.3.3 Immunoblot analysis

SDS-PAGE and immunoblot analysis were performed as described in the Methods (sections 2.3.2 to 2.3.4). For the experiments described in this chapter, the semi-dry transfer method was used to transfer proteins to the support membrane. Details of the antibodies used are provided in the Methods (Tables 2.4 and 2.5).

6.4 Results

6.4.1 Validation of PP2A immunoprecipitation phosphatase assay

6.4.1.1 **Malachite green phosphate detection solution**

To validate the use of malachite green phosphate detection solution, phosphate standards containing between 0 and 2000 pmol phosphate per 25 µL were prepared and 100 µL of the solution was added to 25 µL of each standard. As shown in Figure 6.1 (panel A), the colour intensity increased with increasing phosphate concentration. As shown in Figure 6.1 (panel B), the absorbance of the standards at 650 nm was directly proportional to the phosphate concentration. Thus, malachite green phosphate detection solution can detect small amounts of phosphate and the assay is linear over a wide range of phosphate concentrations.

6.4.1.2 **Immunoprecipitation of PP2A catalytic subunits**

To determine the specificity of PP2A catalytic subunit immunoprecipitation, equal amounts of soluble ARVM lysates were incubated with a mouse monoclonal PP2A catalytic subunit antibody or an equivalent amount of non-immune (normal) mouse IgG. Immunocomplexes were incubated with the substrate Thr phospho-peptide and the presence of inorganic phosphates in 25 µL of diluted or undiluted reaction end-product was determined with malachite green phosphate detection solution. The results of the assay, including the absorbance of the samples and the corresponding phosphate concentration, are shown in Figure 6.2 (panel A). As shown in Figure 6.2 (panel B), although some phosphatase activity was present in the precipitate derived using normal mouse IgG, this was considerably lower than the activity present in the precipitate derived using the PP2A catalytic subunit antibody. To further assess the specificity of the immunoprecipitation, the abundance of PP2A catalytic subunits was determined in each precipitate by immunoblot analysis. As expected, PP2A catalytic subunits were more abundant in the precipitate derived using the subunit-specific antibody (Figure 6.2, panel C). To evaluate the efficiency of the immunoprecipitation, the abundance of PP2A catalytic subunits was determined in equal volumes of pre-immunoprecipitation (pre-IP) lysate,

immunoprecipitate (IP) and post-immunoprecipitation (post-IP) supernatant, by immunoblot analysis. As shown in Figure 6.2 (panel D), PP2A catalytic subunits were substantially enriched in the IP. Together, these results show that immunoprecipitation of PP2A catalytic subunits is specific and efficient.

6.4.2 PP2A activity in ARVM expressing WT or S573A B56δ

To study the role of S573 phosphorylation in β-adrenergic regulation of cardiac PP2A activity, ARVM expressing heterologous B56δ in WT or S573A form were exposed to vehicle or 10 nM ISO and the clarified lysates were subjected to the PP2A immunoprecipitation phosphatase assay. As shown in Figure 6.3 (panel A), the abundance of GFP-B56δ-WT and GFP-B56δ-SA was comparable in the pre-IP lysates. Furthermore, the expression of catalytic subunits was similar in all groups. As shown in Figure 6.3 (panel B), PP2A activity was unchanged in response to ISO stimulation and appeared to not be influenced by the nature of the heterologous subunit that was expressed.

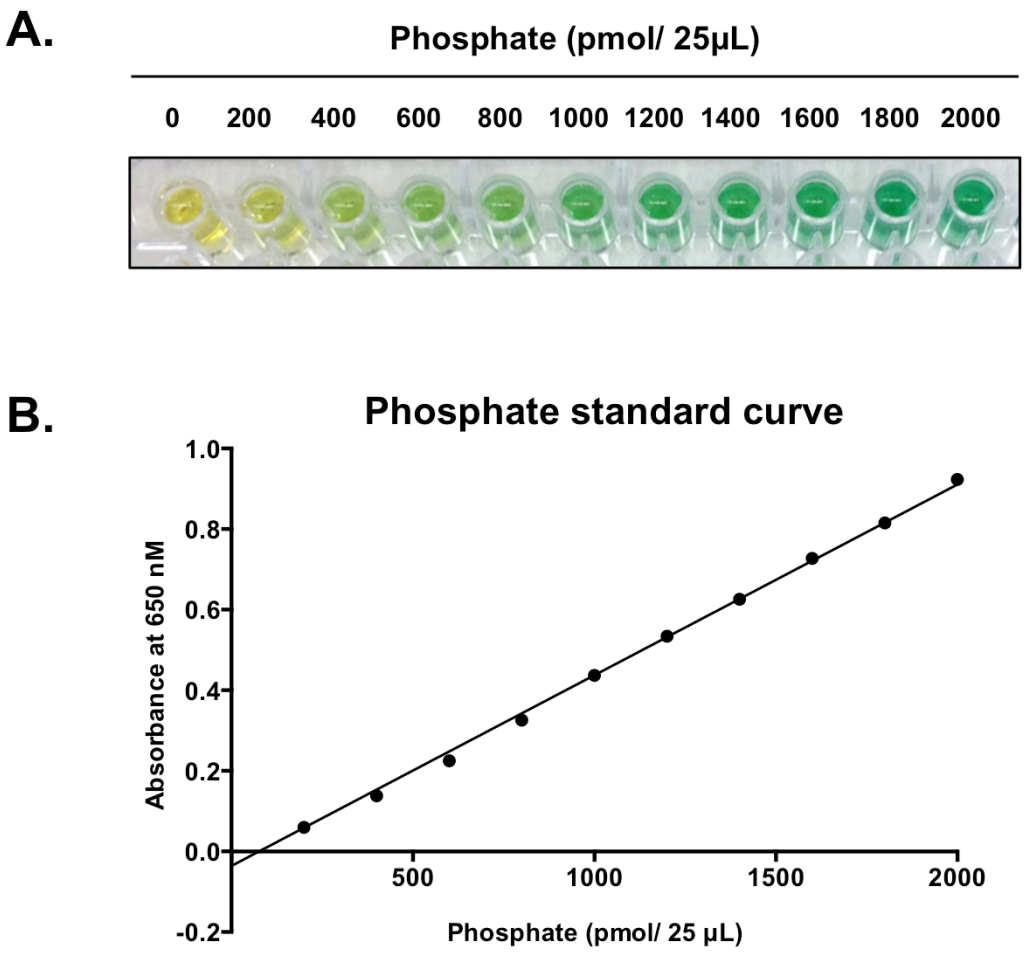

Figure 6.1 Phosphate standard curve

Phosphate standards containing between 0 and 2000 pmol phosphate per 25 µL were prepared from a 0.1 mM phosphate standard working solution. 25 µL of each standard was transferred to wells of a 96-well ½ volume microtiter plate. **A.** Phosphate standards following the addition of malachite green phosphate detection solution. **B.** Phosphate standard curve, generated by plotting the absorbance of each standard (at 650 nm) against the known phosphate concentration.

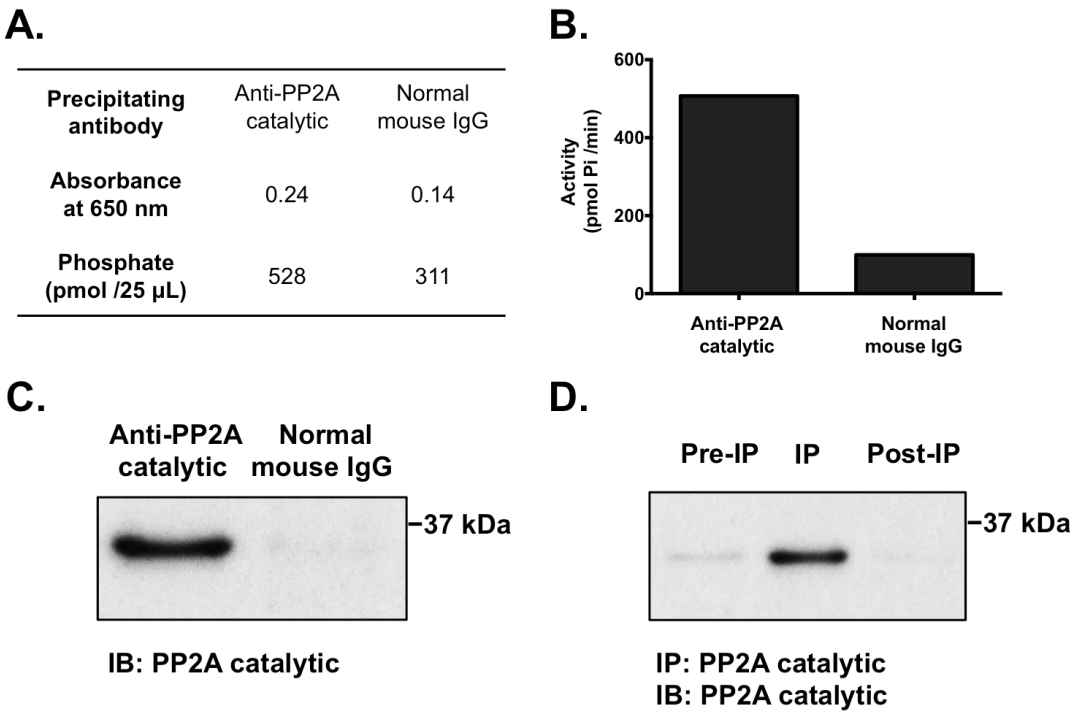

Figure 6.2 Validation of PP2A immunoprecipitation phosphatase assay

Equal amounts of soluble ARVM lysates were incubated with a mouse monoclonal PP2A catalytic subunit antibody (anti-PP2A catalytic) or an equivalent amount of non-immune (normal) mouse IgG. Immunoprecipitates were incubated with a substrate Thr phospho-peptide and inorganic phosphates (Pi) in the reaction end-product were detected with malachite green phosphate detection solution. The absorbance of the samples was measured at 650 nm and the phosphate concentration was interpolated from the phosphate standard curve. **A.** Malachite green phosphatase assay data. **B.** Phosphatase activity. **C.** Immunoprecipitated PP2A catalytic subunits. **D.** Abundance of PP2A catalytic subunits in equal volumes of the Pre-IP lysate, IP and post-IP supernatant.

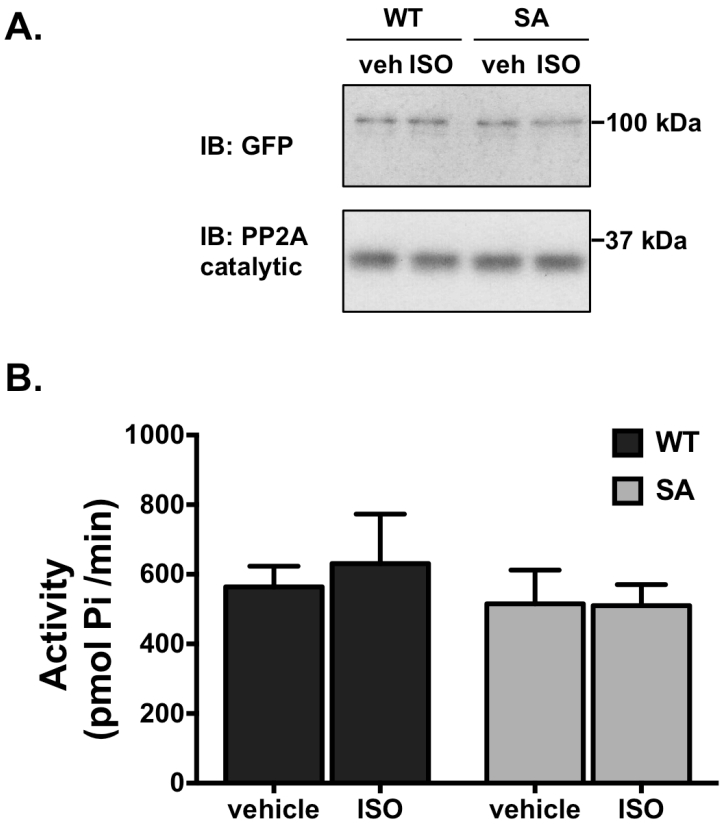

Figure 6.3 PP2A activity in ARVM expressing WT or S573A B56δ

ARVM infected with AdV.GFP-B56δ-WT (WT) or AdV.GFP-B56δ-SA (SA) were exposed to ISO (10 nM) or vehicle (veh) for 10 min, 18 h post-infection. PP2A catalytic subunits were immunoprecipitated with a mouse monoclonal PP2A catalytic subunit antibody. Immunoprecipitates were incubated with a substrate Thr phospho-peptide and inorganic phosphates (Pi) in the reaction end-product were detected with malachite green phosphate detection solution. The absorbance of the samples was measured at 650 nm and the phosphate concentration was interpolated from the phosphate standard curve. **A.** Expression of GFP and PP2A catalytic subunits, as determined by immunoblot analysis of pre-immunoprecipitation lysates. **B.** Phosphatase activity (mean ± SEM). n=3. Data were analysed by two-way ANOVA. No statistical significance was revealed.

6.5 Discussion

The ultimate aim of the studies described in this chapter was to determine the role of B56δ phosphorylation at S573 in β-adrenergic regulation of cardiac PP2A activity. To specifically determine the activity of PP2A, the catalytic subunits were isolated from soluble ARVM lysates by immunoprecipitation and their activity was determined by measuring the amount of inorganic phosphate released from a substrate Thr phospho-peptide.

The sensitivity and specificity of the PP2A immunoprecipitation phosphatase assay were determined in validation studies. The results showed that small (picomolar) concentrations of inorganic phosphates can be detected in this assay and that the relationship between the absorbance and phosphate concentration is linear over a considerably wide range of concentrations. Furthermore, the immunoprecipitation of PP2A catalytic subunits is specific and efficient (Figures 6.1 and 6.2). The PP2A immunoprecipitation phosphatase assay was thus considered an appropriate assay to determine the role of B56δ phosphorylation at S573 in β-adrenergic regulation of cardiac PP2A activity. To this purpose, human WT or non-phosphorylatable (S573A) B56δ was heterologously expressed in ARVM by adenoviral gene transfer and PP2A activity was determined in the absence and presence of ISO stimulation.

In vitro, B-type regulatory subunits can compete for binding to the PP2A core dimer and can displace each other from existing heterotrimers.[207] To minimise the likelihood that heterologously-expressed B56δ might displace other B-type subunits from native PP2A holoenzyme, in the experimental design care was taken to express GFP-B56δ variants at levels comparable to the endogenous protein. PP2A activity was unchanged in response to ISO stimulation and was not different between cells expressing WT or S573A B56δ (Figure 6.3). In non-cardiac cells the phosphorylation of B56δ at S573 is necessary and sufficient to increase the phosphatase activity of the associated catalytic subunit.[114] As was shown in Chapter 5, heterologously expressed WT B56δ is phosphorylated at S573 in response to β-adrenergic stimulation while heterologously expressed S573A B56δ is not phosphorylated at this site. Thus, the lack of a difference in PP2A activity between cells expressing WT

B56δ and those expressing S573A B56δ, particularly following β-adrenergic stimulation, is surprising. The assay used detects *total* PP2A activity and not the specific activity of PP2A holoenzymes targeted by heterologous B56δ subunits. Thus, if the latter represent a relatively small proportion of the total cellular PP2A holoenzyme content, then the results become less surprising. In this context, it is possible that different PP2A holoenzymes respond differentially to β-adrenergic stimulation, such that measuring total PP2A activity would mask the changes in the activity of specific holoenzymes. Furthermore, it is also possible that expression of non-phosphorylatable B56δ was not sufficient to overcome the effect of the endogenous protein.

Based on these considerations, to determine the impact of B56δ phosphorylation at S573 on the activity of the associated PP2A catalytic subunit, an alternative and more appropriate method would be to specifically measure the activity of GFP-B56δ-PP2A. Since the established and characterized PP2A immunoprecipitation phosphatase assay appears to be robust and sensitive, a possible approach towards this aim would be to immunopurify GFP-B56δ-PP2A, rather than the total cellular PP2A catalytic subunit content. This could be achieved by using GFP-Trap®_A beads. With the proviso that catalytic subunits are co-purified and that other B-type subunits are absent from the immunoprecipitates, the phosphatase activity of the immunopurified complexes would then be determined by performing the malachite green phosphatase assay.

7 The Role of B56δ Phosphorylation at S573 in β-Adrenergic Regulation of Cardiac Protein Phosphorylation

7.1 Introduction

As described in previous chapters of this thesis, thus far the functional role of PKA-mediated B56δ phosphorylation at S573 has been explored only in mouse striatal neurons and in rat preovulatory ovarian granulosa cells.

In striatal neurons the phosphorylation of the PP2A regulatory subunit and activation of PP2A represents a positive feedback mechanism.[114] Accordingly, by stimulating the dephosphorylation of the PP1 regulatory protein DARPP-32 at T75, PKA-mediated phosphorylation of T34 is facilitated and DARPP-32 is converted into a potent inhibitor of PP1.[114] Consequently, PP1 activity is inhibited and PKA signaling is amplified. In further studies the B56δ S573 phosphorylation correlated with reduced phosphorylation of DARPP-32 at S97.[208] This was associated with nuclear retention of DARPP-32, reduced activity of nuclear PP1 and increased phosphorylation of histones.

In rat preovulatory ovarian granulosa cells, PKA-mediated phosphorylation of B56δ at S573 induces dephosphorylation of MAP 2D, which is phosphorylated at T256/T259 by glycogen synthase kinase 3β (GSK3β) under basal conditions.[187] The dephosphorylation occurs downstream of LH receptor and is the net effect of simultaneous PKA-mediated inactivation of GSK3β and activation of B56δ-PP2A.

Somewhat more relevant to the field of cardiac biology, although performed in HEK293 cells with heterologously expressed proteins, are studies that describe the regulation of PDE4D3.[177] Accordingly, B56δ-PP2A exists in signaling complexes scaffolded by mAKAP and the phosphorylation of B56δ, by mAKAP-bound PKA, stimulates dephosphorylation of PDE4D3. This reduces degradation of cAMP and prolongs cAMP signaling.

Nevertheless, the role of B56δ phosphorylation at S573 in regulating the phosphorylation of cardiac substrates following β-adrenergic stimulation has not been explored.

7.2 Objectives

The objectives of the studies described in this chapter were to:

- Determine the phosphorylation of generic PKA substrates in ARVM with heterologous expression of GFP, GFP-B56δ-WT or GFP-B56δ-SA, in the absence and presence of β-adrenergic stimulation by ISO.
- Determine the phosphorylation of specific PKA substrates in ARVM with heterologous expression of GFP, GFP-B56δ-WT or GFP-B56δ-SA, in the absence and presence of β-adrenergic stimulation by ISO.

7.3 Methods

7.3.1 ARVM isolation, culture, adenoviral gene transfer and stimulation

For the experiments described in this chapter, ARVM were isolated from the hearts of adult male Wistar rats and cultured as described in the Methods (sections 2.1.1 and 2.1.2). Infection with adenoviral vectors was performed as described in the Methods (section 2.1.3). The cells were exposed to vehicle or ISO (0.1-10 nM) for 10 min (37°C), 18 h post-infection. For immunoblot analysis of protein expression and phosphorylation, the cells were harvested in cell lysis buffer (200 µL per well). The protein concentration was determined as described in the Methods (section 2.5.1).

7.3.2 Immunoblot analysis

SDS-PAGE and immunoblot analysis were performed as described in the Methods (sections 2.5.2 to 2.3.1). For the experiments described in this chapter, proteins were transferred to the support membrane by the semi-dry transfer method. Details of the antibodies used are provided in the Methods (Tables 2.4 and 2.5).

7.4 Results

The ultimate objective of the studies described in this chapter was to determine the role of B56δ phosphorylation at S573 in β-adrenergic regulation of cardiac protein phosphorylation. However, due to difficulties encountered in constructing AdV.GFP-B56δ-SA, the effect of increased B56δ expression was explored first.

7.4.1 Effect of increased B56δ expression on β-adrenergic regulation of cardiac protein phosphorylation

7.4.1.1 **Optimizing the dose of AdV.GFP**

To determine the dose of AdV.GFP that expresses GFP at a level comparable to that achieved by AdV.GFP-B56δ-WT at MOI 30, ARVM were infected with AdV.GFP (MOI 5-30) or AdV.GFP-B56δ-WT (MOI 30). The expression of GFP was determined by immunoblot analysis 18 h post-infection. As shown in Figure 7.1, the expression of GFP (~30-kDa) increased with increasing dose of AdV.GFP and at MOI 5 its expression was comparable to the expression of GFP-B56δ-WT (~100-kDa). Due to differences in molecular weights, under the same electrophoretic transfer conditions the transfer of GFP was probably more efficient than the transfer of GFP-B56δ-WT. Thus, to account for a relative underestimation of GFP-B56δ-WT expression, in subsequent studies AdV.GFP was used at MOI 10. The GFP antibody detected an additional protein with an apparent molecular weight of ~40 kDa. This protein was also detected in uninfected cells and thus, the signal was non-specific.

7.4.1.2 **Phosphorylation of generic PKA substrates**

The phosphorylation of generic PKA substrates was determined in ARVM expressing GFP or GFP-B56δ-WT. These studies were inspired by the evidence, in non-cardiac cells, that PKA-mediated phosphorylation of B56δ at S573 regulates PKA signaling.[114,177] Although aware that in these experiments responses could not be attributed to the phosphorylation at S573, the studies had the potential to reveal novel information on the role of altered B56δ expression *per se*. ARVM expressing either GFP-B56δ-WT or GFP were exposed to

increasing concentrations of ISO (0.1-10 nM) or vehicle and samples of total cellular lysates were resolved by electrophoresis in a 15% acrylamide gel. To determine the phosphorylation status of generic PKA substrates, immunoblot analysis was performed with a rabbit monoclonal antibody that recognizes the RRXS*/T* motif (where R = arginine; X = any amino acid; S*/T* = phosphorylated Ser or Thr). By recognizing phosphorylated Ser/Thr residues in the PKA consensus phosphorylation motif, the phospho-PKA substrate antibody can detect multiple PKA substrates simultaneously. As shown in Figure 7.2 (panel A), the antibody detected several proteins whose phosphorylation was increased by ISO in a dose-dependent manner. Given that the antibody does not recognize the non-phosphorylated motif (as stated by Cell Signaling Technology at the time of these studies), it is implicit that in unstimulated cells the basal phosphorylation of PKA substrates was detected. An interesting observation in this experiment was the increased phosphorylation of some PKA substrates in ARVM that expressed GFP-B56δ-WT. This was most pronounced for proteins with a molecular weight ≥150-kDa, following stimulation by ISO at 1 nM and 10 nM. To determine the relative abundance of heterologous and endogenous B56δ proteins, the samples were subjected to immunoblot analysis with the B56δ antibody. As shown by Figure 7.2 (panel B), the expression of the two proteins was comparable. Together, these first results suggested that ISO-induced phosphorylation of some PKA substrates was increased in cells with a moderate expression of heterologous WT B56δ.

7.4.2 The role of B56δ phosphorylation at S573 in β-adrenergic regulation of cardiac protein phosphorylation

7.4.2.1 **Phosphorylation of generic PKA substrates**

Given the observations described in section 7.4.1.2, when construction of AdV.GFP-B56δ-SA was complete, it seemed reasonable to pursue similar studies in ARVM expressing heterologous B56δ in S573A form. In these further studies the phosphorylation of generic PKA substrates was thus determined in unstimulated and ISO-stimulated ARVM expressing GFP, GFP-B56δ-WT or GFP-B56δ-SA. Again, whole cell lysates were resolved by electrophoresis in a 15% acrylamide gel and immunoblot analysis was performed with the

phospho-PKA substrate antibody. On this occasion, the phosphorylation status of larger proteins was less clear but the phosphorylation status of smaller proteins was readily detected (Figure 7.3, panel A). As expected, the phosphorylation of PKA substrates was increased by ISO in a dose-dependent manner, with strong signals observed at ~30-kDa and <15-kDa. Basal phosphorylation was revealed only for proteins with a molecular weight <15-kDa. A striking result was the reduced phosphorylation of protein(s) migrating at ~30-kDa in cells expressing GFP-B56δ-SA following stimulation with 1 nM ISO.

To gain better insight on the phosphorylation status of larger proteins the lysates of cells harvested in a subsequent experiment were resolved in a 7.5% acrylamide gel. As shown in Figure 7.3 (panel B), the ISO-induced phosphorylation of putative PKA substrates migrating at 150-kDa and ~60-kDa was revealed. Interestingly, whilst the increase in phosphorylation of 150-kDa proteins was dose-dependent, the phosphorylation of proteins migrating at ~60-kDa was similar following stimulation with either 1 nM or 10 nM ISO. Differential phosphorylation of proteins (in cells that expressed a different heterologous protein) was observed in response to stimulation by ISO at 1 nM. Accordingly, when compared to cells that expressed GFP-B56δ-WT, the phosphorylation of 150-kDa and ~60-kDa proteins was reduced in cells that expressed GFP-B56δ-SA. Furthermore, when compared to cells that expressed GFP, the phosphorylation of 150-kDa proteins was increased in cells that expressed GFP-B56δ-WT. Taken together, these studies showed that the ISO-induced phosphorylation of some PKA substrates was reduced in cells that expressed non-phosphorylatable B56δ. Furthermore, it appeared that the phosphorylation of some PKA substrates was amplified by the heterologous expression of WT B56δ.

As shown in Figure 7.4 (panel A), in these experiments GFP-B56δ-WT and GFP-B56δ-SA were expressed at a comparable level. Furthermore, when compared to the expression of endogenous B56δ, the expression of heterologous B56δ moieties was moderate. As shown in Figure 7.4 (panel B), relative to cells expressing GFP alone, the heterologous expression of WT and S573A B56δ corresponded with an increase in the expression of PP2A catalytic subunits that was comparable in magnitude in cells expressing either protein.

7.4.2.2 **Phosphorylation of specific PKA substrates**

In parallel studies the phosphorylation status of specific PKA substrate proteins, which are abundantly expressed in cardiac myocytes where they play important roles in the regulation of contractile responses to β-adrenergic stimuli (and might contribute to the signals observed at <15-kDa, ~30-kDa and 150-kDa), was determined. Thus, the phosphorylation of PLB (6-kDa; S16), cTnI (26-kDa; S23/24) and cMyBP-C (150-kDa; S282) was determined. As shown in Figure 7.5, the phosphorylation of PLB, cTnI and cMyBP-C was increased by ISO in a dose-dependent manner. Furthermore, in the presence of 1 nM ISO the phosphorylation of PLB and cMyBPC appeared reduced in cells expressing GFP-B56δ-SA, when compared to cells expressing GFP-B56δ-WT, and increased in cells expressing GFP-B56δ-WT, when compared to cells expressing GFP.

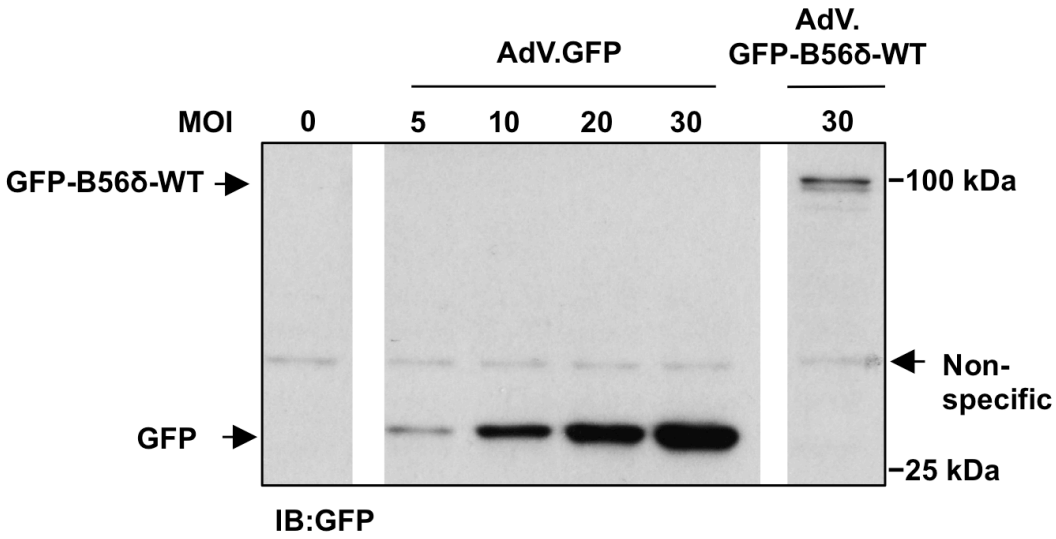

Figure 7.1 Optimizing the dose of AdV.GFP

ARVM were infected with AdV.GFP (MOI 5-30) or AdV.GFP-B56δ-WT (MOI 30). Immunoblot shows the expression of GFP at 18 h post-infection. GFP-B56δ-WT and GFP proteins are indicated on the left. A non-specific signal is indicated on the right.

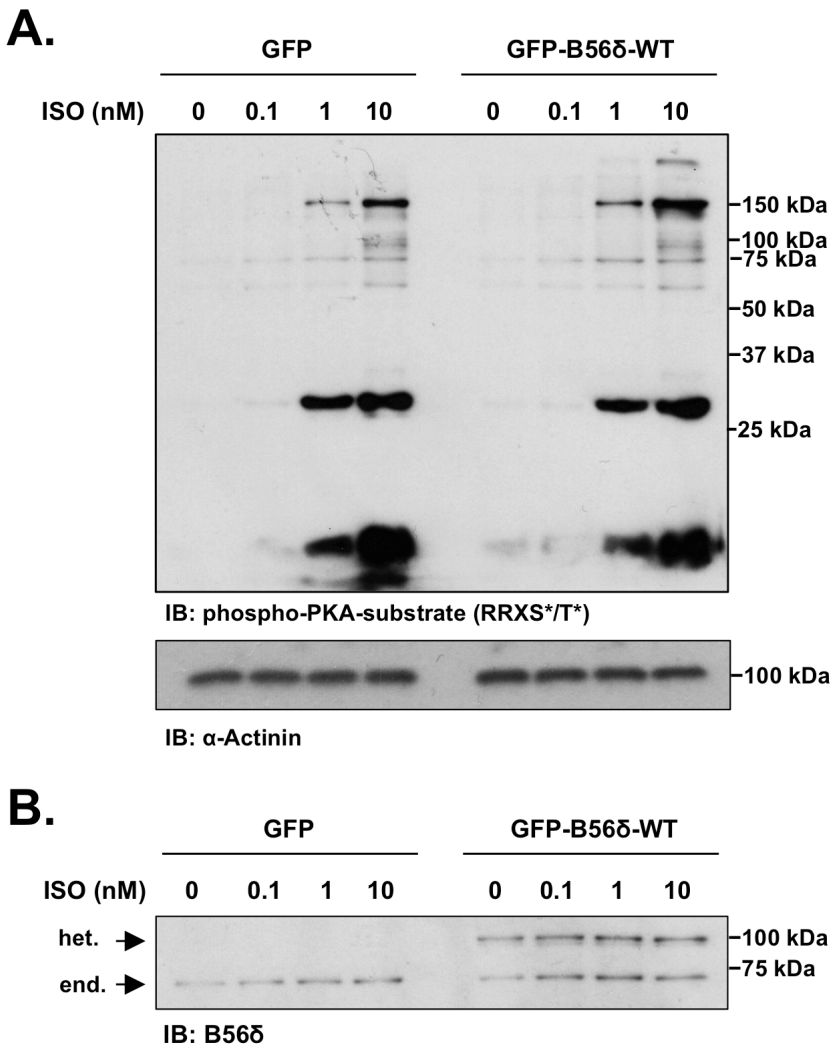

Figure 7.2 The role of B56δ expression in β-adrenergic regulation of generic PKA substrate phosphorylation

ARVM expressing GFP-B56δ-WT or GFP were exposed to ISO (0-10 nM) for 10 min. **A.** Phosphorylation of PKA substrate proteins. **B.** Expression of heterologous (het.) and endogenous (end.) B56δ. In A the immunoblot of α-Actinin demonstrates protein loading.

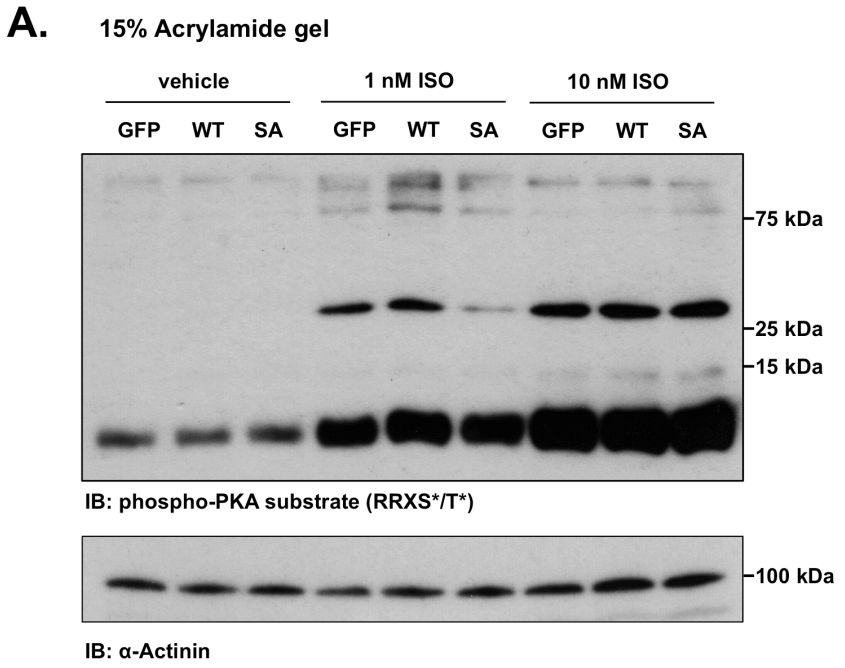
A.
15% Acrylamide gel
vehicle
1 nM ISO
10 nM ISO
GFP WT SA GFP WT SA GFP WT SA
75 kDa
25 kDa
15 kDa
IB: phospho-PKA substrate (RRXS*/T*)
100 kDa
IB: α-Actinin

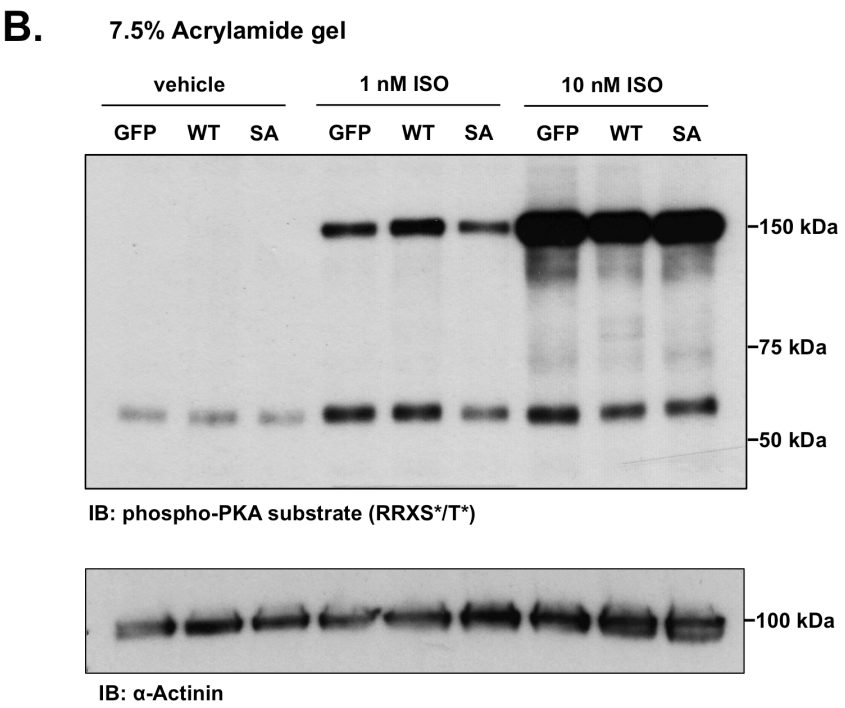
B.
7.5% Acrylamide gel
vehicle
1 nM ISO
10 nM ISO
GFP WT SA GFP WT SA GFP WT SA
150 kDa
75 kDa
50 kDa
IB: phospho-PKA substrate (RRXS*/T*)
100 kDa
IB: α-Actinin

Figure 7.3 The role of B56δ phosphorylation at S573 in β-adrenergic regulation of generic PKA substrate phosphorylation

ARVM expressing GFP, GFP-B56δ-WT or GFP-B56δ-SA were exposed to vehicle (veh) or ISO (1 nM or10 nM) for 10 min. **A.** Phosphorylation of PKA substrate proteins resolved in a 15% acrylamide gel. **B.** Phosphorylation of PKA substrate proteins resolved in a 7.5% acrylamide gel. The results are representative of two biological replicates. Immunoblots of α-Actinin show protein abundance in each sample.

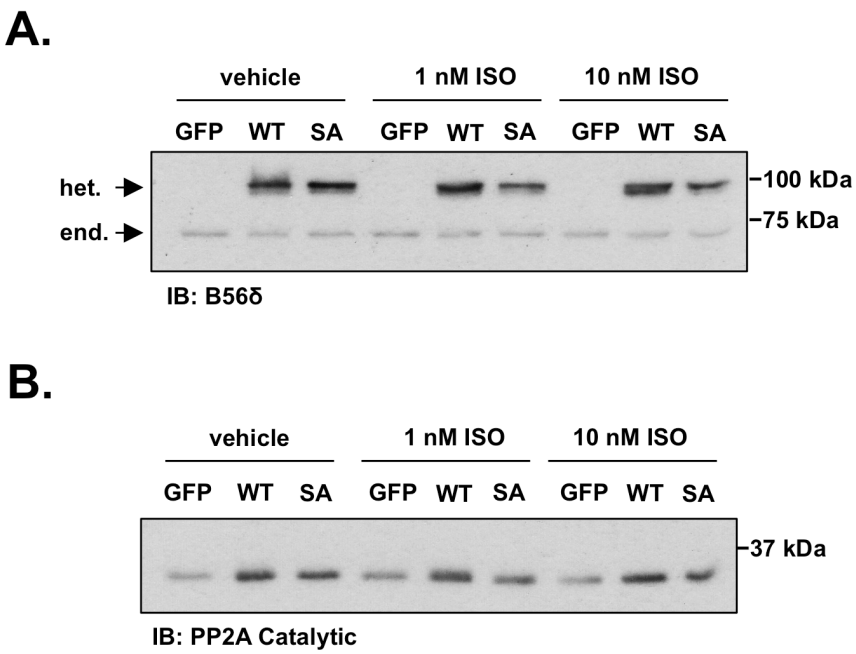

Figure 7.4 PP2A subunit expression

ARVM expressing GFP, GFP-B56δ-WT or GFP-B56δ-SA were exposed to vehicle or ISO (1 nM or 10 nM) for 10 min. Figure shows the expression of **A.** heterologous (het.) and endogenous (end.) B56δ and **B.** PP2A catalytic subunits.

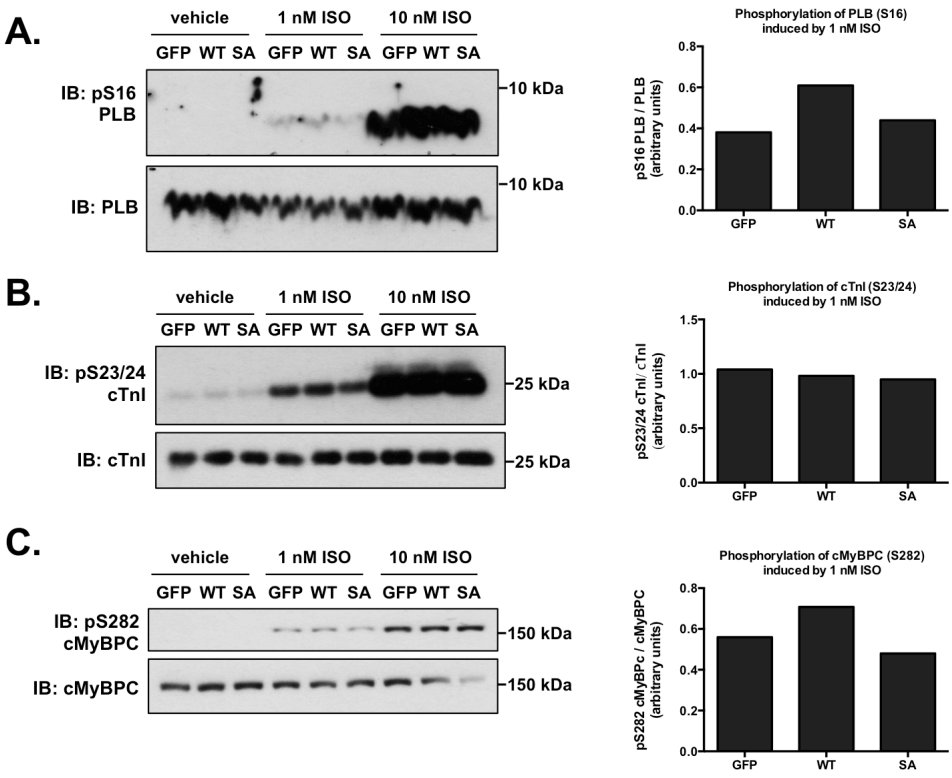

Figure 7.5 The role of B56δ phosphorylation at S573 in β-adrenergic regulation of specific PKA substrate phosphorylation

ARVM expressing GFP, GFP-B56δ-WT or GFP-B56δ-SA were exposed to vehicle (veh) or ISO (1 nM or 10 nM) for 10 min. Figures show the phosphorylation of **A.** PLB at S16; **B.** cTnI at S23/24 and **C.** cMyBP-C at S282. Bar charts show the signals detected in the immunoblots for protein phosphorylation in response to stimulation with 1 nM ISO. The signal generated by the phospho-specific antibody was normalized to the signal generated by the antibody detecting the total protein.

7.5 Discussion

The primary objective of the studies described in this chapter was to explore the role of B56δ phosphorylation at S573 in β-adrenergic regulation of cardiac protein phosphorylation. The studies were performed in ARVM expressing heterologous B56δ in WT or non-phosphorylatable (S573A) form. In these particular studies the impact of S573 phosphorylation was determined in the context of β-adrenergic regulation of PKA substrate phosphorylation.

Whilst the construction of AdV.GFP-B56δ-SA was being completed, the effect of increased B56δ expression, which has been reported in both ischemic and non-ischemic canine models of heart disease,[183] was explored. In these first studies GFP or GFP-B56δ-WT proteins were expressed at a comparable level in ARVM (Figure 7.1). The decision to study the phosphorylation of PKA substrates was guided by the evidence, in non-cardiac cells, that PKA-mediated phosphorylation of B56δ at S573 impacts on PKA signaling.[114,177]

The phosphorylation of generic PKA substrates was determined by immunoblot analysis with a phospho-motif-specific antibody. This antibody recognizes phosphorylated Ser and Thr residues in the PKA consensus phosphorylation motif, with arginine at positions -2 and -3 relative to the site of phosphorylation.[209] By using this antibody, the phosphorylation status of multiple PKA substrate proteins was revealed simultaneously (Figures 7.2 and 7.3). Considering the plethora of proteins phosphorylated by PKA in β-adrenergic signaling,[210] it is clear that in the present studies only a few phospho-proteins, most likely the abundant phospho-proteins, were detected. It is of course also possible that multiple substrates of PKA with an identical or similar molecular weight were detected in clusters. It is also important to be aware of the fact that several targets, including cTnI and cMyBP-C, are phosphorylated by PKA at multiple sites and the phospho-PKA substrate antibody may detect only some of these.

Despite its limitations, novel information was revealed by using the phospho-PKA substrate antibody. First, when compared to ARVM expressing GFP, the phosphorylation of PKA substrates was increased in ARVM expressing GFP-B56δ-WT (Figure 7.2). Second,

when compared to ARVM expressing GFP-B56δ-WT at a comparable abundance, the phosphorylation of PKA substrates was reduced in cells expressing GFP-B56δ-S573A (Figure 7.3 and 7.4). In the light of evidence that the phosphorylation of B56δ at S573 increases the phosphatase activity of the associated catalytic subunit,[114] these findings seemed paradoxical. If the phosphorylation of B56δ induces the *dephosphorylation* of PKA substrates, the phosphorylation of these substrates would be increased, rather than decreased, in cells expressing GFP-B56δ-SA. Furthermore, in cells expressing GFP-B56δ-WT the phosphorylation of the substrates would be reduced, particularly in view of the parallel increase in the expression of PP2A catalytic subunits (Figure 7.4). Thus, an alternative and reasonable explanation is that in cardiac myocytes the phosphorylation of B56δ at S573 mediates positive feedback, enhancing the phosphorylation of PKA substrates. It is worth noting that on most occasions, the discussed effects were observed in the presence of 1 nM but not 10 nM ISO. It is therefore possible that the positive feedback mechanism becomes redundant in the presence of supra-maximal β-AR stimulation.

Studies of generic PKA substrate phosphorylation were supplemented by studies in which the phosphorylation of specific PKA substrates was explored. In these studies phospho-specific antibodies were used to determine the phosphorylation of PLB, cTnI and cMyBP-C at S16, S23/24 and S282, respectively. These specific proteins were studied for three reasons. First, they play important roles in regulating cardiac responses to β-adrenergic stimuli.[211,212] Second, the molecular weights of these proteins correspond to those of the proteins whose phosphorylation appeared to differ on immunoblots of phospho-PKA substrates. Third, the phospho-specific antibodies for each of these sites/proteins were available and validated within the laboratory at the time of the studies. Consistent with the previous results, in the presence of 1 nM ISO the phosphorylation of PLB, and cMyBP-C appeared lowest in cells expressing GFP-B56δ-S573A. Furthermore, when compared to cells expressing GFP, the phoshorylation of these proteins appeared to be increased in cells expressing GFP-B56δ-WT (Figure 7.5). Albeit further studies are necessary to perform statistical analysis and thereby validate these observations, the results further

suggest that in cardiac myocytes B56δ phosphorylation at S573 may mediate positive feedback, amplifying the phosphorylation of at least some PKA substrate proteins.

The findings, although surprising at first, are consistent with some of the proposed roles of B56δ S573 phosphorylation in non-cardiac cells. For example, in mouse striatal neurons the phosphorylation of B56δ (which activates the pertinent PP2A holoenzyme) facilitates the conversion of DARPP-32 into a potent inhibitor of PP1.[114] Consequently, by reducing PP1 phosphatase activity, substrate phosphorylation is enhanced. The second example comes from studies in HEK293 cells. These studies, albeit performed with heterologously expressed proteins, suggest that PKA-mediated B56δ phosphorylation stimulates dephosphorylation of PDE4D3.[177] This reduces the degradation of cAMP, potentiating PKA activation and thereby substrate phosphorylation.[177]

In conclusion, the preliminary data presented in this chapter suggest that in the specific context of β-adrenergic regulation of PKA substrate phosphorylation, the phosphorylation of B56δ at S573 may amplify the phosphorylation of at least some PKA substrates. A key limitation of the studies, however, is that only the phosphorylation of phospho-proteins detected by the pertinent phospho-specific antibodies (phospho-PKA substrate, pS16 PLB, pS23/24 cTnI, pS282 cMyBP-C), all of which are candidate or established PKA substrates, was explored. The substrate specificity of PP2A catalytic subunits, however, is largely determined by the regulatory subunit comprised in the holoenzyme.[105] Thus, the PP2A catalytic subunit can dephosphorylate phosphorylated Ser and Thr residues that do not reside in a PKA motif. It is therefore possible that increased activity of B56δ-PP2A, which arises from the phosphorylation of the regulatory subunit at S573, may induce the dephosphorylation of phospho-proteins that are not detected by the approaches used in the studies reported herein.

8 Summary and Perspectives

B-type subunits determine the subcellular targeting of PP2A holoenzymes and regulate the substrate selectivity and activity of the catalytic subunit. Although cardiac PP2A has been implicated in physiological and pathophysiological events, the roles of the individual B-type subunits and the mechanisms of their regulation are not well defined. Previous work in our laboratory showed that the regulatory B56α subunit is depleted from the myofilaments of ARVM in response to ISO stimulation.[166] This encouraged further investigation of the role of B56 subunits in β-adrenergic regulation of cardiac PP2A, forming the basis of the studies in this thesis.

The studies in chapter 3 assessed the expression of B56α, -γ and -δ at protein level in ARVM and determined their subcellular distribution by fractionation. The data confirmed the ISO-induced translocation of B56α and showed that the response is unique to this isoform. Furthermore, a parallel ISO-induced translocation of PP2A scaffold and catalytic subunits was revealed. Expanding upon previous findings, these results suggested that ISO induces the translocation of *selected* myofilament-residing PP2A *holoenzymes*, rather than of individual regulatory subunits.

In chapter 4, ISO-induced phosphorylation of B56δ was revealed by Phos-tag™ SDS-PAGE and immunoblot analysis. The site of phosphorylation and the upstream signaling pathway were also characterized. The data showed that the phosphorylation occurs at S573 and that it is accomplished by PKA, primarily downstream of β_1-ARs. In light of these novel findings, the possibility that ISO induces the translocation of B56α holoenzymes through the phosphorylation of the regulatory subunit was considered. This was also explored by using Phos-tag™ SDS-PAGE and immunoblot analysis, but changes in the phosphorylation of B56α were not detected (data not shown). The work in chapters 3 and 4 thus demonstrated that cardiac PP2As are differentially regulated by β-ARs, through the translocation of B56α holoenzymes and phosphorylation of B56δ regulatory subunits.

The majority of the studies reported in this thesis focus on the phosphorylation of B56δ at S573 by PKA. *In vitro*, such phosphorylation modulates the substrate specificity of the holoenzyme.[186] Furthermore, in transfected HEK293 cells and in neurons, this phosphorylation is necessary and sufficient to stimulate the activity of the associated PP2A catalytic subunit.[114] This raises the possibility that in ARVM PKA-mediated phosphorylation of B56δ at S573 may facilitate the *dephosphorylation* of B56δ-PP2A substrate proteins. Given the rapid onset of phosphorylation, it is conceivable that in β-adrenergic signaling distinct proteins are phosphorylated and dephosphorylated simultaneously. This could occur to either attenuate the effects of protein kinases that are activated downstream of β-ARs (PKA and CaMKII), or induce other dephosphorylation-dependent responses.

Immunofluorescence studies of B56δ showed that it is present throughout the myocyte, including the nucleus (chapter 4). Given the targeting function of the regulatory subunits, the absence of a more discrete localization was surprising. However, there is evidence in other cell types that B56δ-PP2A regulates the phosphorylation of both nuclear and cytosolic proteins; in trophoblast stem cells, it regulates HAND transcription factors in the nucleus.[213] In neurons and pre-ovulatory follicles, it regulates MAPs in the cytosol.[120,214] Therefore, it is possible that in myocytes the holoenzyme regulates the phosphorylation of specific substrates in multiple subcellular compartments.

The fractionation studies in chapter 3, and the immunofluorescence studies in chapter 4, showed that the subcellular localization of B56δ is not altered by ISO stimulation. It is therefore conceivable that this subunit targets the holoenzyme to its substrates constitutively, and that its phosphorylation by PKA induces their dephosphorylation. Once again, this highlights the differential regulation of B56 holoenzymes. In this context, it may be hypothesized that the translocation of the B56α holoenzyme from the myofilaments of ARVM would lead to the dephosphorylation of B56α-PP2A substrates elsewhere.

To study the role of B56δ phosphorylation at S573, GFP-tagged B56δ in WT or non-phosphorylatable (S573A) form were expressed in ARVM, by adenoviral gene transfer. Interestingly, the heterologous expression of either protein induced a proportional

increase in the expression of PP2A catalytic subunits, suggesting that either heterologous subunit was incorporated into holoenzymes (chapter 5). In future studies, this would be confirmed by immunoprecipitating the heterologous subunits via the GFP-tag and probing the immunoprecipitates for the presence of PP2A catalytic and scaffold subunits. Related to this, the activity of the immunoprecipitated holoenzymes would be determined by performing the malachite green assay. Given the evidence that B56δ S573 phosphorylation stimulates the activity of the associated catalytic subunit,[114] it is expected that ISO stimulation would increase the activity of holoenzymes containing the WT subunit but not the S573A mutant.

Given that a large proportion of cardiac responses to β-adrenergic stimuli result from the phosphorylation of proteins by PKA and that PP2A has been implicated in the regulation of PKA substrate phosphorylation in β-adrenergic signaling,[127] the hypothesis that the phosphorylation of B56δ at S573 impacts on the phosphorylation of PKA substrates was explored (Chapter 7). The phosphorylation of generic PKA substrates was determined by immunoblot analysis with a phospho-PKA substrate antibody in ARVM expressing heterologous WT or S573A B56δ. Although their identity is unknown, the phosphorylation of some proteins appeared increased in cells expressing WT B56δ and decreased in cells expressing S573A B56δ. This was most apparent following stimulation with a lower ISO concentration, suggesting that the phosphorylation of B56δ at S573 may amplify PKA signaling in response to sub-maximal β-AR stimulation.

In further studies it would be necessary to determine the expression of PKA in ARVM expressing heterologous B56δ moieties. If the phosphorylation of B56δ at S573 by PKA opposes the phosphorylation of PKA substrates through increased B56δ-PP2A activity, the expression of PKA might be increased in ARVM expressing the heterologous WT subunit, through a compensatory mechanism, thus explaining the apparent increase in PKA substrate phosphorylation. Similarly, in ARVM expressing the heterologous S573A subunit and thus exhibiting reduced B56δ-PP2A activity, the expression of PKA might be decreased, explaining the decrease in PKA substrate phosphorylation.

Assuming that the expression of PKA is not altered in the experimental system, an alternative explanation for the findings can be proposed. In neurons, the phosphorylation of B56δ at S573 by PKA amplifies cAMP and PKA signaling by reducing PP1 activity.[114] This effect is mediated by B56δ-PP2A-mediated dephosphorylation of the PP1 inhibitor DARPP-32, which increases its PP1-inhibitory activity.[114] This is illustrated schematically in Figure 8.1 (panel A). Given that the expression of DARPP-32 is negligible in non-neuronal cells,[215,216] DARPP-32 is unlikely to regulate PP1 in myocytes. Nevertheless, the structural and functional homologue of DARPP-32 that regulates PP1 activity in cardiomyocytes is I-1, whose activity is regulated by phosphorylation.[217] PKA-mediated phosphorylation at T35 converts I-1 into a potent inhibitor of PP1.[218] Conversely, PKCα-mediated phosphorylation at S67 and T75 attenuates the inhibitory effect of I-1 on PP1.[219,220] This is illustrated in Figure 8.1 (panel B). Given that in neurons B56δ-PP2A-mediated dephosphorylation at T75 increases PP1 inhibition by DARPP-32,[114] it is possible that in myocytes B56δ-PP2A-mediated dephosphorylation of I-1 at the equivalent residue (T75) and possibly also at S67 also promotes I-1-mediated PP1 inhibition. Thus, B56δ S573 phosphorylation status, through its effects on B56δ-PP2A activity and I-1-mediated PP1 inhibition, might regulate the phosphorylation status of PP1 substrate proteins indirectly.

One interesting observation that was reported in chapter 7 was the reduced phosphorylation of cMyBP-C S282 in ARVM expressing heterologous S573A B56δ. This might occur through reduced B56δ-PP2A-mediated dephosphorylation of I-1 and consequent increase in PP1 activity, particularly since it has been reported that cMyBP-C S282 phosphorylation is impaired in transgenic mice with cardiac-specific overexpression of inactive I-1 (i.e. I-1 constitutively phosphorylated at S67 and T75).[221]

Interestingly, PLM phosphorylation at its PKA site (S68) is increased in ARVM with heterologous expression of constitutively active I-1, indicating that this site is dephosphorylated by the I-1-sensitive phosphatase PP1.[222] Given this evidence, in future studies PLM S68 phosphorylation status could be used an indicator of PP1 activity, to establish whether the phosphorylation of B56δ at S573 regulates I-1 and thereby PP1 activities, at least in the relevant subcellular compartment. If the hypothesis is correct, the

phosphorylation of PLM at S68 would be increased in ARVM expressing WT B56δ and decreased in ARVM expressing S573A B56δ, through decreased or increased PP1 activity, respectively (Figure 8.1). In these future studies one might consider determining the phosphorylation of PP1 substrates (including cMyBP-C and PLM) in the absence and presence of the non-selective AR agonist noradrenaline. This would activate PKCα *and* PKA simultaneously and thus would result in a more physiological regulation of I-1 phosphorylation. Depending on the outcome of such studies, it may then be necessary to also determine the phosphorylation of I-1 at its regulatory sites. Given that endogenous I-1 is not readily detected by immunoblot analysis in cardiac cells,[223] however, these studies would need to be performed in ARVM co-transduced with an adenovirus that expresses the protein of interest.

A final important point to consider, is that both PP1 and PP2A catalytic subunits can also dephosphorylate phosphorylated Ser and Thr residues that do not reside in PKA substrate motifs. Thus, future work would also involve investigating the phosphorylation of non-PKA substrate phospho-proteins in ARVM with heterologous expression of WT or S573A B56δ proteins, in the absence and presence of ISO stimulation. A possible approach towards this aim would be to use a selection of phospho-motif antibodies and phosphorylation site-specific antibodies, to determine the phosphorylation of unknown and specific substrates, respectively. Any phospho-proteins that appear to be regulated through B56δ phosphorylation could then be identified by mass spectrometry approaches.

In conclusion, it is clear that further work is necessary to elucidate the physiological role of B56δ S573 phosphorylation in β-adrenergic regulation of cardiac PP2A (and thereby possibly also PP1) activity, protein phosphorylation and function. Ultimately, a better understanding of this role may facilitate the modulation of the specific holoenzyme in cardiac pathophysiology, for therapeutic benefit.

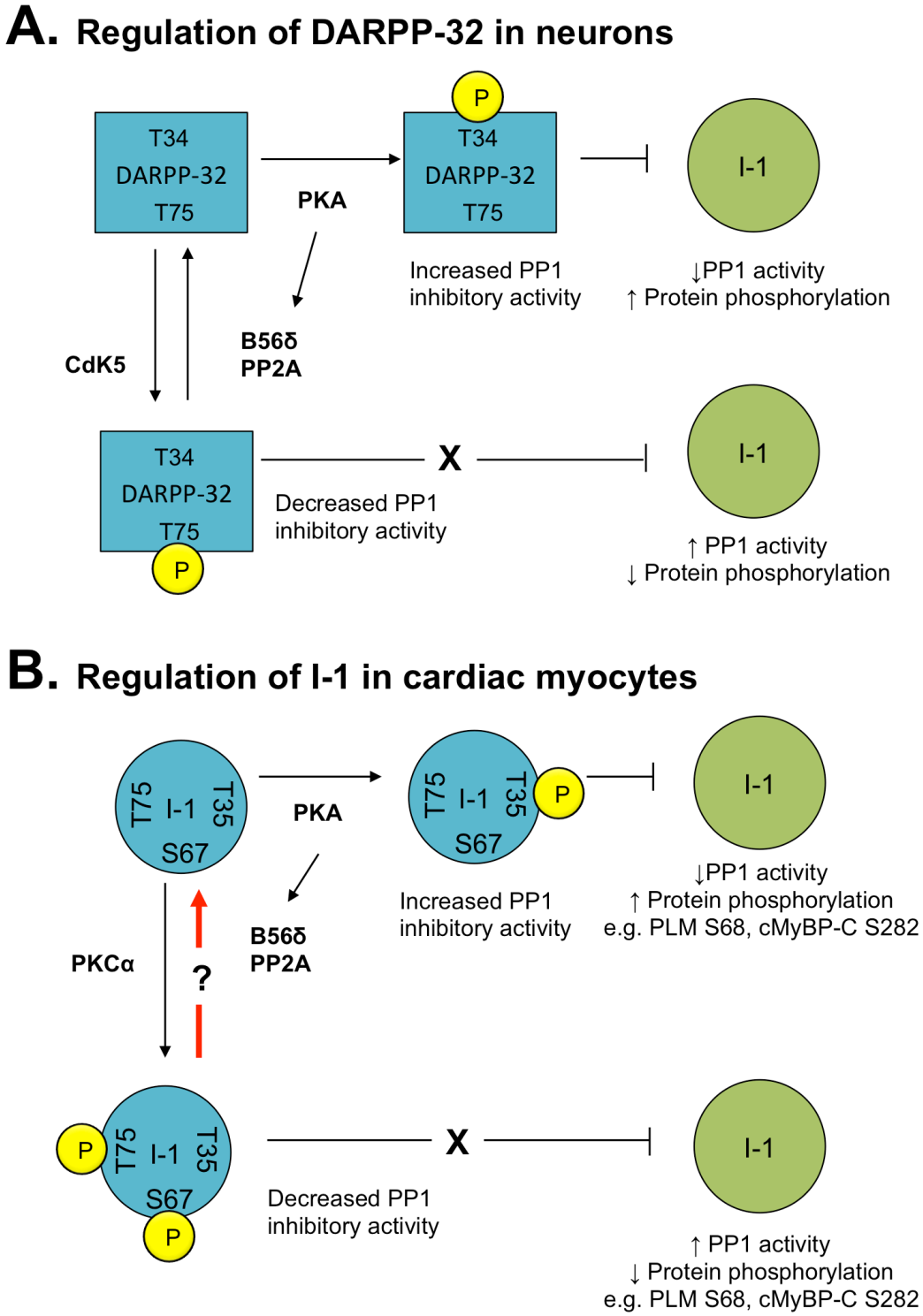
A. Regulation of DARPP-32 in neurons
T34
DARPP-32
T75
P
PKA
Increased PP1
inhibitory activity
I-1
↓PP1 activity
↑ Protein phosphorylation
CdK5
B56δ
PP2A
X
Decreased PP1
inhibitory activity
↑ PP1 activity
↓ Protein phosphorylation
B. Regulation of I-1 in cardiac myocytes
T75
I-1
T35
S67
PKA
Increased PP1
inhibitory activity
↓PP1 activity
↑ Protein phosphorylation
e.g. PLM S68, cMyBP-C S282
PKCα
?
B56δ
PP2A
Decreased PP1
inhibitory activity
↑ PP1 activity
↓ Protein phosphorylation
e.g. PLM S68, cMyBP-C S282

Figure 8.1 Phospho-regulation of DARPP-32 and I-1

A. In striatal neurons, PKA-mediated phosphorylation at T34 converts DARPP-32 into a potent inhibitor of PP1. This reduces PP1 activity and thereby increases the phosphorylation of PP1 substrate proteins. Conversely, cyclin-dependent kinase 5 (Cdk5)-mediated phosphorylation at T75 reduces the inhibitory effect of DARPP-32 on PP1. This results in increased PP1 activity and thereby reduced phosphorylation of PP1 substrate proteins. PKA-mediated phosphorylation of B56δ at S573 and consequent increase in B56δ-PP2A activity promotes the dephosphorylation of DARPP-32 at T75 and thereby facilitates the phosphorylation at T34. **B.** In cardiac myocytes, PKA-mediated phosphorylation at T35 converts I-1 into a potent inhibitor of PP1. This reduces PP1 activity and thereby increases the phosphorylation of PP1 substrate proteins. Conversely, PKCα-mediated phosphorylation at S67 and T75 reduces the inhibitory effect of I-1 on PP1. This results in increased PP1 activity and thereby reduced phosphorylation of PP1 substrate proteins. PKA-mediated phosphorylation of B56δ at S573 and consequent increase in B56δ-PP2A activity might promote the dephosphorylation of I-1 at S67/T75, thereby producing an apparently paradoxical increase in protein phosphorylation through PP1 inhibition.

References

1. Cohen P. The regulation of protein function by multisite phosphorylation-a 25 year update. *Trends Biochem Sci*. 2000;25:596-601.

2. Cohen P. The role of protein phosphorylation in human health and disease. The Sir Hans Krebs Medal Lecture. *Eur J Biochem*. 2001;268:5001-10.

3. Rapundalo ST. Cardiac protein phosphorylation: functional and pathophysiological correlates. *Cardiovasc Res*. 1998;38:559-88.

4. Walker LA, Fullerton DA and Buttrick PM. Contractile protein phosphorylation predicts human heart disease phenotypes. *Am J Physiol Heart Circ Physiol*. 2013;304:H1644-50.

5. Triposkiadis F, Karayannis G, Giamouzis G, Skoularigis J, Louridas G and Butler J. The sympathetic nervous system in heart failure physiology, pathophysiology, and clinical implications. *J Am Coll Cardiol*. 2009;54:1747-62.

6. Rockman HA, Koch WJ and Lefkowitz RJ. Seven-transmembrane-spanning receptors and heart function. *Nature*. 2002;415:206-12.

7. Xiang Y and Kobilka BK. Myocyte adrenoceptor signaling pathways. *Science*. 2003;300:1530-2.

8. Wettschureck N and Offermanns S. Mammalian G proteins and their cell type specific functions. *Physiol Rev*. 2005;85:1159-204.

9. Brodde OE, Michel MC and Zerkowski HR. Signal transduction mechanisms controlling cardiac contractility and their alterations in chronic heart failure. *Cardiovasc Res*. 1995;30:570-84.

10. Lohse MJ, Engelhardt S and Eschenhagen T. What is the role of β-adrenergic signaling in heart failure? *Circ Res*. 2003;93:896-906.

11. Taylor SS, Yang J, Wu J, Haste NM, Radzio-Andzelm E and Anand G. PKA: a portrait of protein kinase dynamics. *Biochim Biophys Acta*. 2004;1697:259-69.

12. Kopperud R, Christensen AE, Kjarland E, Viste K, Kleivdal H and Doskeland SO. Formation of inactive cAMP-saturated holoenzyme of cAMP-dependent protein kinase under physiological conditions. *J Biol Chem*. 2002;277:13443-8.

13. Saucerman JJ and McCulloch AD. Cardiac β-adrenergic signaling: from subcellular microdomains to heart failure. *Ann N Y Acad Sci*. 2006;1080:348-61.

14. Wong W and Scott JD. AKAP signalling complexes: focal points in space and time. *Nat Rev Mol Cell Biol*. 2004;5:959-70.

15. Ruehr ML, Russell MA and Bond M. A-kinase anchoring protein targeting of protein kinase A in the heart. *J Mol Cell Cardiol*. 2004;37:653-65.

16. Bender AT and Beavo JA. Cyclic nucleotide phosphodiesterases: molecular regulation to clinical use. *Pharmacol Rev*. 2006;58:488-520.

17. Zaccolo M and Movsesian MA. cAMP and cGMP signaling cross-talk: role of phosphodiesterases and implications for cardiac pathophysiology. *Circ Res*. 2007;100:1569-78.

18. Vandecasteele G, Rochais F, Abi-Gerges A and Fischmeister R. Functional localization of cAMP signalling in cardiac myocytes. *Biochem Soc Trans*. 2006;34:484-8.

19. Zaccolo M. cAMP signal transduction in the heart: understanding spatial control for the development of novel therapeutic strategies. *Br J Pharmacol*. 2009;158:50-60.

20. Di Benedetto G, Zoccarato A, Lissandron V, Terrin A, Li X, Houslay MD, Baillie GS and Zaccolo M. Protein kinase A type I and type II define distinct intracellular signaling compartments. *Circ Res*. 2008;103:836-44.

21. Xiang YK. Compartmentalization of β-adrenergic signals in cardiomyocytes. *Circ Res*. 2011;109:231-44.

22. Redden JM and Dodge-Kafka KL. AKAP phosphatase complexes in the heart. *J Cardiovasc Pharmacol*. 2011;58:354-62.

23. DiFrancesco D and Tortora P. Direct activation of cardiac pacemaker channels by intracellular cyclic AMP. *Nature*. 1991;351:145-7.

24. Houslay MD. Underpinning compartmentalised cAMP signalling through targeted cAMP breakdown. *Trends Biochem Sci*. 2010;35:91-100.

25. de Rooij J, Zwartkruis FJ, Verheijen MH, Cool RH, Nijman SM, Wittinghofer A and Bos JL. Epac is a Rap1 guanine-nucleotide-exchange factor directly activated by cyclic AMP. *Nature*. 1998;396:474-7.

26. Dao KK, Teigen K, Kopperud R, Hodneland E, Schwede F, Christensen AE, Martinez A and Doskeland SO. Epac1 and cAMP-dependent protein kinase holoenzyme have similar cAMP affinity,

but their cAMP domains have distinct structural features and cyclic nucleotide recognition. *J Biol Chem*. 2006;281:21500-11.

27. Ruiz-Hurtado G, Morel E, Dominguez-Rodriguez A, Llach A, Lezoualc'h F, Benitah JP and Gomez AM. Epac in cardiac calcium signaling. *J Mol Cell Cardiol*. 2013;58:162-71.

28. Oestreich EA, Malik S, Goonasekera SA, Blaxall BC, Kelley GG, Dirksen RT and Smrcka AV. Epac and phospholipase Cε regulate Ca2+ release in the heart by activation of protein kinase Cε and calcium-calmodulin kinase II. *J Biol Chem*. 2009;284:1514-22.

29. Pereira L, Rehmann H, Lao DH, Erickson JR, Bossuyt J, Chen J and Bers DM. Novel Epac fluorescent ligand reveals distinct Epac1 vs. Epac2 distribution and function in cardiomyocytes. *Proc Natl Acad Sci U S A*. 2015;112:3991-6.

30. Grimm M and Brown JH. β-adrenergic receptor signaling in the heart: role of CaMKII. *J Mol Cell Cardiol*. 2010;48:322-30.

31. De Koninck P and Schulman H. Sensitivity of CaM kinase II to the frequency of Ca2+ oscillations. *Science*. 1998;279:227-30.

32. Wegener AD, Simmerman HK, Lindemann JP and Jones LR. Phospholamban phosphorylation in intact ventricles. Phosphorylation of serine 16 and threonine 17 in response to β-adrenergic stimulation. *J Biol Chem*. 1989;264:11468-74.

33. Huke S and Bers DM. Ryanodine receptor phosphorylation at Serine 2030, 2808 and 2814 in rat cardiomyocytes. *Biochem Biophys Res Commun*. 2008;376:80-5.

34. Zhu WZ, Wang SQ, Chakir K, Yang D, Zhang T, Brown JH, Devic E, Kobilka BK, Cheng H and Xiao RP. Linkage of β1-adrenergic stimulation to apoptotic heart cell death through protein kinase A-independent activation of Ca2+/calmodulin kinase II. *J Clin Invest*. 2003;111:617-25.

35. Hausdorff WP, Caron MG and Lefkowitz RJ. Turning off the signal: desensitization of β-adrenergic receptor function. *FASEB J*. 1990;4:2881-9.

36. Moore CA, Milano SK and Benovic JL. Regulation of receptor trafficking by GRKs and arrestins. *Annu Rev Physiol*. 2007;69:451-82.

37. Lefkowitz RJ and Shenoy SK. Transduction of receptor signals by β-arrestins. *Science*. 2005;308:512-7.

38. Noma T, Lemaire A, Naga Prasad SV, Barki-Harrington L, Tilley DG, Chen J, Le Corvoisier P, Violin JD, Wei H, Lefkowitz RJ and Rockman HA. β-arrestin-mediated β1-adrenergic receptor transactivation of the EGFR confers cardioprotection. *J Clin Invest*. 2007;117:2445-58.

39. Steinberg SF. The molecular basis for distinct β-adrenergic receptor subtype actions in cardiomyocytes. *Circ Res*. 1999;85:1101-11.

40. Xiao RP. β-Adrenergic signaling in the heart: dual coupling of the β2-adrenergic receptor to G_s and G_i proteins. *Sci STKE*. 2001;2001:re15.

41. Kuznetsov V, Pak E, Robinson RB and Steinberg SF. β2-adrenergic receptor actions in neonatal and adult rat ventricular myocytes. *Circ Res*. 1995;76:40-52.

42. Zhu WZ, Zheng M, Koch WJ, Lefkowitz RJ, Kobilka BK and Xiao RP. Dual modulation of cell survival and cell death by β2-adrenergic signaling in adult mouse cardiac myocytes. *Proc Natl Acad Sci U S A*. 2001;98:1607-12.

43. De Jongh KS, Murphy BJ, Colvin AA, Hell JW, Takahashi M and Catterall WA. Specific phosphorylation of a site in the full-length form of the α1 subunit of the cardiac L-type calcium channel by adenosine 3',5'-cyclic monophosphate-dependent protein kinase. *Biochemistry*. 1996;35:10392-402.

44. Wehrens XH, Lehnart SE, Reiken S, Vest JA, Wronska A and Marks AR. Ryanodine receptor/calcium release channel PKA phosphorylation: a critical mediator of heart failure progression. *Proc Natl Acad Sci U S A*. 2006;103:511-518.

45. MacLennan DH and Kranias EG. Phospholamban: a crucial regulator of cardiac contractility. *Nat Rev Mol Cell Biol*. 2003;4:566-77.

46. Fuller W and Shattock MJ. Phospholemman and the cardiac sodium pump: protein kinase C, take a bow. *Circ Res*. 2006;99:1290-2.

47. Layland J, Solaro RJ and Shah AM. Regulation of cardiac contractile function by troponin I phosphorylation. *Cardiovasc Res*. 2005;66:12-21.

48. Sadayappan S, Gulick J, Osinska H, Barefield D, Cuello F, Avkiran M, Lasko VM, Lorenz JN, Maillet M, Martin JL, Brown JH, Bers DM, Molkentin JD, James J and Robbins J. A critical function for Ser-282 in cardiac Myosin binding protein-C phosphorylation and cardiac function. *Circ Res*. 2011;109:141-50.

49. El-Armouche A, Rau T, Zolk O, Ditz D, Pamminger T, Zimmermann WH, Jackel E, Harding SE, Boknik P, Neumann J and Eschenhagen T. Evidence for protein phosphatase inhibitor-1 playing an amplifier role in β-adrenergic signaling in cardiac myocytes. *FASEB J*. 2003;17:437-9.

50. Shaywitz AJ and Greenberg ME. CREB: a stimulus-induced transcription factor activated by a diverse array of extracellular signals. *Annu Rev Biochem*. 1999;68:821-61.

51. Collins S, Altschmied J, Herbsman O, Caron MG, Mellon PL and Lefkowitz RJ. A cAMP response element in the β2-adrenergic receptor gene confers transcriptional autoregulation by cAMP. *J Biol Chem*. 1990;265:19330-5.

52. Backs J and Olson EN. Control of cardiac growth by histone acetylation/deacetylation. *Circ Res*. 2006;98:15-24.

53. Backs J, Worst BC, Lehmann LH, Patrick DM, Jebessa Z, Kreusser MM, Sun Q, Chen L, Heft C, Katus HA and Olson EN. Selective repression of MEF2 activity by PKA-dependent proteolysis of HDAC4. *J Cell Biol*. 2011;195:403-15.

54. Ha CH, Kim JY, Zhao J, Wang W, Jhun BS, Wong C and Jin ZG. PKA phosphorylates histone deacetylase 5 and prevents its nuclear export, leading to the inhibition of gene transcription and cardiomyocyte hypertrophy. *Proc Natl Acad Sci U S A*. 2010;107:15467-72.

55. Haworth RS, Stathopoulou K, Candasamy AJ and Avkiran M. Neurohormonal regulation of cardiac histone deacetylase 5 nuclear localization by phosphorylation-dependent and phosphorylation-independent mechanisms. *Circ Res*. 2012;110:1585-95.

56. Stanley WC, Recchia FA and Lopaschuk GD. Myocardial substrate metabolism in the normal and failing heart. *Physiol Rev*. 2005;85:1093-129.

57. Dyck JR, Kudo N, Barr AJ, Davies SP, Hardie DG and Lopaschuk GD. Phosphorylation control of cardiac acetyl-CoA carboxylase by cAMP-dependent protein kinase and 5'-AMP activated protein kinase. *Eur J Biochem*. 1999;262:184-90.

58. Morisco C, Condorelli G, Trimarco V, Bellis A, Marrone C, Condorelli G, Sadoshima J and Trimarco B. Akt mediates the cross-talk between β-adrenergic and insulin receptors in neonatal cardiomyocytes. *Circ Res*. 2005;96:180-8.

59. Neumann J, Boknik P, Herzig S, Schmitz W, Scholz H, Gupta RC and Watanabe AM. Evidence for physiological functions of protein phosphatases in the heart: evaluation with okadaic acid. *Am J Physiol*. 1993;265:H257-66.

60. Neumann J, Maas R, Boknik P, Jones LR, Zimmermann N and Scholz H. Pharmacological characterization of protein phosphatase activities in preparations from failing human hearts. *J Pharmacol Exp Ther*. 1999;289:188-93.

61. Heijman J, Dewenter M, El-Armouche A and Dobrev D. Function and regulation of serine/threonine phosphatases in the healthy and diseased heart. *J Mol Cell Cardiol*. 2013;64:90-8.

62. Manning G, Whyte DB, Martinez R, Hunter T and Sudarsanam S. The protein kinase complement of the human genome. *Science*. 2002;298:1912-34.

63. Johnson SA and Hunter T. Kinomics: methods for deciphering the kinome. *Nat Methods*. 2005;2:17-25.

64. Ubersax JA and Ferrell JE, Jr. Mechanisms of specificity in protein phosphorylation. *Nat Rev Mol Cell Biol*. 2007;8:530-41.

65. Virshup DM and Shenolikar S. From promiscuity to precision: protein phosphatases get a makeover. *Mol Cell*. 2009;33:537-45.

66. Shi Y. Serine/threonine phosphatases: mechanism through structure. *Cell*. 2009;139:468-484.

67. Brautigan DL. Protein Ser/Thr phosphatases-the ugly ducklings of cell signalling. *FEBS J*. 2013;280:324-45.

68. Virshup DM. Protein phosphatase 2A: a panoply of enzymes. *Curr Opin Cell Biol*. 2000;12:180-185.

69. Janssens V and Goris J. Protein phosphatase 2A: a highly regulated family of serine/threonine phosphatases implicated in cell growth and signalling. *Biochem J*. 2001;353:417-39.

70. Janssens V, Goris J and Van Hoof C. PP2A: the expected tumor suppressor. *Curr Opin Genet Dev*. 2005;15:34-41.

71. Janssens V and Rebollo A. The role and therapeutic potential of Ser/Thr phosphatase PP2A in apoptotic signalling networks in human cancer cells. *Curr Mol Med*. 2012;12:268-87.

72. Chen W, Wang Z, Jiang C and Ding Y. PP2A-Mediated Anticancer Therapy. *Gastroenterol Res Pract*. 2013;2013:675429.

73. Ramaswamy K, Spitzer B and Kentsis A. Therapeutic Re-Activation of Protein Phosphatase 2A in Acute Myeloid Leukemia. *Front Oncol*. 2015;5:16.

74. Arnaud L, Chen S, Liu F, Li B, Khatoon S, Grundke-Iqbal I and Iqbal K. Mechanism of inhibition of PP2A activity and abnormal hyperphosphorylation of tau by I2(PP2A)/SET. *FEBS Lett*. 2011;585:2653-9.

75. Voronkov M, Braithwaite SP and Stock JB. Phosphoprotein phosphatase 2A: a novel druggable target for Alzheimer's disease. *Future Med Chem*. 2011;3:821-33.

76. Virshup DM. Protein phosphatase 2A: a panoply of enzymes. *Curr Opin Cell Biol*. 2000;12:180-5.

77. Janssens V, Longin S and Goris J. PP2A holoenzyme assembly: in cauda venenum (the sting is in the tail). *Trends Biochem Sci*. 2008;33:113-21.

78. Stone SR, Hofsteenge J and Hemmings BA. Molecular cloning of cDNAs encoding two isoforms of the catalytic subunit of protein phosphatase 2A. *Biochemistry*. 1987;26:7215-7220.

79. Arino J, Woon CW, Brautigan DL, Miller TB, Jr. and Johnson GL. Human liver phosphatase 2A: cDNA and amino acid sequence of two catalytic subunit isotypes. *Proc Natl Acad Sci U S A*. 1988;85:4252-6.

80. Khew-Goodall Y and Hemmings BA. Tissue-specific expression of mRNAs encoding α- and β-catalytic subunits of protein phosphatase 2A. *FEBS Lett*. 1988;238:265-8.

81. Gotz J, Probst A, Ehler E, Hemmings B and Kues W. Delayed embryonic lethality in mice lacking protein phosphatase 2A catalytic subunit Cα. *Proc Natl Acad Sci U S A*. 1998;95:12370-5.

82. Hemmings BA, Adams-Pearson C, Maurer F, Müller P, Goris J, Merlevede W, Hofsteenge J and Stone SR. α- and β-forms of the 65-kDa subunit of protein phosphatase 2A have a similar 39 amino acid repeating structure. *Biochemistry*. 1990;29:3166-3173.

83. Groves MR, Hanlon N, Turowski P, Hemmings BA and Barford D. The structure of the protein phosphatase 2A PR65/A subunit reveals the conformation of its 15 tandemly repeated HEAT motifs. *Cell*. 1999;96:99-110.

84. Xu Y, Xing Y, Chen Y, Chao Y, Lin Z, Fan E, Yu JW, Strack S, Jeffrey PD and Shi Y. Structure of the protein phosphatase 2A holoenzyme. *Cell*. 2006;127:1239-1251.

85. Cho US and Xu W. Crystal structure of a protein phosphatase 2A heterotrimeric holoenzyme. *Nature*. 2007;445:53-57.

86. Stanevich V, Zheng A, Guo F, Jiang L, Wlodarchak N and Xing Y. Mechanisms of the scaffold subunit in facilitating protein phosphatase 2A methylation. *PLoS One*. 2014;9:e86955.

87. Sents W, Ivanova E, Lambrecht C, Haesen D and Janssens V. The biogenesis of active protein phosphatase 2A holoenzymes: a tightly regulated process creating phosphatase specificity. *FEBS J*. 2012.

88. Kong M, Ditsworth D, Lindsten T and Thompson CB. α4 is an essential regulator of PP2A phosphatase activity. *Mol Cell*. 2009;36:51-60.

89. Jiang L, Stanevich V, Satyshur KA, Kong M, Watkins GR, Wadzinski BE, Sengupta R and Xing Y. Structural basis of protein phosphatase 2A stable latency. *Nat Commun*. 2013;4:1699.

90. De Baere I, Derua R, Janssens V, Van Hoof C, Waelkens E, Merlevede W and Goris J. Purification of porcine brain protein phosphatase 2A leucine carboxyl methyltransferase and cloning of the human homologue. *Biochemistry*. 1999;38:16539-47.

91. Ogris E, Du X, Nelson KC, Mak EK, Yu XX, Lane WS and Pallas DC. A protein phosphatase methylesterase (PME-1) is one of several novel proteins stably associating with two inactive mutants of protein phosphatase 2A. *J Biol Chem*. 1999;274:14382-91.

92. Tolstykh T, Lee J, Vafai S and Stock JB. Carboxyl methylation regulates phosphoprotein phosphatase 2A by controlling the association of regulatory B subunits. *EMBO J*. 2000;19:5682-91.

93. Wu J, Tolstykh T, Lee J, Boyd K, Stock JB and Broach JR. Carboxyl methylation of the phosphoprotein phosphatase 2A catalytic subunit promotes its functional association with regulatory subunits in vivo. *EMBO J*. 2000;19:5672-81.

94. Evans DR and Hemmings BA. Mutation of the C-terminal leucine residue of PP2Ac inhibits PR55/B subunit binding and confers supersensitivity to microtubule destabilization in Saccharomyces cerevisiae. *Mol Gen Genet*. 2000;264:425-32.

95. Longin S, Zwaenepoel K, Louis JV, Dilworth S, Goris J and Janssens V. Selection of protein phosphatase 2A regulatory subunits is mediated by the C terminus of the catalytic subunit. *J Biol Chem*. 2007;282:26971-26980.

96. Chen J, Martin BL and Brautigan DL. Regulation of protein serine-threonine phosphatase type-2A by tyrosine phosphorylation. *Science*. 1992;257:1261-1264.

97. Begum N and Ragolia L. cAMP counter-regulates insulin-mediated protein phosphatase-2A inactivation in rat skeletal muscle cells. *J Biol Chem*. 1996;271:31166-71.

98. Longin S, Zwaenepoel K, Louis JV, Dilworth S, Goris J and Janssens V. Selection of protein phosphatase 2A regulatory subunits is mediated by the C terminus of the catalytic Subunit. *J Biol Chem*. 2007;282:26971-80.

99. Wu F and Wilson JX. Peroxynitrite-dependent activation of protein phosphatase type 2A mediates microvascular endothelial barrier dysfunction. *Cardiovasc Res*. 2009;81:38-45.

100. Kotlo K, Xing Y, Lather S, Grillon JM, Johnson K, Skidgel RA, Solaro RJ and Danziger RS. PR65A phosphorylation regulates PP2A complex signaling. *PLoS One*. 2014;9:e85000.

101. Li M, Guo H and Damuni Z. Purification and characterization of two potent heat-stable protein inhibitors of protein phosphatase 2A from bovine kidney. *Biochemistry*. 1995;34:1988-96.

102. Anazawa Y, Nakagawa H, Furihara M, Ashida S, Tamura K, Yoshioka H, Shuin T, Fujioka T, Katagiri T and Nakamura Y. PCOTH, a novel gene overexpressed in prostate cancers, promotes

prostate cancer cell growth through phosphorylation of oncoprotein TAF-Iβ/SET. *Cancer Res*. 2005;65:4578-86.

103. Switzer CH, Cheng RY, Vitek TM, Christensen DJ, Wink DA and Vitek MP. Targeting SET/I(2)PP2A oncoprotein functions as a multi-pathway strategy for cancer therapy. *Oncogene*. 2011;30:2504-13.

104. Cristobal I, Rincon R, Manso R, Carames C, Zazo S, Madoz-Gurpide J, Rojo F and Garcia-Foncillas J. Deregulation of the PP2A inhibitor SET shows promising therapeutic implications and determines poor clinical outcome in patients with metastatic colorectal cancer. *Clin Cancer Res*. 2015;21:347-56.

105. Slupe AM, Merrill RA and Strack S. Determinants for Substrate Specificity of Protein Phosphatase 2A. *Enzyme Res*. 2011;2011:398751.

106. Strack S, Chang D, Zaucha JA, Colbran RJ and Wadzinski BE. Cloning and characterization of Bδ, a novel regulatory subunit of protein phosphatase 2A. *FEBS Lett*. 1999;460:462-6.

107. Mayer RE, Hendrix P, Cron P, Matthies R, Stone SR, Goris J, Merlevede W, Hofsteenge J and Hemmings BA. Structure of the 55-kDa regulatory subunit of protein phosphatase 2A: evidence for a neuronal-specific isoform. *Biochemistry*. 1991;30:3589-97.

108. McCright B and Virshup DM. Identification of a new family of protein phosphatase 2A regulatory subunits. *J Biol Chem*. 1995;270:26123-8.

109. Flegg CP, Sharma M, Medina-Palazon C, Jamieson C, Galea M, Brocardo MG, Mills K and Henderson BR. Nuclear export and centrosome targeting of the protein phosphatase 2A subunit B56α: role of B56α in nuclear export of the catalytic subunit. *J Biol Chem*. 2010;285:18144-54.

110. McCright B, Rivers AM, Audlin S and Virshup DM. The B56 family of protein phosphatase 2A (PP2A) regulatory subunits encodes differentiation-induced phosphoproteins that target PP2A to both nucleus and cytoplasm. *J Biol Chem*. 1996;271:22081-9.

111. Gigena MS, Ito A, Nojima H and Rogers TB. A B56 regulatory subunit of protein phosphatase 2A localizes to nuclear speckles in cardiomyocytes. *Am J Physiol Heart Circ Physiol*. 2005;289:H285-94.

112. Price NE and Mumby MC. Effects of regulatory subunits on the kinetics of protein phosphatase 2A. *Biochemistry*. 2000;39:11312-8.

113. Xu Y, Chen Y, Zhang P, Jeffrey PD and Shi Y. Structure of a protein phosphatase 2A holoenzyme: insights into B55-mediated Tau dephosphorylation. *Mol Cell*. 2008;31:873-85.

114. Ahn J-H, McAvoy T, Rakhilin SV, Nishi A, Greengard P and Nairn AC. Protein kinase A activates protein phosphatase 2A by phosphorylation of the B56δ subunit. *Proc Natl Acad Sci U S A*. 2007;104:2979-2984.

115. Kirchhefer U, Heinick A, König S, Kristensen T, Müller FU, Seidl MD and Boknik P. Protein phosphatase 2A is regulated by PKCα-dependent phosphorylation of its targeting subunit B56α at Ser41. *J Biol Chem*. 2013.

116. Csortos C, Zolnierowicz S, Bako E, Durbin SD and DePaoli-Roach AA. High complexity in the expression of the B' subunit of protein phosphatase 2A. Evidence for the existence of at least seven novel isoforms. *J Biol Chem*. 1996;271:2578-88.

117. McCright B, Brothman AR and Virshup DM. Assignment of human protein phosphatase 2A regulatory subunit genes B56α, B56β, B56γ, B56δ, and B56ε (PPP2R5A-PPP2R5E), highly expressed in muscle and brain, to chromosome regions 1q41, 11q12, 3p21, 6p21.1, and 7p11.2 --> p12. *Genomics*. 1996;36:168-70.

118. Tehrani MA, Mumby MC and Kamibayashi C. Identification of a novel protein phosphatase 2A regulatory subunit highly expressed in muscle. *J Biol Chem*. 1996;271:5164-70.

119. Bhasin N, Cunha SR, Mudannayake M, Gigena MS, Rogers TB and Mohler PJ. Molecular basis for PP2A regulatory subunit B56α targeting in cardiomyocytes. *Am J Physiol Heart Circ Physiol*. 2007;293:H109-19.

120. Louis JV, Martens E, Borghgraef P, Lambrecht C, Sents W, Longin S, Zwaenepoel K, Pijnenborg R, Landrieu I, Lippens G, Ledermann B, Gotz J, Van Leuven F, Goris J and Janssens V. Mice lacking phosphatase PP2A subunit PR61/B'δ (Ppp2r5d) develop spatially restricted tauopathy by deregulation of CDK5 and GSK3β. *Proc Natl Acad Sci U S A*. 2011;108:6957-6962.

121. Shouse GP, Nobumori Y, Panowicz MJ and Liu X. ATM-mediated phosphorylation activates the tumor-suppressive function of B56γ-PP2A. *Oncogene*. 2011;30:3755-65.

122. Ahn J-H, Kim Y, Kim H-S, Greengard P and Nairn AC. Protein kinase C-dependent dephosphorylation of tyrosine hydroxylase requires the B56δ heterotrimeric form of protein phosphatase 2A. *PLoS One*. 2011;6:e26292.

123. Margolis SS, Perry JA, Forester CM, Nutt LK, Guo Y, Jardim MJ, Thomenius MJ, Freel CD, Darbandi R, Ahn JH, Arroyo JD, Wang XF, Shenolikar S, Nairn AC, Dunphy WG, Hahn WC, Virshup DM and Kornbluth S. Role for the PP2A/B56δ phosphatase in regulating 14-3-3 release from Cdc25 to control mitosis. *Cell*. 2006;127:759-73.

124. Ruvolo VR, Kurinna SM, Karanjeet KB, Schuster TF, Martelli AM, McCubrey JA and Ruvolo PP. PKR regulates B56α-mediated BCL2 phosphatase activity in acute lymphoblastic leukemia-derived REH cells. *J Biol Chem*. 2008;283:35474-85.

125. Low ICC, Loh T, Huang Y, Virshup DM and Pervaiz S. Sustained Ser70 phosphorylation of Bcl-2 by selective tyrosine nitration of protein phosphatase 2A-B56δ stabilizes its anti-apoptotic activity. *Blood*. 2014.

126. Bialojan C and Takai A. Inhibitory effect of a marine-sponge toxin, okadaic acid, on protein phosphatases. Specificity and kinetics. *Biochem J*. 1988;256:283-90.

127. De Arcangelis V, Soto D and Xiang Y. Phosphodiesterase 4 and phosphatase 2A differentially regulate cAMP/protein kinase a signaling for cardiac myocyte contraction under stimulation of β_1 adrenergic receptor. *Mol Pharmacol*. 2008;74:1453-62.

128. Davare MA, Horne MC and Hell JW. Protein phosphatase 2A is associated with class C L-type calcium channels (Cav1.2) and antagonizes channel phosphorylation by cAMP-dependent protein kinase. *J Biol Chem*. 2000;275:39710-39717.

129. Hall DD, Feekes JA, Arachchige Don AS, Shi M, Hamid J, Chen L, Strack S, Zamponi GW, Horne MC and Hell JW. Binding of protein phosphatase 2A to the L-type calcium channel Cav1.2 next to Ser1928, its main PKA site, is critical for Ser1928 dephosphorylation. *Biochemistry*. 2006;45:3448-59.

130. Xu H, Ginsburg KS, Hall DD, Zimmermann M, Stein IS, Zhang M, Tandan S, Hill JA, Horne MC, Bers D and Hell JW. Targeting of protein phosphatases PP2A and PP2B to the C-terminus of the L-type calcium channel Cav1.2. *Biochemistry*. 2010;49:10298-10307.

131. Marx SO, Reiken S, Hisamatsu Y, Jayaraman T, Burkhoff D, Rosemblit N and Marks AR. PKA phosphorylation dissociates FKBP12.6 from the calcium release channel (ryanodine receptor): defective regulation in failing hearts. *Cell*. 2000;101:365-376.

132. Mustafa SJ, Morrison RR, Teng B and Pelleg A. Adenosine receptors and the heart: role in regulation of coronary blood flow and cardiac electrophysiology. *Handb Exp Pharmacol*. 2009:161-88.

133. Gupta RC, Neumann J, Durant P and Watanabe AM. A1-adenosine receptor-mediated inhibition of isoproterenol-stimulated protein phosphorylation in ventricular myocytes. Evidence against a cAMP-dependent effect. *Circ Res*. 1993;72:65-74.

134. Liu Q and Hofmann PA. Antiadrenergic effects of adenosine A1 receptor-mediated protein phosphatase 2a activation in the heart. *Am J Physiol Heart Circ Physiol*. 2002;283:H1314-21.

135. Gupta RC, Neumann J, Boknik P and Watanabe AM. M2-specific muscarinic cholinergic receptor-mediated inhibition of cardiac regulatory protein phosphorylation. *Am J Physiol*. 1994;266:H1138-44.

136. Herzig S, Meier A, Pfeiffer M and Neumann J. Stimulation of protein phosphatases as a mechanism of the muscarinic-receptor-mediated inhibition of cardiac L-type Ca^{2+} channels. *Pflugers Arch*. 1995;429:531-8.

137. Vasudevan NT, Mohan ML, Gupta MK, Hussain AK and Naga Prasad SV. Inhibition of protein phosphatase 2A activity by PI3Kγ regulates β-adrenergic receptor function. *Mol Cell*. 2011;41:636-48.

138. Daniels RH and Bokoch GM. p21-activated protein kinase: a crucial component of morphological signaling? *Trends Biochem Sci*. 1999;24:350-5.

139. Westphal RS, Coffee RL, Jr., Marotta A, Pelech SL and Wadzinski BE. Identification of kinase-phosphatase signaling modules composed of p70 S6 kinase-protein phosphatase 2A (PP2A) and p21-activated kinase-PP2A. *J Biol Chem*. 1999;274:687-92.

140. Ke Y, Wang L, Pyle WG, de Tombe PP and Solaro RJ. Intracellular localization and functional effects of P21-activated kinase-1 (Pak1) in cardiac myocytes. *Circ Res*. 2004;94:194-200.

141. Sheehan KA, Ke Y and Solaro RJ. p21-Activated kinase-1 and its role in integrated regulation of cardiac contractility. *Am J Physiol Regul Integr Comp Physiol*. 2007;293:R963-73.

142. Liu L and Eisen HJ. Epidemiology of heart failure and scope of the problem. *Cardiol Clin*. 2014;32:1-8, vii.

143. Mann DL and Bristow MR. Mechanisms and models in heart failure: the biomechanical model and beyond. *Circulation*. 2005;111:2837-49.

144. Olson EN. A decade of discoveries in cardiac biology. *Nat Med*. 2004;10:467-74.

145. Kemp CD and Conte JV. The pathophysiology of heart failure. *Cardiovasc Pathol*. 2012;21:365-71.

146. Boknik P, Fockenbrock M, Herzig S, Knapp J, Linck B, Lüss H, Müller FU, Müller T, Schmitz W, Schröder F and Neumann J. Protein phosphatase activity is increased in a rat model of long-term β-adrenergic stimulation. *Naunyn Schmiedebergs Arch Pharmacol*. 2000;362:222-31.

147. Larsen KO, Lygren B, Sjaastad I, Krobert KA, Arnkvaern K, Florholmen G, Larsen AK, Levy FO, Tasken K, Skjonsberg OH and Christensen G. Diastolic dysfunction in alveolar hypoxia: a role for interleukin-18-mediated increase in protein phosphatase 2A. *Cardiovasc Res*. 2008;80:47-54.

148. Ai X and Pogwizd SM. Connexin 43 downregulation and dephosphorylation in nonischemic heart failure is associated with enhanced colocalized protein phosphatase type 2A. *Circ Res*. 2005;96:54-63.

149. Beardslee MA, Lerner DL, Tadros PN, Laing JG, Beyer EC, Yamada KA, Kleber AG, Schuessler RB and Saffitz JE. Dephosphorylation and intracellular redistribution of ventricular connexin43 during electrical uncoupling induced by ischemia. *Circ Res*. 2000;87:656-62.

150. Ai X, Jiang A, Ke Y, Solaro RJ and Pogwizd SM. Enhanced activation of p21-activated kinase 1 in heart failure contributes to dephosphorylation of connexin 43. *Cardiovasc Res*. 2011;92:106-14.

151. Cheng G, Kasiganesan H, Baicu CF, Wallenborn JG, Kuppuswamy D and Cooper Gt. Cytoskeletal role in protection of the failing heart by β-adrenergic blockade. *Am J Physiol Heart Circ Physiol*. 2012;302:H675-87.

152. Marshall M, Anilkumar N, Layland J, Walker SJ, Kentish JC, Shah AM and Cave AC. Protein phosphatase 2A contributes to the cardiac dysfunction induced by endotoxemia. *Cardiovasc Res*. 2009;82:67-76.

153. Bone RC, Sprung CL and Sibbald WJ. Definitions for sepsis and organ failure. *Crit Care Med*. 1992;20:724-6.

154. Merx MW and Weber C. Sepsis and the heart. *Circulation*. 2007;116:793-802.

155. Tavernier B, Li JM, El-Omar MM, Lanone S, Yang ZK, Trayer IP, Mebazaa A and Shah AM. Cardiac contractile impairment associated with increased phosphorylation of troponin I in endotoxemic rats. *FASEB J*. 2001;15:294-6.

156. Ling S, Sun Q, Li Y, Zhang L, Zhang P, Wang X, Tian C, Li Q, Song J, Liu H, Kan G, Cao H, Huang Z, Nie J, Bai Y, Chen S, Li Y, He F, Zhang L and Li Y. CKIP-1 inhibits cardiac hypertrophy by regulating class II histone deacetylase phosphorylation through recruiting PP2A. *Circulation*. 2012;126:3028-40.

157. Gergs U, Boknik P, Buchwalow I, Fabritz L, Matus M, Justus I, Hanske G, Schmitz W and Neumann J. Overexpression of the catalytic subunit of protein phosphatase 2A impairs cardiac function. *J Biol Chem*. 2004;279:40827-34.

158. Zhang T, Johnson EN, Gu Y, Morissette MR, Sah VP, Gigena MS, Belke DD, Dillmann WH, Rogers TB, Schulman H, Ross J, Jr. and Brown JH. The cardiac-specific nuclear delta(B) isoform of Ca2+/calmodulin-dependent protein kinase II induces hypertrophy and dilated cardiomyopathy associated with increased protein phosphatase 2A activity. *J Biol Chem*. 2002;277:1261-7.

159. Brewis N, Ohst K, Fields K, Rapacciuolo A, Chou D, Bloor C, Dillmann W, Rockman H and Walter G. Dilated cardiomyopathy in transgenic mice expressing a mutant A subunit of protein phosphatase 2A. *Am J Physiol Heart Circ Physiol*. 2000;279:H1307-18.

160. Liu Q and Hofmann PA. Protein phosphatase 2A-mediated cross-talk between p38 MAPK and ERK in apoptosis of cardiac myocytes. *Am J Physiol Heart Circ Physiol*. 2004;286:H2204-12.

161. Morrison DK. MAP kinase pathways. *Cold Spring Harb Perspect Biol*. 2012;4.

162. Snabaitis AK, D'Mello R, Dashnyam S and Avkiran M. A novel role for protein phosphatase 2A in receptor-mediated regulation of the cardiac sarcolemmal Na^+/H^+ exchanger NHE1. *J Biol Chem*. 2006;281:20252-62.

163. Fliegel L. Molecular biology of the myocardial Na^+/H^+ exchanger. *J Mol Cell Cardiol*. 2008;44:228-37.

164. Cunha SR and Mohler PJ. Cardiac ankyrins: Essential components for development and maintenance of excitable membrane domains in heart. *Cardiovasc Res*. 2006;71:22-9.

165. Cunha SR and Mohler PJ. Obscurin targets ankyrin-B and protein phosphatase 2A to the cardiac M-line. *J Biol Chem*. 2008;283:31968-80.

166. Yin X, Cuello F, Mayr U, Hao Z, Hornshaw M, Ehler E, Avkiran M and Mayr M. Proteomics analysis of the cardiac myofilament subproteome reveals dynamic alterations in phosphatase subunit distribution. *Mol Cell Proteomics*. 2010;9:497-509.

167. Bartel DP. MicroRNAs: genomics, biogenesis, mechanism, and function. *Cell*. 2004;116:281-97.

168. Thum T, Galuppo P, Wolf C, Fiedler J, Kneitz S, van Laake LW, Doevendans PA, Mummery CL, Borlak J, Haverich A, Gross C, Engelhardt S, Ertl G and Bauersachs J. MicroRNAs in the human heart: a clue to fetal gene reprogramming in heart failure. *Circulation*. 2007;116:258-67.

169. Terentyev D, Belevych AE, Terentyeva R, Martin MM, Malana GE, Kuhn DE, Abdellatif M, Feldman DS, Elton TS and Gyorke S. miR-1 overexpression enhances Ca^{2+} release and promotes cardiac arrhythmogenesis by targeting PP2A regulatory subunit B56α and causing CaMKII-dependent hyperphosphorylation of RyR2. *Circ Res*. 2009;104:514-21.

170. Liang Q and Molkentin JD. Redefining the roles of p38 and JNK signaling in cardiac hypertrophy: dichotomy between cultured myocytes and animal models. *J Mol Cell Cardiol*. 2003;35:1385-94.

171. Glaser ND, Lukyanenko YO, Wang Y, Wilson GM and Rogers TB. JNK activation decreases PP2A regulatory subunit B56α expression and mRNA stability and increases AUF1 expression in cardiomyocytes. *Am J Physiol Heart Circ Physiol*. 2006;291:H1183-92.

172. Kirchhefer U, Brekle C, Eskandar J, Isensee G, Kucerova D, Mueller FU, Pinet F, Schulte JS, Seidl MD and Boknik P. Cardiac function is regulated by B56α-mediated targeting of PP2A to contractile relevant substrates. *J Biol Chem*. 2014.

173. Zhou XW, Mudannayake M, Green M, Gigena MS, Wang G, Shen RF and Rogers TB. Proteomic studies of PP2A-B56γ1 phosphatase complexes reveal phosphorylation-regulated partners in cardiac local signaling. *J Proteome Res*. 2007;6:3433-42.

174. Ding JH, Xu X, Yang D, Chu PH, Dalton ND, Ye Z, Yeakley JM, Cheng H, Xiao RP, Ross J, Chen J and Fu XD. Dilated cardiomyopathy caused by tissue-specific ablation of SC35 in the heart. *EMBO J*. 2004;23:885-96.

175. Xu X, Yang D, Ding JH, Wang W, Chu PH, Dalton ND, Wang HY, Bermingham JRJ, Ye Z, Liu F, Rosenfeld MG, Manley JL, Ross JJ, Chen J, Xiao RP, Cheng H and Fu XD. ASF/SF2-regulated CaMKIIδ alternative splicing temporally reprograms excitation-contraction coupling in cardiac muscle. *Cell*. 2005;120:59-72.

176. Varadkar P, Despres D, Kraman M, Lozier J, Phadke A, Nagaraju K and McCright B. The protein phosphatase 2A B56γ regulatory subunit is required for heart development. *Dev Dyn*. 2014.

177. Dodge-Kafka KL, Bauman A, Mayer N, Henson E, Heredia L, Ahn J, McAvoy T, Nairn AC and Kapiloff MS. cAMP-stimulated protein phosphatase 2A activity associated with muscle A kinase-anchoring protein (mAKAP) signaling complexes inhibits the phosphorylation and activity of the cAMP-specific phosphodiesterase PDE4D3. *J Biol Chem*. 2010;285:11078-86.

178. Marx SO, Reiken S, Hisamatsu Y, Gaburjakova M, Gaburjakova J, Yang YM, Rosemblit N and Marks AR. Phosphorylation-dependent regulation of ryanodine receptors: a novel role for leucine/isoleucine zippers. *J Cell Biol*. 2001;153:699-708.

179. Janssens V, Jordens J, Stevens I, Van Hoof C, Martens E, De Smedt H, Engelborghs Y, Waelkens E and Goris J. Identification and functional analysis of two Ca2+-binding EF-hand motifs in the B"/PR72 subunit of protein phosphatase 2A. *J Biol Chem*. 2003;278:10697-706.

180. Marx SO, Reiken S, Hisamatsu Y, Jayaraman T, Burkhoff D, Rosemblit N and Marks AR. PKA phosphorylation dissociates FKBP12.6 from the calcium release channel (ryanodine receptor): defective regulation in failing hearts. *Cell*. 2000;101:365-76.

181. Nicklin SA and Baker AH. Simple methods for preparing recombinant adenoviruses for high-efficiency transduction of vascular cells. *Methods Mol Med*. 1999;30:271-83.

182. Strack S, Cribbs JT and Gomez L. Critical role for protein phosphatase 2A heterotrimers in mammalian cell survival. *J Biol Chem*. 2004;279:47732-9.

183. DeGrande ST, Little SC, Nixon DJ, Wright P, Snyder J, Dun W, Murphy N, Kilic A, Higgins R, Binkley PF, Boyden PA, Carnes CA, Anderson ME, Hund TJ and Mohler PJ. Molecular mechanisms underlying cardiac protein phosphatase 2A regulation in heart. *J Biol Chem*. 2013;288:1032-46.

184. Tanabe O, Gomez GA, Nishito Y, Usui H and Takeda M. Molecular heterogeneity of the cDNA encoding a 74-kDa regulatory subunit (B" or delta) of human protein phosphatase 2A. *FEBS Lett*. 1997;408:52-6.

185. Tanabe O, Nagase T, Murakami T, Nozaki H, Usui H, Nishito Y, Hayashi H, Kagamiyama H and Takeda M. Molecular cloning of a 74-kDa regulatory subunit (B″ or δ) of human protein phosphatase 2A. *FEBS Lett*. 1996;379:107-111.

186. Usui H, Inoue R, Tanabe O, Nishito Y, Shimizu M, Hayashi H, Kagamiyama H and Takeda M. Activation of protein phosphatase 2A by cAMP-dependent protein kinase-catalyzed phosphorylation of the 74-kDa B'' (δ) regulatory subunit in vitro and identification of the phosphorylation sites. *FEBS Lett*. 1998;430:312-6.

187. Flynn MP, Maizels ET, Karlsson AB, McAvoy T, Ahn JH, Nairn AC and Hunzicker-Dunn M. Luteinizing hormone receptor activation in ovarian granulosa cells promotes protein kinase A-dependent dephosphorylation of microtubule-associated protein 2D. *Mol Endocrinol*. 2008;22:1695-710.

188. Kinoshita E, Kinoshita-Kikuta E and Koike T. Separation and detection of large phosphoproteins using Phos-tag SDS-PAGE. *Nat Protoc*. 2009;4:1513-21.

189. Dooley DJ, Bittiger H and Reymann NC. CGP 20712 A: a useful tool for quantitating β_1- and β_2-adrenoceptors. *Eur J Pharmacol*. 1986;130:137-9.

190. Bilski AJ, Halliday SE, Fitzgerald JD and Wale JL. The pharmacology of a β2-selective adrenoceptor antagonist (ICI 118,551). *J Cardiovasc Pharmacol*. 1983;5:430-7.

191. Murray AJ. Pharmacological PKA inhibition: all may not be what it seems. *Sci Signal*. 2008;1:re4.

192. Stuenaes JT, Bolling A, Ingvaldsen A, Rommundstad C, Sudar E, Lin FC, Lai YC and Jensen J. β-adrenoceptor stimulation potentiates insulin-stimulated PKB phosphorylation in rat cardiomyocytes via cAMP and PKA. *Br J Pharmacol*. 2010;160:116-29.

193. Candasamy AJ, Haworth RS, Cuello F, Ibrahim M, Aravamudhan S, Kruger M, Holt MR, Terracciano CM, Mayr M, Gautel M and Avkiran M. Phosphoregulation of the titin-cap protein telethonin in cardiac myocytes. *J Biol Chem*. 2014;289:1282-93.

194. Green SA, Holt BD and Liggett SB. β1- and β2-adrenergic receptors display subtype-selective coupling to Gs. *Mol Pharmacol*. 1992;41:889-93.

195. Alexander S, Mathie A and Peters J. Guide to Receptors and Channels (GRAC), 4th Edition. *Br J Pharmacol*. 2009;158 Suppl 1:S1-254.

196. Haworth RS, Roberts NA, Cuello F and Avkiran M. Regulation of protein kinase D activity in adult myocardium: novel counter-regulatory roles for protein kinase Cε and protein kinase A. *J Mol Cell Cardiol*. 2007;43:686-695.

197. Shizukuda Y and Buttrick PM. Subtype specific roles of β-adrenergic receptors in apoptosis of adult rat ventricular myocytes. *J Mol Cell Cardiol*. 2002;34:823-831.

198. Davies SP, Reddy H, Caivano M and Cohen P. Specificity and mechanism of action of some commonly used protein kinase inhibitors. *Biochem J*. 2000;351:95-105.

199. Lochner A and Moolman JA. The many faces of H89: a review. *Cardiovasc Drug Rev*. 2006;24:261-74.

200. Penn RB, Parent J-L, Pronin AN, Panettieri RA and Benovic JL. Pharmacological Inhibition of Protein Kinases in Intact Cells: Antagonism of β Adrenergic Receptor Ligand Binding by H-89 Reveals Limitations of Usefulness. *J Pharmacol Exp Ther*. 1999;288:428-437.

201. Nagase T, Murakami T, Nozaki H, Inoue R, Nishito Y, Tanabe O, Usui H and Takeda M. Tissue and subcellular distributions, and characterization of rat brain protein phosphatase 2A containing a 72-kDaδ/B" subunit. *J Biochem*. 1997;122:178-87.

202. Luo J, Deng ZL, Luo X, Tang N, Song WX, Chen J, Sharff KA, Luu HH, Haydon RC, Kinzler KW, Vogelstein B and He TC. A protocol for rapid generation of recombinant adenoviruses using the AdEasy system. *Nat Protoc*. 2007;2:1236-47.

203. He TC, Zhou S, da Costa LT, Yu J, Kinzler KW and Vogelstein B. A simplified system for generating recombinant adenoviruses. *Proc Natl Acad Sci U S A*. 1998;95:2509-14.

204. Strack S, Ruediger R, Walter G, Dagda RK, Barwacz CA and Cribbs JT. Protein phosphatase 2A holoenzyme assembly: identification of contacts between B-family regulatory and scaffolding A subunits. *J Biol Chem*. 2002;277:20750-5.

205. McAvoy T and Nairn AC. Serine/threonine protein phosphatase assays. *Curr Protoc Mol Biol*. 2010;Chapter 18:Unit18 18.

206. Shanley TP, Vasi N, Denenberg A and Wong HR. The serine/threonine phosphatase, PP2A: endogenous regulator of inflammatory cell signaling. *J Immunol*. 2001;166:966-72.

207. Kamibayashi C, Estes R, Lickteig RL, Yang SI, Craft C and Mumby MC. Comparison of heterotrimeric protein phosphatase 2A containing different B subunits. *J Biol Chem*. 1994;269:20139-48.

208. Stipanovich A, Valjent E, Matamales M, Nishi A, Ahn JH, Maroteaux M, Bertran-Gonzalez J, Brami-Cherrier K, Enslen H, Corbille AG, Filhol O, Nairn AC, Greengard P, Herve D and Girault JA. A

phosphatase cascade by which rewarding stimuli control nucleosomal response. *Nature*. 2008;453:879-84.

209. Pearson RB and Kemp BE. Protein kinase phosphorylation site sequences and consensus specificity motifs: tabulations. *Methods Enzymol*. 1991;200:62-81.

210. Lundby A, Andersen MN, Steffensen AB, Horn H, Kelstrup CD, Francavilla C, Jensen LJ, Schmitt N, Thomsen MB and Olsen JV. In vivo phosphoproteomics analysis reveals the cardiac targets of β-adrenergic receptor signaling. *Sci Signal*. 2013;6:rs11.

211. Li L, Desantiago J, Chu G, Kranias EG and Bers DM. Phosphorylation of phospholamban and troponin I in β-adrenergic-induced acceleration of cardiac relaxation. *Am J Physiol Heart Circ Physiol*. 2000;278:H769-79.

212. Sadayappan S, Gulick J, Osinska H, Martin LA, Hahn HS, Dorn GW, 2nd, Klevitsky R, Seidman CE, Seidman JG and Robbins J. Cardiac myosin-binding protein-C phosphorylation and cardiac function. *Circ Res*. 2005;97:1156-63.

213. Firulli BA, Howard MJ, McDaid JR, McIlreavey L, Dionne KM, Centonze VE, Cserjesi P, Virshup DM and Firulli AB. PKA, PKC, and the protein phosphatase 2A influence HAND factor function: a mechanism for tissue-specific transcriptional regulation. *Mol Cell*. 2003;12:1225-1237.

214. Karlsson AB, Maizels ET, Flynn MP, Jones JC, Shelden EA, Bamburg JR and Hunzicker-Dunn M. Luteinizing hormone receptor-stimulated progesterone production by preovulatory granulosa cells requires protein kinase A-dependent activation/dephosphorylation of the actin dynamizing protein cofilin. *Mol Endocrinol*. 2010;24:1765-81.

215. Hemmings HC, Jr. and Greengard P. DARPP-32, a dopamine- and adenosine 3':5'-monophosphate-regulated phosphoprotein: regional, tissue, and phylogenetic distribution. *J Neurosci*. 1986;6:1469-81.

216. Hemmings HC, Jr., Girault JA, Nairn AC, Bertuzzi G and Greengard P. Distribution of protein phosphatase inhibitor-1 in brain and peripheral tissues of various species: comparison with DARPP-32. *J Neurochem*. 1992;59:1053-61.

217. Williams KR, Hemmings HC, Jr., LoPresti MB, Konigsberg WH and Greengard P. DARPP-32, a dopamine- and cyclic AMP-regulated neuronal phosphoprotein. Primary structure and homology with protein phosphatase inhibitor-1. *J Biol Chem*. 1986;261:1890-903.

218. Endo S, Zhou X, Connor J, Wang B and Shenolikar S. Multiple structural elements define the specificity of recombinant human inhibitor-1 as a protein phosphatase-1 inhibitor. *Biochemistry*. 1996;35:5220-8.

219. Braz JC, Gregory K, Pathak A, Zhao W, Sahin B, Klevitsky R, Kimball TF, Lorenz JN, Nairn AC, Liggett SB, Bodi I, Wang S, Schwartz A, Lakatta EG, DePaoli-Roach AA, Robbins J, Hewett TE, Bibb JA, Westfall MV, Kranias EG and Molkentin JD. PKC-α regulates cardiac contractility and propensity toward heart failure. *Nat Med*. 2004;10:248-54.

220. Rodriguez P, Mitton B, Waggoner JR and Kranias EG. Identification of a novel phosphorylation site in protein phosphatase inhibitor-1 as a negative regulator of cardiac function. *J Biol Chem*. 2006;281:38599-608.

221. Florea S, Anjak A, Cai WF, Qian J, Vafiadaki E, Figueria S, Haghighi K, Rubinstein J, Lorenz J and Kranias EG. Constitutive phosphorylation of inhibitor-1 at Ser67 and Thr75 depresses calcium cycling in cardiomyocytes and leads to remodeling upon aging. *Basic Res Cardiol*. 2012;107:279.

222. El-Armouche A, Wittkopper K, Fuller W, Howie J, Shattock MJ and Pavlovic D. Phospholemman-dependent regulation of the cardiac Na/K-ATPase activity is modulated by inhibitor-1 sensitive type-1 phosphatase. *FASEB J*. 2011;25:4467-75.

223. El-Armouche A, Pamminger T, Ditz D, Zolk O and Eschenhagen T. Decreased protein and phosphorylation level of the protein phosphatase inhibitor-1 in failing human hearts. *Cardiovasc Res*. 2004;61:87-93.